APPLICATION OF 3D IMAGING TECHNOLOGY TO ANTERIOR CRUCIATE LIGAMENT SURGERY

Sarah Dawson

Supervisor: Prof. C.L. Vaughan
Co-Supervisors: Dr W. van der Merwe, Dr. D. Fitzpatrick

Thesis submitted to the Faculty of Health Sciences at the University of Cape Town in partial fulfilment of the requirements for the degree of Master of Science in Biomedical Engineering.

Cape Town, February 2006

DECLARATION

I, SARAH PENELOPE DAWSON, hereby declare that the work on which this thesis is based is my own original work (except where acknowledgements indicate otherwise) and that neither the whole, nor any part of it, has been, is being, or is to be submitted for any other degree in this or any other University.

I empower the University to reproduce for purpose of research either the whole or part of the contents of this thesis in any manner.

Signed by candidate

Signature

08 - 02 - 06

Date

ABSTRACT

Two aspects of anterior cruciate ligament (ACL) reconstruction surgery were investigated in this thesis. The first was the feasibility of adapting an existing image guided neurosurgery system for use in ACL reconstruction surgery. The second was the creation of 3D models of the knee from MRI scans, and the use of these models to analyse anatomical details of the knee and ACL reconstructed knee. An orthopaedic surgeon specialising in ACL reconstruction, Dr Willem van der Merwe, was consulted during the project.

A stereo-photogrammetric image guided neurosurgery system was developed at the University of Cape Town in 2004. This system uses computer tomography (CT) images, surface fiducials for registration, a reference frame for calibration, a tracked pointer and two smart cameras to register theatre space with CT space. This gives neurosurgeons accurate anatomic guidance on the CT scans during surgery. The system was to be adapted for use in ACL reconstruction. In this arthroscopic procedure a torn ACL is reconstructed by drilling tunnels through the tibia and femur and fixing an autograft through these tunnels. Positioning the tunnels accurately is the most critical step in the success of the procedure. The task was to adapt the system for use with magnetic resonance images (MRI) instead of CT and bony anatomic landmarks instead of surface fiducials. A further problem to address was the movement of the knee during surgery with regard to maintaining registration and navigation accuracy.

Separate tests were performed with dry bones, a plastinated specimen and finally a cadaver knee. A clinical scan protocol, a T1 weighted transverse high resolution gradient echo sequence (TR = 1260ms; TE = 16 ms) with 3 mm slices, was used. The tibia and femur were registered separately. The bony femoral landmarks which gave the best registration accuracy were: the highest point of the articular cartilage laterally; the highest point of the articular cartilage medially and the highest point in the femoral notch. The most accurate tibial bony landmarks were: the lateral tibial spine; the medial tibial spine and the tibial tuberosity (palpated through the skin). The proposed navigation method to eliminate the drilling of invasive tracking devices would be to register each bone when the tunnel position on that bone is to be marked. The bone would then be held still whilst the navigation information is used. Once the bone is manipulated, it would have to be re-registered if further information should be required. The best accuracies achieved were average navigation displacement errors of 1.4 mm for the femur and 2.2 mm for the tibia with the plastinated specimen. The arthroscopic cadaver test gave average errors of 2.2 mm for the femur and 4.8 mm for the tibia. Thus the conclusion is that the system is feasible for use in ACL reconstruction surgery and with slight modifications will provide simple and useful navigation for orthopaedic surgeons.

The second task of the thesis was to reconstruct 3D models of knees from MRI scans. These models allowed detailed anatomical study of the insertion sites of the healthy ACL, and how these compared to the position of the tunnels in ACL reconstruction. Guidance for this part of the project was given by Dr David Fitzpatrick at University College Dublin (UCD). The scan protocol found to be most effective for model generation was a sagittal T2 spin echo sequence with 2 mm slices (TR = 4960 ms; TE = 80 ms). Scans of the left and right knees of 13 healthy subjects and 13 subjects with one ACL reconstructed knee (all performed by Dr van der Merwe) were taken, making 52 knees in total. Each set of scans was converted into a 3D model of tibia, femur and ACL (or ACL reconstruction) using Mimics software. Reference axes were then set on these models using the Arthron software program from UCD. These reference axes defined the following directions: Positive x was medial; Positive y was posterior; Positive z was proximal. 3D measurements of the four 'corners' of the tibial and femoral ACL footprint were taken on healthy knees, and of the four 'corners' of the tibial and femoral tunnel exits on reconstructed knees. These four positions were averaged to give the centre of the insertion or tunnel. The measurements were normalised for size using an AP measurement of the thickness of the femur at the femoral notch, and an anterior-posterior (AP) measurement of the tibial plateau and expressed as a percentage.

A 2-way ANOVA was run on these measurements to answer four questions. The results showed that the ACL insertion varies quite widely between people with standard deviations of up to 12% in the tibia and femur. Secondly, the results show that the ACL is bi-laterally symmetric, i.e. in healthy knees, the ACL in the right and left knee of the same person is in the same place on both the tibia and femur. Thirdly it was shown that the healthy ACL of those patients whose other knee had undergone ACL reconstruction inserted in a similar place to all the other healthy knees in the study, demonstrating that there is no outright anatomic or modelling difference between the two groups. Finally, a comparison between the tunnel position in the reconstructed knee and the healthy ACL insertion in the opposite knee of each ACL reconstruction patient was performed. This showed that in general, tunnels are placed in the anatomical footprint of the ACL. However, the femoral tunnel is drilled more proximally than the ACL's femoral insertion and the tibial tunnel is drilled more posteriorly than the ACL's tibial insertion. This could indicate a need to change surgical procedure. However, it must be noted that on examination of the knee models, the autograft and natural ACL did align well, which could indicate that despite tunnel 'misplacement', the reconstruction is effective. The results also show that MRIs of a patient's healthy knee could be used to give the ideal position for their ACL reconstruction, since the ACL is bi-laterally symmetrical.

ACKNOWLEDGEMENTS

I wish to thank the following people for their help during this project:

1. Prof. Kit Vaughan for all his advice and guidance.
2. Dr David Fitzpatrick for his support and interest during my time at University College Dublin.
3. Dr Willem van der Merwe for his invaluable advice and insight into ACL reconstruction and orthopaedic surgery.
4. The National Research Foundation (NRF), Innovation fund and Wellcome trust for financial assistance.
5. Andre Bester for his patience and time with the setting up and details of the neurosurgery system.
6. Goodwin Lawlor for his permission to use Arthron and his troubleshooting advice.
7. The post-graduate engineering students at UCD for their help with the Mimics software.
8. The radiographers at the Sports Science Institute for their assistance with patients and the MRI machine.
9. Andrew Whiley for his thorough proof-reading.

TABLE OF CONTENTS

LIST OF FIGURES

LIST OF TABLES

ABBREVIATIONS

ACL:	Anterior Cruciate Ligament
AP:	Anterior-Posterior
ANOVA:	Analysis of Variance
CAD:	Computer Aided Design
CAS:	Computer Assisted Surgery
CAOS:	Computer Assisted Orthopaedic Surgery
CT:	Computer Tomography
IGS:	Image Guided Surgery
ML:	Medial-Lateral
MRI:	Magnetic Resonance Imaging
OR:	Operating Room
PD:	Posterior-Distal
TKR:	Total Knee Replacement

1 INTRODUCTION

1.1 Subject of this Thesis

This thesis concerns two areas of Anterior Cruciate Ligament (ACL) econstruction. The first is the adaptation of an existing Image Guided Surgery (IGS) system for use during ACL reconstruction surgery. The second area that is dealt with is the creation and analysis of three-dimensional (3D) models of the knee from Magnetic Resonance Imaging (MRI) scans. These models are used to attain anatomical information about healthy and reconstructed ACLs.

1.2 Background to the Problem

1.2.1 Image Guided Neurosurgery System

In 2004, a stereo-photogrammetric system for guiding neurosurgeons during surgery was developed and tested at the University of Cape Town (UCT) [Watson, 2004]. The aim in developing the system was to provide a cost-effective system that would be available to hospitals in developing countries. The system consists of two smart cameras, a trackable probe, a reference frame and a laptop with software, as shown in Figure 1.1 below.

Figure 1.1 The smart cameras and laptop (left) and the reference frame and trackable probe (right) of the image guided neurosurgery system [Watson, 2004].

The first step in using the system is to place three surface fiducials on the patient's skull. The patient is then scanned using Computer Tomography (CT). The patient is then moved into the operating theatre, where the reference frame is used to calibrate the space above the patient's head ('theatre space'), as shown in Figure 1.2 on the next page.

Figure 1.2 The reference frame being used to calibrate the theatre space above the patient's head.

Each fiducial is then pointed to in turn, using the trackable probe which is tracked by the smart cameras, as shown in Figure 1.3 below. This process registers the theatre space to the CT scans ('scan space') via a mathematical transformation which relates the known positions of the fiducials both in theatre and on the scans. The pointer can now be used to point anywhere on the patient's head or brain, and the position of the pointer can be seen on the CT scans. This enables the surgeon to operate with an accurate knowledge of the patient's anatomy, and the location of tumours and other important structures. A detailed explanation of the neurosurgery system and its operation can be found in Appendix A.

Figure 1.3 An image from a smart camera showing the probe pointing to one of the surface fiducials on the head [Watson, 2004].

Following the success of this system it was decided that an application in orthopaedic surgery, specifically ACL reconstruction surgery, would be useful.

1.2.2 Anterior Cruciate Ligament Reconstruction

Anterior cruciate ligament reconstruction is a frequently performed operation of the knee. The ACL attaches to a fossa on the posterior aspect of the medial surface of the lateral femoral condyle, and to a fossa in front of, and lateral to, the anterior tibial spine. The function of the ACL is to resist anterior movement of the tibia with respect to the femur. It also helps to resist hyperextension of the knee, and contributes to the rotational stability of the knee [Jackson *et al.*, 1993].

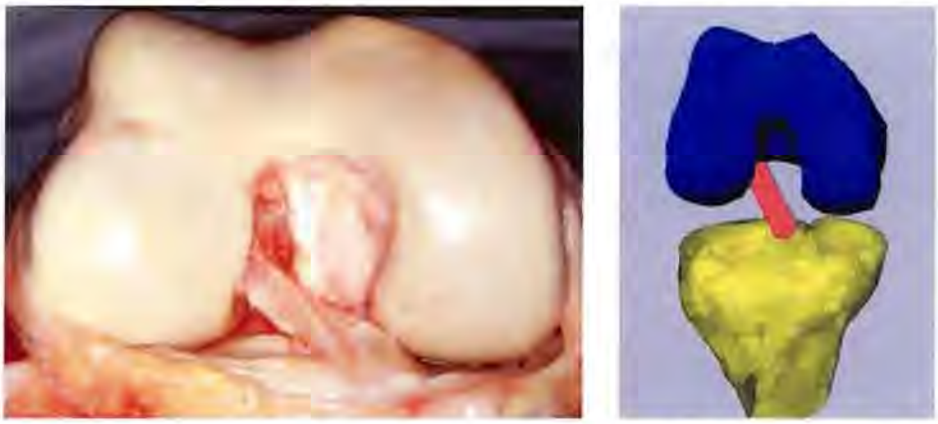

Figure 1.4 A dissection of a human knee joint showing the ACL (left), and a 3D model of the knee joint showing femur (blue), tibia (yellow) and ACL (red) (right) [Neyret *et al.*, 2000; Duthon *et al.*, 2000].

The ACL is fairly easily torn in high impact sports such as soccer or rugby, and reconstruction of the ligament is essential in restoring normal knee function and thus preventing osteoporosis and further knee injuries [Nebelung and Wuschech, 2005].

ACL reconstruction is an arthoscopically performed operation. After clearing any ACL remnants from the knee, the surgeon drills a tunnel through the tibia, starting at the anteromedial aspect. Through this tunnel, the femoral tunnel is then drilled, exiting from the anterolateral aspect of the femur, as shown in Figure 1.5 below.

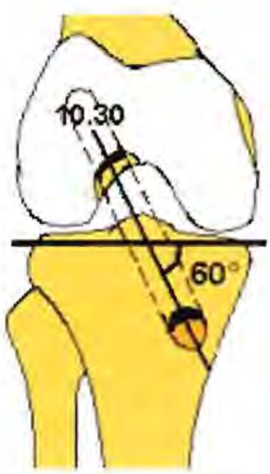

Figure 1.5 A possible orientation for the femoral and tibial tunnels in ACL reconstruction [Giron *et al.*, 2000].

Through these tunnels, an autograft is then fixed. This is usually either the bone-patellar tendon-bone autograft, or the semitendinosus (and sometimes gracilis) tendon of the hamstrings, as in Figure 1.6 below.

Figure 1.6 The hamstrings tendons being threaded through the tibial and femoral tunnels in ACL reconstruction surgery.

Once the autograft is fixed in place, the surgery is completed, and the patient begins rehabilitation [Jackson *et al.*, 1993; Hughston 1993].

1.2.3 Mimics Software

Mimics is a software package developed by the Materialise company. It is a 3D image-processing and editing software which is based on scanner data. Dicom images from either MRI or CT scanners can be imported into the program, segmented and manipulated and used to create full 3D models of the object which was imaged.

This software was made available at University College Dublin (UCD), and was used to convert MRI images of the knee into 3D format so that these images could be analysed, and various anatomical parameters measured.

1.3 Description of the Problem

There are two main tasks in this thesis. The first concerns the adaptation of the IGS Neurosurgery system for use in orthopaedic surgery, and more specifically, ACL reconstruction. The second involves the use of MRI scans to create 3D models of knees in order to provide more information about the ACL and ACL reconstruction techniques.

1.3.1 Feasibility of Adapting the Neurosurgery System for Orthopaedic use

Although there are existing image guided ACL reconstruction systems, the reason for developing this system is to create an affordable, simple and user-friendly system which is complimentary to the orthopaedic surgeon's procedure, and does not introduce unnecessary invasiveness to the surgery. The problem of adapting the system from the neurosurgery environment to the orthopaedic environment involves several parts, since the two applications are fairly different from one another. The major differences are:

- In the neurosurgery system, computer tomography scans were used, whereas in ACL reconstruction, the clinical norm is to use magnetic resonance imaging. Thus, adaptations had to be made to allow the use of the different imaging medium.
- In neurosurgery, surface fiducials are used since the skin on the head is relatively immobile. However, around the knee, the skin is relatively loose, requiring a different method to be used for registration. The method proposed and investigated in this thesis is that of anatomical, landmark-based registration i.e. using the bony landmarks of the knee as registration points.
- The skull is a single body, whereas the knee is made up of the femur, tibia and patella. Furthermore, these bones move relative to each other, and are manipulated in surgery whereas the skull is held in a fixed position during surgery. This means that once registration takes place, it is maintained throughout the neurosurgery procedure. In order to adapt this to the ACL reconstruction surgery, a more involved registration process is required, and some simplifying assumptions must be made about the knee.

These problems are dealt with in this thesis in terms of assessing the feasibility of adapting the neurosurgery system for use in ACL reconstruction. An orthopaedic surgeon specialising in knee surgery, Dr Willem van der Merwe, at the Sports Science Institute in Newlands, Cape Town, provided information on the ACL reconstruction procedure, and was consulted during the testing of the system.

1.3.2 Creating and Analysing 3D Models of the Knee

The process followed was to take detailed MRI scans of the knee, and to import these into the Mimics program. Each knee was then carefully segmented in order to create a 3D model of the femur, tibia and ACL or ACL reconstruction. These models are used to make measurements and determine various statistical relationships.

The purpose of this investigation was twofold. Firstly, the models were used to gain detailed information on the healthy ACL since cadaveric and dissection studies of the ACL are necessarily limited in their approach. Secondly, information on the placement of ACL tunnels, and how this relates to the insertion of the healthy ACL was obtained from the models. This seems to be one of the only studies comparing the position of the native ACL to the position of the reconstructed tunnel using a computer model, since it is difficult to perform on cadavers. The information gained may shed light on current ACL reconstruction procedures, and on the need for greater accuracy in tunnel placement.

The details looked at are:

- Position of the attachments of the ACL in healthy knees
- Bilateral symmetry of the ACL in healthy knees
- Position of the tunnels in reconstructed ACLs
- The correlation between tunnel position and original ACL position in reconstructed knees

This investigation was partly undertaken at University College Dublin, Ireland, under the supervision of Dr David Fitzpatrick, due to his experience in using Mimics and the 3D models obtained from Mimics. Dr Willem van der Merwe was also consulted during the analysis of the measurements obtained from the models.

1.4 Objectives

The objectives of the thesis are as follows:

- To test the use of the image guided neurosurgery system for providing navigation information during ACL reconstruction.
- To conclude from these tests as to the feasibility of the system for use in image guided ACL reconstruction surgery.
- To master the use of the Mimics segmentation and 3D modelling software.
- To use the resulting knee models to gain insight into the anatomical properties of the healthy and reconstructed ACL.

1.5 Limitations and Scope of the Project

This project covers only the assessment of the *feasibility* of adapting the neurosurgery system to orthopaedic surgery, as opposed to the actual creation of an adapted system. It wa thus limited in that neither specific hardware nor software for the system were developed.

In the area of 3D model analysis, only the measurements and statistics which are applicable to the accuracy of ACL reconstruction surgery were studied, although many more figures could be obtained from the 3D models.

1.6 Plan of Development

This thesis begins with a literature review section in which Computer Assisted Orthopaedic Surgery (CAOS) is discussed. This is followed by an analysis of the literature with regard to anterior cruciate ligaments, and anterior cruciate ligament reconstruction. A chapter outlining the investigative procedure used in this thesis follows the literature review.

The investigations involved in the thesis are set out in two sections. The first section discusses the process of testing the feasibility of adapting the image guided neurosurgery system for use in ACL reconstruction surgery. A full discussion of the problem and proposed solutions is given, and is followed by three chapters discussing the tests undertaken to assess the feasibility of image guided surgery in ACL reconstruction.

The second part of the thesis discussing the creation and analysis of 3D models follows. A chapter discussing the problem and proposed solution is followed by two chapters discussing the various procedures examined for creation and analysis of 3D models of the knee. This is followed by a chapter discussing the results of measurements made on the models, and statistical analysis performed on the models.

Conclusions and recommendations for both the preceding sections are presented in the final two chapters.

2 LITERATURE REVIEW

In this section, a detailed examination of the literature pertinent to this project is given. To begin with, an overview of what Computer Assisted Orthopaedic Surgery (CAOS) is, and the pros and cons of the various different available systems, is given. This is followed by a section on anterior cruciate ligament reconstruction surgery, specifically dealing with the placement of the tunnels in surgery, and how this compares to the anatomical placement of the healthy ACL.

2.1 Computer Assisted Orthopaedic Surgery (CAOS)

Nolte and Beutler (2004) define CAOS as a term which "*summarizes approaches that aim to improve visibility to the surgical field and increase geometrical accuracy by means of robotic devices or so-called navigation systems when carrying out surgical actions. These goals are achieved by virtually linking the bony anatomy being operated on with a virtual, often radiological, representation.*"

The basic principle of CAOS is to couple medical images and anatomical data through a registration process, and to enhance this information by displaying surgical tools or pre-operative plans in real time with this data [Nolte and Beutler, 2004].

2.1.1 Classification of Different Systems

There are various ways of classifying CAOS systems

CAOS is divided into three categories, based on how the relevant image data is obtained, as shown in Table 2.1 below.

Table 2.1 Table showing the division of CAOS systems according to the imaging data used [Sikorski and Chauhan, 2003].

Image-based		Image-free
Pre-operatively Imaged	CT/MRI scans taken before surgery.	Model of the anatomy is updated through registration process.
Per-operatively Imaged	Images acquired in surgery using modified fluoroscopy techniques.	

Figure 2.1 below shows the components of an image-based CAOS system.

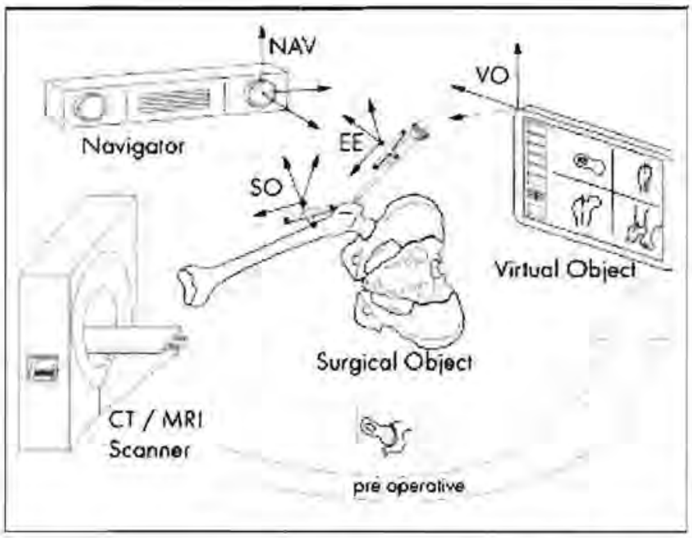

Figure 2.1 The components of an image-based CAOS system [Nolte and Beutler, 2004].

A second way of classifying CAOS systems is according to the level of independence given to computers or devices in the system, as shown in Table 2.2 below.

Table 2.2 Table showing the division of CAOS system according to surgeon/device control [DiGioia *et al.*, 1998; Müller-Alsbach and Stäubli, 2004].

Passive Systems	Semi-Active Systems	Active Systems
Perform no action independently.	Guide according to a pre-defined strategy.	Entire tasks performed by robotic devices.
Augment information available to the surgeon.	Surgeon has the final control.	Surgeon oversees the action.

For the purposes of this literature review, systems will be divided into Image-based or Image-free systems, and only passive systems will be dealt with.

2.1.2 Basic CAOS Procedure

There are three important aspects to any CAOS surgery. First, there is patient-specific pre-operative planning. This involves modelling the effects of various surgical interactions, and deciding which will be used in surgery.

Once in surgery, one of the most crucial steps in CAOS, that of registration, is performed. This relates the pre-operative plan and medical images with the position of the patient at the time of surgery [Langlotz, 2004].

The bones and surgical tools must be tracked throughout the surgery, and this is accomplished by attaching tracking devices to the patient and tools. Most commonly these are either active (generate an infra-red signal) or passive (reflect infra-red from a source) optical devices known as Dynamic Reference Bases (DRBs), which are monitored by camera. However, this has the disadvantage that a direct line-of-sight between the camera, tools and bones is required at all times. Other systems, such as acoustic or magnetic systems, do not require line-of sight but are less accurate and more difficult to adapt to current operating environments [DiGioia *et al.*, 1998; Sikorski and Chauhan, 2003].

Figure 2.2 A CAOS system in theatre showing the navigation screen (1), cameras (2) and drilled DRBs for tracking (3) [Jenny and Boeri, 2004].

2.1.3 Image-Based Systems

In the pre-operative phase using image-based systems, CT or MR images of the patient are taken. These are used to perform various planning procedures such as assessing the condition of the knee, gaining anatomical information about the patient, and modelling various surgical interventions to assess their predicted outcome [Joskowicz and Taylor, 2001].

This data is then transferred to theatre, where registration must take place so that the operating reality can be correlated with the pre-operative planning data. There are two broad categories of registration – paired points and surface registration.

Paired-points registration is sub-divided into landmark- and fiducial-based registration. Here, operatively or cutaneously attached fiducial markers, or anatomical landmarks, are defined on the pre-operative images. The same points are then identified on the patient in theatre and this set of matched points defines a relationship between the images and operating theatre [Nolte and Beutler, 2004; Langlotz, 2004].

Surface registration is based on the unique shape of bones. Many intra-operative data points are collected by direct contact with a probe (usually ultrasound) on the surfaces of the bones. These are then matched with pre-operative images of the patient's bones, and this constitutes registration [DiGioia *et al.*, 1998].

The bones and tools are then fitted with optical tracking devices which track the anatomy and maintain the correlation between the medical images and the theatre.

2.1.4 Image-Free Systems

Image-free systems do not make use of any pre-operatively obtained images. Instead, the tracking system (as mentioned above) is used to establish anatomical landmarks, structures and surfaces which are used as the features of a virtual representation of the object. This is also known as surgeon-defined anatomy [Nolte and Beutler, 2004].

There are three ways of obtaining surgeon-defined anatomy. Firstly, the tracked pointing devices can be used to determine anatomical landmarks through direct intra-operative digitisation. Secondly, joints are passively moved in pivoting procedures to determine joint centres and other kinematic parameters. Finally, bone-morphing is used. Here, the surgeon acquires a set or 'cloud' of points on each anatomical region. These are then fitted to a library of standard statistical models of the anatomy to form 3D images which more closely represent the patient's anatomy [Langlotz, 2004; Nolte and Beutler 2004].

Using these methods, an accurate representation of the patient's anatomy is developed without using any medical imaging. The anatomy is tracked in the same way as in Image-based systems.

2.1.4.1 Image-Based versus Image-Free Systems

There are pros and cons to both the CAOS methods.

The greatest weakness in image-based systems is the registration process. Should this be inaccurately performed, either by the surgeon or due to poor matching algorithms, all subsequent navigation data will be erroneous. To ensure an accurate registration, extra pre-operative planning time is required. This pre-operative time is not necessary in Image-free systems [Nolte and Beutler, 2004; Langlotz, 2004; Hüfner *et al.,* 2004].

However, despite the time involved, the images provided pre-operatively in image-based systems allow for superior pre-operative planning and visualisation of the patient's anatomy. This can aid the surgeon greatly when performing the operation. The opportunity for such planning is absent in Image-free systems (unless extra radiographs are taken). DiGioia (1998) states that one of the limitations of non-computer assisted surgery is an "*inability to integrate medical images or pre-operative plans directly in the operating room*". It would seem that Image-based computer-assisted systems address this need most directly.

An inherent downfall of image-free systems is that the data on which all subsequent navigation takes place is defined by the surgeon – the navigation system cannot verify the plausibility of the acquired information. Errors in all three types of data collection are possible, for instance, poor co-ordination during point collection and insufficient range-of-motion in pivoting procedures. It is also important to remember that the 3D image generated from bone morphing is not necessarily exactly that of the patient - particularly in cases of atypical anatomy [Langlotz, 2004].

One of the advantages of image-free systems is the "*relative technical simplicity and the superior workflow of the associated surgical modules*" [Nolte and Beutler, 2004]. They eliminate the sometimes complicated registration processes of image-based systems. Sikorski and Chauhan (2003) describe them as "*quicker, simpler and cheaper*". However, they caution that the lack of anatomical detail in image-free systems could result in deficiencies, especially in the case of major anatomical deformities.

In a study performed by Bäthis *et al.* (2004), a CT-based and an image-free system were compared in Total Knee Replacement (TKR) operations. There was no significant difference between the two systems, and both were described as precise tools for component orientation. Thus it seems that both systems have their place in CAOS, and both display similar accuracy qualities. However, it would seem that the increased time involved in planning and registration in image-based systems is outweighed by the added information and anatomical detail available both pre- and intra-operatively.

2.1.5 Accuracy Validation and Sources of Error

It has been shown that computer assisted surgery presents an improvement on current orthopaedic surgery methods. However, it is important to establish exactly how the accuracy of these systems is to be validated, and to identify the most common sources of error.

2.1.5.1 Sources of Error

There are various sources of error in the CAOS process. These will be discussed, as well as suggestions for how to overcome/reduce these errors.

In image-based navigation, one of the earliest sources of error is from the CT or MR imaging process. Noise, limited spatial and contrast resolution and image artefacts are all present in the imaging step of CAOS. Whilst these are inherent qualities of CT and MRI, it is vital to ensure that the best data possible is acquired – this is particularly important at this stage, since errors at this first step impact every following step in the process [Simon *et al.*, 1995; Amiot and Poulin, 2004, Sikorski and Chauhan, 2003].

Registration is one of the most important stages in image-based CAOS. Noisy data in a paired-points registration process will result in poor registration accuracy. Also, some paired-points matching algorithms may seem to be very accurate, when, in fact, they are not matching corresponding points with each other. It is vital for a surgeon to ensure that the registration process has taken place as accurately as possible [Simon *et al.*, 1995; Langlotz, 2004; Amiot and Poulin, 2004; Sikorski and Chauhan, 2003].

An equivalent to the CT imaging and registration errors present in image-based systems are surface model generation errors in image-free systems. If these models are not geometrically accurate all subsequent navigation will be erroneous. Sources of error include poor co-ordination of triggering and point collection and insufficient range-of-motion when performing a pivoting procedure. It is thus necessary to verify that the resulting feedback of the CAOS system is reasonable [Langlotz, 2004].

Errors are also introduced when affixing the tracking devices to the patient's anatomy. Firstly, this fixation may result in deformation of the bone, thus making any previous images of the anatomy inaccurate. It is also possible for these tracking devices to move in relation to the anatomy and surgical tools, thus changing the registration between patient and computer-assisted tools. This change results in a serious degradation of the performance of the navigation systems. It is vital to ensure that these tracking devices do not move during surgery, and that if they do, the navigation system is abandoned [Simon *et al.*, 1995; Langlotz, 2004; Sikorski and Chauhan, 2003].

If any of the tracked tools are deformed in surgery, the supplied navigation data will no longer be accurate because the CAOS system still assumes the instrument to be in its original shape. Again, the navigation system should be abandoned if this occurs [Langlotz, 2004; Amiot and Poulin, 2004].

2.1.5.2 Accuracy Validation

In order to analyse the accuracy of any CAOS system, it is necessary to have an accurate ground truth to compare the system to. Various proposals for this have been suggested in the literature.

Simon *et al.,* (1995) suggest that a way to measure the accuracy of the anatomical paired-points registration is to use fiducial based registration of the same object as the ground truth. They also suggest that a ground truth for surface model generation would be to accurately image the bone's surface using other methods, such as an optical range sensor, and to compare this to the surface model generated by the system.

However, even in a well validated and tested system with proven accuracy, it is still possible for any of the previously described errors to occur. This is particularly dangerous because the transition between exact and inexact feedback is smooth, thus the loss of accuracy in the system is not obvious. It must always fall to the surgeon to judge whether the displayed navigation data is accurate or not [Langlotz, 2004; Sikorski and Chauhan, 2003].

2.1.6 Improved Surgery

It has been shown that CAOS has the potential to achieve better levels of accuracy than conventional surgery, and that improved accuracy results in better orthopaedic surgery. But what really constitutes overall improved surgery? What is required of CAOS to make a successful surgical intervention, and is it meeting these demands? Are the perceived benefits of CAOS really proven?

The important measures of a successful surgical intervention are as follows:

- Accuracy, and its impact on clinical outcome
- Time in theatre
- Cost
- Simplicity of set-up, integration and use
- Patient risks e.g. invasiveness and radiation exposure

These will be dealt with as they are discussed in the literature.

2.1.6.1 Accuracy

The major perceived benefit in CAOS is that of improved accuracy. Although many studies have shown that CAOS does allow for improved tunnel placement, and that improved placement results in improved graft longevity and knee functionality, there are still some question marks over this issue.

Many researchers say that this accuracy can only be shown through large-scale, randomised outcome studies. This is problematic in several ways. Firstly, these studies are expensive due to the nature of CAOS technology and it is difficult to justify them when conventional surgery is reasonably low cost and reasonably successful. Secondly, in order to establish that improved accuracy really does have long-term clinical benefits, long-term studies are necessary. However, some patients may not survive the 10 – 20 year period necessary (in the case of total knee replacement surgery), and the CAOS technology will be obsolete by the end of the study. Also, there are many other factors that affect ACL reconstruction success such as rehabilitation procedure, patient lifestyle etc. These and other complications make it difficult to prove that greater accuracy has significant patient or healthcare benefits [Mohsen and Phillips, 2004].

It is clear that this relationship between theoretical achievements and real patient outcomes still needs to be established and that CAOS will not be widely accepted until it is. Improved accuracy means nothing to a patient unless it aids their return to normal activities and keeps them functional and pain free [Sikorski and Chauhan, 2003; Nizard *et al.*, 2004; Stulberg, 2003; Delp *et al.*, 1998].

2.1.6.2 Time in Theatre

One of the most common concerns in the use of CAOS is that operating time will increase significantly. Julliard *et al.* (1998) report increased theatre time to be only 15 – 30 minutes, whilst Degenhart (2004) quotes even less extra time, at 10 – 15 minutes. These low values of extra time spent in theatre would seem to be more than compensated for by the improvement in accuracy gained when using a CAOS system.

2.1.6.3 Cost

Cost is a huge factor in medicine today. CAOS, as a new and fairly complex technology, has many associated costs including increased operating time, cost of hardware and software, cost of surgeon and staff training, and cost of extra radiological procedures. CAOS systems are currently expensive, but as with all new technology, the cost may decrease if the volume of users increases [Sikorski and Chauhan, 2003; Porter *et al.*, 2004; Noble *et al.*, 2003]. *"The feasibility of a treatment is defined not only by it clinical excellence, but also by the operation costs."* [Jyrkinsen *et al.*, 2000]. Unless the costs associated with CAOS become more reasonable, it is unlikely that its use will ever be widely justifiable.

2.1.6.4 Simplicity of Set-up, Integration and Use

A benefit and even a clinical requirement of any new technology is that it fits well into the existing Operating Room (OR) environment and is easy for the surgeon and staff to use. However, at present this is not the case with CAOS, as the OR set-up must be changed with the addition of foreign and often complex machinery. CAOS will only be accepted by medical staff when it becomes more simple to use and less invasive to the OR [Gebhard *et al.*, 2004; Di Gioia *et al.*, 1998].

2.1.6.5 Patient Risks

One of the currently unavoidable problems in CAOS is the infra-red beacons which are drilled into the bone of the patient. This increased invasiveness, although minor, still adds risk to the surgery, and ideally should be eliminated from the procedure [Sikorski and Chauhan, 2003].

Another added risk in CAOS is the increased radiation exposure if CT scans are used in image-based navigation systems [Delp *et al.*, 1998].

Whether these risks are outweighed by a more effective surgery remains to be seen.

2.1.7 Conclusion

It is clear that the ultimate goal of CAOS systems must be to assist the surgeon in performing surgery more accurately, with fewer complications, in less time and less invasively than existing methods, and that this will improve patient outcomes in a cost-effective manner [DiGioia *et al.*, 1998]. When all of these factors are achieved, CAOS will become a truly successful surgical procedure.

2.2 Anterior Cruciate Ligament Reconstruction Surgery

100 000 anterior cruciate ligament (ACL) reconstructions are performed each year in the United States alone [Fu and Musahl, 2001]. The literature indicates that accurate femoral and tibial tunnel positioning is critical to the success of ACL reconstruction. Indeed, Schep *et al.* (2005) view it as the most important step in the reconstruction procedure [Eriksson, 1997; Julliard *et al.*, 1998; Schep *et al.*, 2005; Burkart *et al.*, 2001; Musahl *et al.*, 2002 *i* and 2003; Picard *et al.*, 2001]. However, Musahl *et al.* (2003) report misplacement of tunnels in 10% to 40% of cases. Furthermore, long-term clinical success rates do not exceed 85 – 90% [Fu and Musahl, 2001]. This means that at least 10 000 revision ACL reconstructions need to be performed in the USA each year [Musahl et al., 2002 *ii*]. Clearly this high rate of revision surgery calls for an examination of the ACL reconstruction procedure – what are its aims, how are surgeons performing the operation, and how can the clinical success rate be improved?

Figure 2.3 Image from an ACL reconstruction surgery.

2.2.1 Tunnel Positioning

The goal in positioning the tunnels is to place them such that stability and the full range of knee motion is restored, whilst at the same time avoiding excessive graft stretching or impingement on the femoral notch during movement of the knee. Other important factors for ligament placement include proper graft tensioning and correct graft fixation [Sati *et al.*, 2002; Picard *et al.*, 2001].

Misplacement of the tunnels results in graft failure, diminished range of motion, and graft impingement with the femoral notch [Musahl *et al.*, 2002*i*]. Further complications include interference with the posterior cruciate ligament (PCL), graft tightening and slacking, and knee instability [Sati *et al.*, 2002; Schep *et al.*, 2005; Julliard *et al.*, 1998].

As mentioned above, it is generally accepted that precise femoral and tibial tunnel placement is a critical factor in the success of ACL reconstruction surgery [Musahl *et al.*, 2005, Shea *et al.*, 2002, Lintner *et al.*, 1996]. Tunnel misplacement is the most common technical error in ACL reconstruction, and the most important variable which surgeons can control [Topliss and Webb, 2001].

2.2.2 Current Accuracy in Tunnel Placement

In an audit of 114 ACL reconstruction cases, Topliss and Webb (2001) found that 65% of femoral and 59% of tibial tunnels were placed outside acceptable margins. In only 10% of cases were both tunnels placed correctly in both sagittal and coronal planes. In a report on the second ESSKA scientific workshop concerning cruciate ligament reconstruction, Amis and Jakob (1998) affirm these results, saying there is much evidence to show that even experienced, excellently trained surgeons cannot drill the tunnels for ACL reconstruction accurately.

Both Kohn *et al.* (1998) and Jonsson *et al.* (1998) found that tunnels were placed too anteriorly, even amongst experienced surgeons. Futhermore, in a follow-up on 100 ACL reconstruction patients, Järvelä *et al.* (2001) show that the standard deviation in tunnel placement was 11.1% and 6.8% for the tibia and femur respectively, indicating a large variability and unpredictability in tunnel placement.

Thus it seems clear that although accurate and repeatable placement of the femoral and tibial tunnels is the most important factor in ensuring a successful ACL reconstruction, current accuracies in tunnel placement leave much to be desired.

2.2.3 Describing the Position of the ACL Attachment

Before discussing the placement of tunnels in ACL reconstruction, and the position of the ACL in the healthy knee, it is important to review the methods used in the literature to describe these positions.

Due to the 3-dimensional nature of the bones, the ACL and the tunnels, describing where the tunnels or ligament are placed can be difficult. There are two main methods used in the literature to describe the femoral position of tunnels or the femoral ACL attachment – the clock referencing method and the grid method, which are discussed further below.

Describing the tibial attachment is slightly easier, due to the nearly 'flat' surface of the tibia, and the relatively simpler shape of the tibial ACL insertion. Thus the position of the tunnel or ligament footprint is usually given as a measurement in the anteroposterior (AP) direction, either as a percentage of the total AP distance of the tibia, or simply as a measurement from the anterior border of the tibial plateau [Musahl *et al.*, 2005; Amis and Jakob, 1998; Shea *et al.*, 2002].

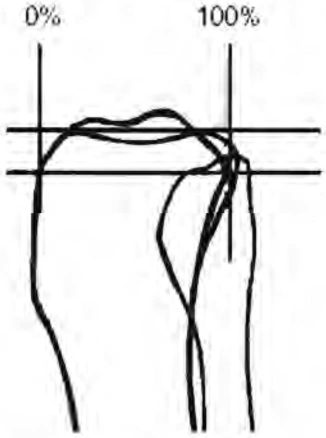

Figure 2.4 Measurement of AP distance on the tibia – the ACL position is given as a percentage of this distance [Amis and Jakob, 1998].

2.2.3.1 The Clock Positioning Method

This method is most widely used in the literature because it is intuitive and correlates well to what is visible arthroscopically, i.e. to what the surgeon sees in theatre [Musahl *et al.*, 2003; Giron *et al.*, 2005].

In this method, the roof of the femoral notch serves as the 12 o'clock reference position when viewed posteriorly, with the knee in 90° flexion. This is also known as Blumensaat's line when seen in the lateral view [Musahl *et al.*, 2003]. A clock face is fitted inside the femoral notch, and the 'time' is used to describe the position of the ACL or femoral tunnel [Giron *et al.*, 2005]. Millimetre measurements are sometimes also given to describe the AP offset, since the 'clock' describes only two dimensions.

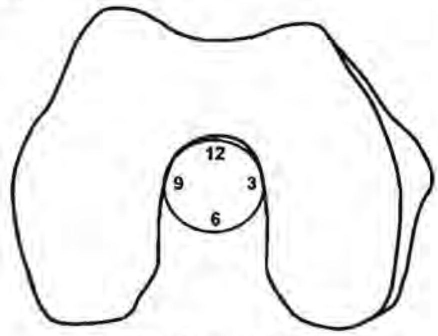

Clock position

Figure 2.5 The clock position as used to describe the placement of the ACL footprint or tunnel [Giron *et al.*, 2005]

2.2.3.2 The Quadrant Method

The quadrant method is more useful and precise for anatomical studies, but does not translate well into the surgical environment. It is, however, independent of variation in knee size, and is reproducible, according to Bernard *et al.* (1997).

As seen in Figure 2.6 below, the method uses a lateral roentgenogram of the femur, with the condyles lined up exactly. A rectangle is then drawn underneath Blumensaat's line. The sides of the rectangle are the depth of the notch (A_2) and the width of the femoral condyles (B_2). Measurements are then taken of the distance from the centre of the ACL (X) to Blumensaat's line (A_1) and to the posterior margin of the femoral condyles (B_1). The position of the ACL centre is then given in percentage values $A = A_1/A_2$ and $B = B_1/B_2$ [Musahl *et al.*, 2003; Bernard *et al.*, 1997].

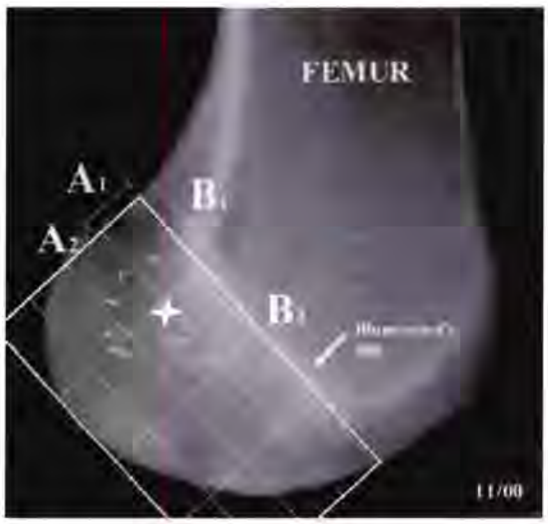

Figure 2.6 The measurements used in the quadrant method shown on a lateral roentgenogram. X represents the centre of the ACL [Musahl *et al.*, 2003].

2.2.4 Ideal Tunnel Placement

One of the biggest obstacles in the way of improving tunnel placement is a lack of consensus as to exactly where the best place for the tunnels is. Despite much research into the area, the best tunnel positioning still remains a highly controversial topic and, specifically for the femoral tunnel, an important area requiring more work [Musahl *et al.*, 2005; Zavras *et al.*, 2005, Fu and Musahl, 2001].

In a study by Picard *et al.* (2001), the *ideal* tunnel locations marked by two experienced surgeons were different, for the femur and tibia, in both the coronal and sagittal planes. Furthermore, in a symposium to establish global trends in current sports related injuries, it was found that of the fourteen surgeons on the panel, eight surgeons used an 11:00/1:00 placement, four a 10:30/1:30 placement, one a 9:00/3:00 placement and one an over the top reconstruction, illustrating the range of tunnel placements used. [Harner *et al.*, 2001].

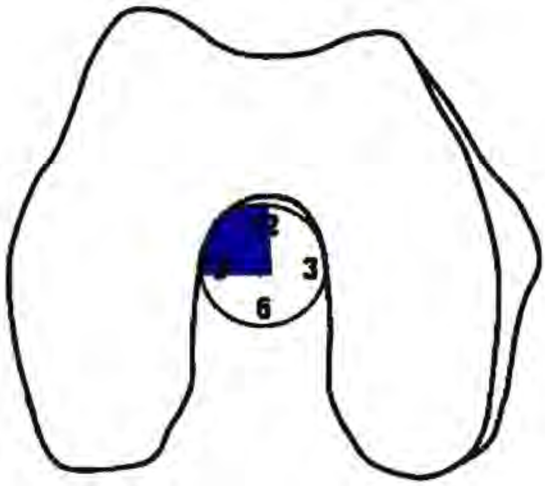

Figure 2.7 Range over which surgeons place the reconstructed ACL [Giron *et al.*, 2005].

These varied choices of tunnel position indicate that, despite extensive research, the optimal location for tunnel placement is, in fact, not known, or has not been conclusively proven [Musahl *et al.*, 2002 *ii*].

There are two main theories regarding tunnel placement. The first is to place the graft isometrically and the second is to place it anatomically, with the femoral tunnel often being sited as the most important area of concern for both these methods [Musahl *et al.*, 2005].

2.2.5 Isometric Placement

Placing the graft isometrically means that its length does not change, or changes very little, over the entire range of knee motion. The reasoning for this placement is that if cyclic stretching of the graft is avoided, it will be under less stress and therefore be less likely to change shape in response to normal knee motion. Theoretically this results in a stronger graft, more able to fulfil its stabilising roll and less likely to get damaged, stretched or broken, and there is some laboratory evidence to support this theory [Zavras *et al.*, 2005; Giron *et al.*, 2005; Schep *et al.*, 2005].

An isometrically placed graft is placed high in the femoral notch (when viewed distally, in a flexed position) i.e. close to the posterior end of Blumensaat's line [Musahl *et al.*, 2005; Zavras *et al.*, 2005]. Zavras *et al.*, (2005) describe the isometric position as being at the 10:30 to 11:00 o'clock position (right knee), 3 mm distal to the posterior edge of the roof of the notch, at the antero-proximal edge of the anatomic ACL insertion. However, Arnold *et al.* (2001) say the isometric location is at about 11:00 – 12:00 o'clock, showing variability even among supporters of the same theory.

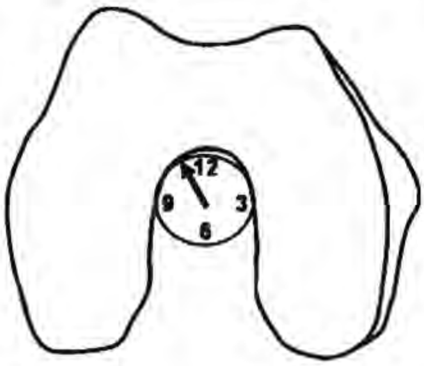

Figure 2.8 The approximate tunnel location for isometric placement [Giron *et al.*, 2005].

2.2.6 Anatomic Placement

Anatomic placement of the ACL graft is based on the reasoning that in order for the graft to replicate the function of the original ACL accurately, it should be placed where the original ACL inserted into the knee. The theory is that this more physiological placement will restore normal knee function and kinematics [Markolf *et al.*, 2002; Zavras *et al.*, 2005; Cain and Clancy, 2002; Bernard *et al.*, 1997].

An anatomically placed graft is located lower in the femoral notch than an isometrically placed graft according to most authors [Musahl *et al.*, 2005].

Markolf *et al.* (2002) say the anatomical tunnel position for the femoral tunnel is at 11 o'clock (right knee), 6 – 7 mm anterior and distal to the posterior femoral wall. However, Zavras *et al.* (2005) say the position is 9:30 – 10:00 o'clock, corresponding to the Anteromedial bundle of the natural ACL, which Cain and Clancy (2002) agree with. Arnold *et al.* (2001) say the anatomical tunnel should be placed even lower than this – below 10 o'clock.

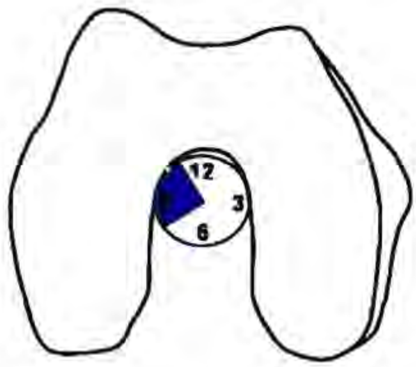

Figure 2.9 Range of values for anatomical placement of an ACL graft [Giron *et al.*, 2005].

The tibial anatomical placement is said to be 43% from the anterior edge of the medial tibial plateau [Musahl *et al.*, 2003].

2.2.7 Isometric versus Anatomic Tunnel Placement

Obviously the two theories of tunnel placement are incompatible with each other. Anatomical positioning for the tunnels does not result in an ACL which is isometric in its behaviour, just as the original ACL is not isometric in its behaviour [Musahl *et al.*, 2005; Zavras *et al.*, 2005]. In fact, some authors reject the concept of isometric placement outright, saying that a graft placement that achieves perfect isometry does not exist, even under ideal conditions [Klos *et al.*, 1998; Julliard *et al.*, 1998]. However, despite the physiological contradiction and other contrary evidence, some authors still think that isometry is desirable in a graft, and important to achieve [Giron *et al.*, 2005; Fleute *et al.*, 1999].

Various studies have been performed to decide which of the two placements is best. In a cadaveric study, Musahl *et al.* (2005) loaded knees in which the femur had been reconstructed either anatomically or isometrically. Their conclusion was that grafts placed anatomically resulted in knee kinematics closer to those of an intact knee than isometrically placed grafts did. Zavras *et al.* (2005) found that both isometric and anatomic femoral graft placements where best able to restore normal laxity in the knee, when compared to more anterior positions, but that the anatomic placement performed slightly better than the isometric placement. In a report on the general state of cruciate ligament reconstruction, Amis and Jakob (1998) say that placing the femoral graft in or near the normal ACL attachment is a more important criterion for successful reconstruction than placing the graft isometrically.

However, Aglietti *et al.* (1998) compared knees where the tibial tunnel was drilled either anatomically or not, and found no significant difference in range of motion or symptoms between the patients.

Despite the mixed results and lingering controversy, it seems the current trend is to move to a more anatomic graft placement. This makes sense in terms of modelling the reconstructed ACL on the normal ACL in order to restore normal knee function [Harner *et al.*, 1999; Amis and Jakob, 1998; Arnold *et al.*, 2001].

However, has the 'anatomical position' of the ACL been well defined? And can the same position be used for all patients? The next section explores where exactly a healthy ACL is placed, and how this information can be used to improve ACL reconstruction procedures.

2.2.8 Anatomic Insertions of the ACL

The ACL consists of two distinct bundles – the anteromedial (AM) and posterolateral (PL) bundles. These bundles behave differently during the range of knee motion [Giron *et al.*, 2005]. However, discussion of their functions is beyond the scope of this literature review. Instead, a comparison of how the literature presents the anatomical insertions of the ACL will be given, in order to determine if there is a generally agreed 'anatomic' point, and how much this differs between individuals.

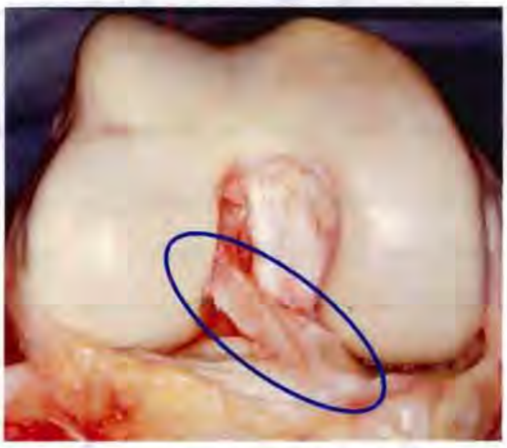

Figure 2.10 A dissected knee showing the insertions of the ACL on the femur and tibia [Giron *et al.*, 2000].

2.2.8.1 Femur

The femoral attachment of the ACL is in the shape of an egg, or a segment of a circle with the anterior side almost straight and the posterior side convex. The insertion is deep in the notch on the medial wall of the lateral femoral condyle [Yasuda *et al.*, 2004; Giron *et al.*, 2005; Arnold *et al.*, 2001; Girgis *et al.*, 1975]. The femoral attachment area is 113 ± 27 mm^2 according to Harner *et al.* (1999).

2.2.8.2 Tibia

The tibial attachment of the ACL is oval and larger in the anteroposterior (AP) direction (17 ± 2 mm average) than the mediolateral (ML) direction [Giron *et al.*, 2005]. The tibial attachment area is 136 ± 33 mm^2 according to Harner *et al.* (1999).

In the tibia, all measurements are made in a very similar way, making values easier to compare. It seems that different authors correspond well with one another, with an average tibial insertion point being at approximately 45% of the total AP width (from the anterior end).

What is most striking, however, is the *range* of values obtained. In normalised measures, there is intra-patient variation of over 10%, which indicates that the ACL position in different people is not as standardised as one supposes. Whether this variety of insertion sites between people should affect ACL reconstruction procedure is debatable.

Because of the large anatomical variation between different people, some authors have come to the conclusion that an individualised anatomical placement for each person would be best. Since the ACL is located near the rotational centre of the knee, small errors in placement can have large errors in kinematics [Musahl *et al.*, 2002*ii*]. These errors could be generated as a matter of course, if one standard placement was used for all subjects, regardless of individual anatomy.

Howell (1998) says "*there is not one ideal .. tunnel placement for all knees*". He recommends customising the tunnel placement to accommodate anatomic variability and says this will allow for more conservative surgical techniques as well as improving the function and stability of the reconstructed knee. This opinion is supported by Amis and Jakob's (1998) report on the second ESSKA scientific workshop concerning cruciate ligament reconstruction.

2.2.9 Arthroscopic Identification

Even assuming that one ideal ACL tunnel position could be defined for tibia and femur, it still remains very difficult for the surgeon to identify this position intra-operatively, and this explains the high level of variability and inaccuracy in ACL reconstructive surgery.

A main problem is that the remnants of the original ACL are often missing or difficult to identify, especially on the femur [Giron *et al.*, 2005; Arnold *et al.*, 2001]. Furthermore, Arnold *et al.* (2001) found that with a correctly drilled tibial tunnel, the guide-pin for the drill could not physically be placed within the original ACL footprint, making it impossible to drill the correct femoral tunnel.

The use of an arthroscopic procedure is another major factor in tunnel misplacement. Arthroscopic views could contribute to the inaccuracy of tunnel placement due to limited range of view, lens distortion, 2D views (i.e. no depth perception), a limited number of arthroscopically identifiable landmarks, no global placement and tensioning perspective etc. [Sati *et al.*, 2002; Picard *et al.*, 2001, Musahl *et al.*, 2002 *i*].

Figure 2.15 Examples of the surgeon's arthroscopic view during ACL reconstruction [Giron *et al.*, 2000].

Klos *et al.* (2000) also suggest that the use of mobile soft tissue landmarks as opposed to consistently identifiable landmarks also contributes to tunnel placement inaccuracy. Fleute *et al.* (1999) suggest that the use of free-hand drill guides, whose position is judged visually, is highly objective and therefore inaccurate.

Harner *et al.* (2001) say that 70% of ACL graft failures are due to technical error. The lack of technical accuracy in tunnel placement during ACL reconstruction points to the need for improved tunnel positioning methods, whereby a precise tunnel location can be achieved. CAOS is a proposed method for doing this, and the next sections will look at how CAOS can aid the surgeon and improve the surgery, and whether there is any proof to show that it does.

2.2.10 The Benefits of CAOS in ACL Reconstruction

The question to be answered when considering the use of CAOS in ACL reconstruction is whether, considering the reasons for tunnel misplacement in current techniques, computer assisted techniques can overcome these problems and ultimately improve the surgical outcomes.

As seen previously, apart from the variety of preferred tunnel placements, the primary problem in ACL surgery is a lack of visual information to verify tunnel placement and orientation. The use of an image-based computer assisted system would overcome this problem by providing the surgeon both with pre-operative images, which could be used for planning, as well as these images used as navigation devices during the surgery to provide feedback on tool and bony anatomy position [Burkart *et al.*, 2001].

In their discussion of an x-ray based computerised ACL graft placement system, Sati *et al.* (2002) say "*this concept has tremendous potential to provide the surgeon with accurate and valuable information regarding bone geometry*". Picard *et al.* (2001), in their comparison between conventional and computer assisted tunnel placement, note that the computer assisted system provided superior navigation to the conventional techniques and that, in fact, this could not even be exploited fully due to the limitations of conventional instruments.

Other authors support these opinions, saying that computer assisted navigation provides detailed topographical information of the entire knee joint, where in the conventional technique the operative field is restrictive. They find that there are consistently identifiable radiographic features on the femur and tibia that can be used for computer assisted ACL graft placement [Müller-Alsbach and Stäubli, 2004; Fu and Musahl, 2001; Musahl *et al.*, 2003; Klos *et al.*, 1998 and 2000; Julliard *et al.*, 1998; Moody *et al.*, 2002].

Clearly, therefore, CAOS has the ability to improve intra-operative visibility, and thus the accuracy with which tunnels are drilled during ACL reconstruction surgery.

However, this is not the only advantage of using a computer assisted system. Other advantages stem largely from the fact that it is possible to create a virtual graft and examine its placement, whether notch impingement occurs, and what the isometry profile is, before drilling any tunnels. This simulated graft means the behaviour of the graft can be predicted and visualised in any given position, and then adjusted until the required behaviour (e.g. no notch impingement, optimal isometry profile etc.) is achieved. Only then need any holes be drilled [Julliard *et al.*, 1998; Burkart *et al.*, 2001; Müller-Alsbach and Stäubli, 2004].

Julliard *et al.* (1998) state that "*even for an experienced surgeon, obtaining isometric and physiologic behavior of the graft while preventing notch impingement for each case is a difficult task when using a standard technique.*"

One of the major benefits of CAOS is that the superior pre-operative planning, as well as the added navigational information during surgery, allows even inexperienced surgeons to achieve high levels of accuracy in tunnel placement [Schep *et al.*, 2005; Degenhart, 2004; Burkart *et al.*, 2001].

Another benefit of this pre-operative planning (with image based systems) is that it allows consideration of patient-specific anatomy, and thus the development of a surgical plan which is tailored to each individual patient. This has the inherent benefits of reconstructing, as far as possible, the original anatomy of the patient, as opposed to that of a generic anatomical model [Musahl *et al.*, 2003].

Thus it has been shown that CAOS clearly has the qualities necessary to improve current ACL reconstruction techniques.

2.2.11 Results of using CAOS for ACL Reconstruction

The only question left to answer is whether it has, in fact, been shown, that the application of CAOS to ACL reconstruction has yielded any improved outcomes, and whether it has any disadvantages.

When evaluating improved accuracy, tunnel placement will be the only criterion considered, as it has the most impact on graft success, and is the most objectively measurable factor.

However, due to the great variation in preferred tunnel placement between surgeons, it is difficult to compare results to one specific 'ideal' tunnel site. Instead, most studies compare the accuracy with which the originally planned 'perfect tunnel position' was achieved, even though these specific positions may differ between surgeons.

Klos *et al.* (1998) studied the effect of adding computer graphic overlays to the arthroscopic view. The resulting improvements in accuracy were a decrease in standard deviation of 6% to 3% for the tibial tunnel, and 9% to 3% for the femoral tunnel, which is a significant improvement. Good results were also achieved by Picard *et al.* (2001) using an image-based CAOS system. Surgical error in tunnel placement was reduced from 4.6 ± 2.12 mm for the conventional technique to 3.1 ± 2.14 mm for the computer assisted technique (using the same two surgeons each time) – this was a statistically significant improvement.

Using a non-image based system, Sati *et al.* (2002) report accuracy to be in the order of 1 mm. Also in a non-image based system, Schep *et al.* (2005) allowed three surgeons of varying experience to perform ACL reconstructions using both a passive CAS system, and conventionally. They report the difference in tunnel positions planned and drilled with a computer assisted system, and those drilled conventionally was 6.2 ± 2.49 mm for the femur and 6.46 ± 2.27 mm for the tibia. They found that CAS reduces the inter-surgeon variance in tunnel placement and reduces the effect of experience i.e. reduces the number of misplaced tunnels by surgeons with limited experience.

Musahl *et al.* (2005) used an active robotic system in a study on ACL placement. CAOS was not the focus of the study, but they report that it allowed a high precision and accuracy of tunnel placement, and decreased inter- and intra- specimen variability in tunnel placement. In an earlier study, Musahl *et al.* (2003) also say that CAS has benefits as a research tool and to increase precision in surgery.

Although the available literature is limited, these results show a clear improvement in tunnel position accuracy when using a computer assisted technique, compared to a conventional technique.

2.2.12 Conclusion

It can be seen from the above information that there is a lack of accuracy in tunnel placement during ACL surgery, and that this contributes to a high percentage of graft failures and unsuccessful surgical outcomes. Moreover, it has been shown that computer assisted surgery provides the tools necessary to improve pre-operative planning and intra-operative visualisation, and thus the accuracy with which tunnels can be positioned. In addition to this, preliminary studies show that various different systems do, indeed, result in an increase in accuracy and repeatability of tunnel placement, for a relatively insignificant increase in operating time.

Despite all this positive information, it is important to remember that there are a variety of opinions as to the optimal tunnel location to achieve the best outcome. Therefore, although computer assisted ACL surgery may be able to achieve highly accurate tunnel positions, this does not necessarily indicate that improved clinical outcomes can be expected [Musahl *et al.*, 2002 *i*].

3 OVERVIEW OF INVESTIGATIVE PROCESS

This chapter gives an overview of the investigative process used in this thesis.

3.1 Assessing the Feasibility of Adapting the IGS Neurosurgery System for use in Orthopaedics

The first investigation which was undertaken was that of determining whether the image guided neurosurgery system could be adapted for use in ACL reconstruction surgery, and whether this was feasible. The three main issues addressed were:

- Can MR imaging be used to provide the navigation information in surgery and, if so, what is the best protocol to use?
- Can anatomical landmarks be used for registration and, if so, which landmarks give the best accuracy?
- How can the movement of the bones during surgery, and relative to each other, be addressed?

These questions were answered during a series of experiments, briefly introduced below and discussed in the following chapters. Detailed results of the experiments can be found in Appendix B.

3.1.1 Dry Bone Experiments

During these experiments dry human bones were used to ascertain the accuracy of registration using anatomical landmarks. Later tests with the dry bones were also used to determine whether the two bones could be registered separately. The availability and ease of use of the dry bones meant they were useful in forming a first idea of whether the registration procedures would be accurate or not.

Figure 3.1 The dry bones used in the registration tests.

3.1.2 Plastinated Specimen Experiments

These tests used a plastinated specimen of an intact human knee joint (with skin removed). This specimen provided better magnetic resonance imaging (MRI) quality, and the bone was a better approximation to how the knee would look in surgery. The plastinated specimen was used to determine which anatomical landmarks provided the best registration results, and which landmarks allowed separate registration of the tibia and femur. The plastinated specimen allowed confirmation and extension of the results obtained in the dry bone tests, owing to the greater accuracy and more realistic set-up it provided.

Figure 3.2 The plastinated specimen used in the registration tests.

3.1.3 Arthroscopic Testing

Having obtained preliminary results from the dry bones and plastinated specimen, an arthroscopic procedure was carried out on a cadaver knee to test the modified IGS procedure in an environment approximating that of the operating theatre. The accuracy of the registration procedure, as well as its ease of use, practicality and usefulness were tested.

Figure 3.3 The cadaver leg used in the arthroscopic testing.

3.2 Creating and Analysing 3D Models of the Knee

The second investigation that took place was that of determining the anatomic relationships between healthy ACLs and reconstructed ACLs. This investigation relied on MR imaging and computer graphic simulation, as well as final statistical analysis of measurement results.

The investigation took place in two parts. The first was a 'trial and error' investigation of the best MRI protocols, Mimics procedure and measurement format to use. This took place at the Mechanical Engineering Department of University College Dublin, Ireland, under the supervision of Dr David Fitzpatrick. The Biomedical division of this department has much experience in using Mimics to create and analyse 3D images, and was thus the ideal place to investigate the best methods for the tests in this thesis.

The second part of the investigation was the implementation of the final methods, and the statistical analysis and interpretation of this data. This took place at the University of Cape Town, South Africa, in consultation with Dr Willem van der Merwe, who provided insight on the ACL reconstruction procedure and analysis of the associated results.

3.2.1 Magnetic Resonance Imaging

Bilateral (i.e. left and right) MRI scans of healthy people and patients who had undergone ACL reconstruction surgery were taken on an Esaote E-Scan 0.18 Tesla scanner. Various different protocols were experimented with until one best suited for creating 3D models was found.

Figure 3.4 The Esaote 0.18 Tesla scanner used in the experiments.

3.2.2 Creation of 3D Models using Mimics

Once the scans were obtained, they were imported into the Mimics software. They were then segmented and manipulated to produce 3D models of the patient's knee, including femur, tibia and ACL (or autograft). A process of trial and error regarding the various 3D reconstruction options was undertaken in order to master the process of creating 3D models.

3.2.3 Measurement of ACL and Tunnel Positions

Once the 3D models were created, they were imported into the Arthron software program. This was used to create a set of consistent reference axes on each knee so they could be compared to each other. Reference axes with clinical significance were set up on both the tibia and femur so that separate and meaningful measurements could be made on each bone.

A procedure of measuring the 3D positions of the ACL insertions, or tunnel positions, was then decided on and these positions were obtained for each patient, for both tibia and femur. Normalising measurements were also taken, so that the positions could be compared across all patients, regardless of bone size.

3.2.4 Statistical Analysis

The final, normalised measurements of each patient were then imported into a statistical analysis package, Statistica. A 2-way ANOVA (Analysis of Variance) was then performed on the data, followed by Tukey HSD post-hoc tests. Questions regarding the bi-lateral symmetry of the ACL in healthy people and the difference in position between the un-injured and reconstructed ACL in patients were answered for x, y and z directions.

4 ADAPTATION OF THE NEUROSURGERY SYSTEM FOR ORTHOPAEDIC SURGERY

This chapter describes how the feasibility of adapting the image guided neurosurgery system to orthopaedic surgery was tested.

4.1 Discussion of the Problem

4.1.1 Reason for Developing Another CAOS system for ACL Reconstruction

The main aim of an image guided system in ACL reconstruction is to provide the surgeon (who has a limited arthroscopic view) with information on where to drill the tibial and femoral tunnels. As discussed in Chapter 2, the accurate placement of these tunnels is critical to the success of the surgery. However, the accuracy of this placement in current techniques is questionable. Computer Assisted Orthopaedic Surgery (CAOS) systems for ACL reconstruction have been developed to meet this need. However, these systems are extremely expensive and fairly complicated to use. For these reasons, and others, they are not making their way into the operating rooms of orthopaedic surgeons.

The image guided neurosurgery system was designed to meet the dual needs of providing navigation during surgery, and doing so at a reasonable cost – specifically one that made the system affordable to hospitals in developing countries.

The purpose, therefore, in adapting the system for use in orthopaedic surgery, was to develop an accurate and useful system that is more readily available to surgeons than existing navigated ACL reconstruction systems. This means that it is simple to use, and is not invasive to the normal operating theatre environment, whilst at the same time being affordable. For this reason, an orthopaedic surgeon specialising in ACL reconstruction surgery, Dr Willem van der Merwe, was consulted, specifically for his input on what type of system an orthopaedic surgeon would use – including all that is necessary to assist with the surgery, whilst at the same time not over-complicating the surgery by adding unnecessary information.

Figure 4.1 The crowded surgical environment of ACL reconstruction surgery.

It is important to realise that the main purpose of an image guided system for ACL reconstruction is to allow the surgeon to navigate to the best positions to place the tibial and femoral tunnels, since this is the most critical step in the surgery. Once these positions are known, the navigation system is essentially no longer required. Current CAOS systems for ACL reconstruction provide navigation throughout the surgery, at the expense of the patient, since trackable frames are drilled into the tibia and femur to allow this. Therefore another goal of developing this new system was to provide navigation without this added invasiveness.

4.1.2 Problems of Adapting the IG Neurosurgery System for ACL Reconstruction

As discussed in Chapter 1, there are several significant differences between how the image guided procedure works in neurosurgery, and how it must be applied to orthopaedic surgery, specifically ACL reconstruction.

The first of these problems is the fact that MRI is used clinically as a pre-operative examination in ACL reconstruction patients. It therefore makes sense that this scanning technology should also be used to provide the navigational images in the image guided surgery system. However, CT scans are used in the neurosurgery system. It is generally accepted that CT scanning provides clearer images, so the feasibility of using MRI, with its reduced image quality, was ascertained as the various experiments were being carried out.

The second major problem that was addressed is the fact that surface fiducials cannot be used in knee surgery, due to the relatively loose skin around the knee. Movement of this skin, and thus the fiducials, would create an erroneous registration and a highly inaccurate navigation system. The proposed solution to this problem was to use bony landmarks which can be identified arthroscopically. It is important that these landmarks are easily and consistently identifiable and that they can be reached in the limited arthroscopic environment. It is similarly important that they can be consistently identified on the MRI scans. It is also vital that the number and combination of landmarks chosen provides enough 3D orientation information so that the navigation system can accurately register the theatre space with the image space.

The third major problem in adapting the system is that the tibia and femur move relative to one another, whereas the skull is a single object. Similarly, the knee is constantly being manipulated during surgery, whereas the skull is clamped in one position. If registration is to be maintained throughout surgery the bones must be tracked somehow. In current systems this is done by drilling trackable reference frames into the tibia and femur. However, if this added invasiveness is to be avoided in what is an otherwise minimally invasive procedure, another approach must be taken. Some simplifying assumptions must be made that the knee can be held still for some portion of the surgery, and/or that navigational information is not required throughout the surgery. These assumptions cannot be at the expense of either the quality of surgery (i.e. the surgeon's normal practice in theatre) or the level of navigational information supplied.

A series of experiments was undertaken to further examine these problems, as outlined in Chapter 3. The details of the imaging, registration and accuracy testing procedures used in these experiments are discussed below.

4.2 Landmark Registration Tests

The first 'phantom' used in the experiments was a dry bone phantom. This consisted of a dry human tibia and femur, strapped together on a board to resemble an articulated knee in extension.

The second 'phantom' used was a plastinated specimen. This was an articulated knee, complete with ligaments, muscles and tendons. The skin and patella were removed from the knee. Although stiff, the knee could be manipulated slightly.

Final testing of the system was done on a cadaver knee. The specimen was the leg of a fresh frozen cadaver which had been defrosted overnight at room temperature.

4.2.1 Magnetic Resonance Imaging of the Dry Bones

The first step in using the dry bones was to obtain MR images of them. However, MRI works by exciting hydrogen atoms, mainly present in water. The dry bones contained very few hydrogen atoms, and thus the first images of them were poor, as shown in Figure 4.2 below.

Sagittal Gradient Echo STIR
24 images, 2 mm thick slices
TR = 2320 ms, TE = 25 ms

Figure 4.2 Gradient Echo STIR sequence of the dry bones.

In an attempt to make the dry bones more visible to the MRI scanner, various methods were proposed e.g. painting the bones, coating them in varnish etc. Eventually it was decided that soaking the bones in a salt solution pricr to imaging would result in the absorption of some water around the outside of the bones, which would improve their MR images. The first scans taken of the bones used a Sagittal T1-weighted sequence as shown in Figure 4.3 below.

Sagittal Spin Echo T1
21 images, 2 mm thick slices
TR = 1100 ms, TE = 26 ms

Figure 4.3 Spin Echo, T1 weighted sequence of the soaked dry bones

These images were reasonable, but not excellent. Further images were taken using Turbo Multi Echo and High resolution Gradient Echo T1 sequences. The best protocol for the soaked dry bones was decided as a transverse T2 weighted sequence as shown in Figure 4.4 below.

Transverse Turbo Multi Echo
54 images, 3 mm thick slices
TR = 4380 ms, TE = 90 ms

Figure 4.4 Turbo Multi Echo T2 weighted sequence of the soaked dry bones.

All the images were taken using the standard knee coil.

4.2.2 Magnetic Resonance Imaging of the Plastinated Specimen

The imaging of the plastinated specimen was easier, as it had more hydrogen in it, and therefore provided better images. After some experimentation is was decided that the same sequence as that used for the dry bones would be used. This created good images, as shown below, and allowed for consistency between the different experiments.

Transverse Turbo Multi Echo
54 images, 3 mm thick slices
TR = 4380 ms, TE = 90 ms

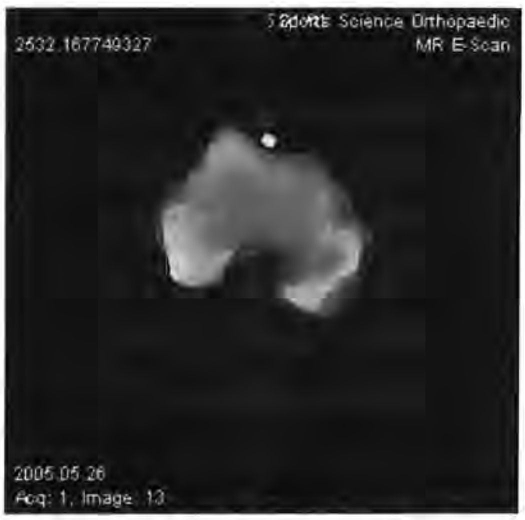

Figure 4.5 Turbo Multi Echo T2 weighted sequence of the plastinated specimen.

For final plastinated specimen testing, an MRI sequence that is used clinically was chosen, in order to test the navigation system using images that would be routinely available. This was a T1 weighted sequence, as shown in Figure 4.6 below.

Transverse High Resolution Gradient Echo T1
36 images, 3 mm slices
TR = 1260 ms, TE = 16 ms

Figure 4.6 T1 weighted sequence of the plastinated bones, as used in the clinical setting.

Again, both these protocols were performed using the standard knee coil.

4.2.3 Magnetic Resonance Imaging of the Cadaver

Obtaining good MR images of the cadaver should have been similar to the normal imaging of patient's knees. However, due to the size of the cadaver leg, a larger coil (hip coil) had to be used, and even so, the leg was tightly fitted into this coil.

The same T1 weighted sequence used for the final plastinated specimen testing was chosen for the imaging of the cadaver knee, and fairly good images were obtained as shown in Figure 4.7 below.

Transverse High Resolution Gradient Echo T1
36 images, 3 mm slices
TR = 1260 ms, TE = 16 ms

Figure 4.7 T1 weighted sequence of the cadaver, as used in the clinical setting.

4.2.4 Fiducial Markers for Accuracy Testing

In order to test the accuracy of a registration process, a ground truth was needed. In other words, markers of known positions were placed on the specimens before scanning. Once registration had taken place, these markers were pointed to in turn on the specimen using the tracked probe. The position of the probe according to the navigation system appears on the MRI scans on screen, and was compared to the actual position of the marker on those scans. The difference between the two positions provided a measurement of the error in the system and the quality of the registration process.

The navigation system provided a way of measuring this difference. The probe's position appears on screen on the MRI scan. The mouse cursor can also be moved onto these scans. The program provides an error measurement in two dimensions (dx and dy) indicating the distance between the probe's position and the mouse cursor's position on a particular slice of the scans, as shown in Figure 4.8 below. A dy and dz error measurement was provided on a second section of the screen. However, it proved difficult to utilise both these screens at once. Thus, only dx and dy error measurements were taken. It was assumed that if the marker was visible on the 2D (dx and dy) image, then the dz error was negligible, as the system had chosen the correct 'depth' (z distance) of scan. This is a fairly reasonable assumption since if there was error in the z direction, the marker would not be visible on the 2D (dx, dy) image at all. Thus, a visible marker on the 2D image indicates at least a reasonable dz error.

Figure 4.8 The x and y error between the tracked probe (blue circle) and the mouse cursor (white arrow).

As Figure 4.8 shows, if the probe is pointing to the accuracy marker on the specimen, and the mouse cursor is pointing to the same marker's position on the MRI scan, the difference between the two positions is the error in the navigational information supplied by the system.

The markers used in these experiments were small, fat-filled (vitamin E) capsules. These were ellipsoidal in shape, 7 mm in length and 5 mm in diameter. They were chosen for their relatively small size, and because fat images brightly on MRI scans, making them easy to identify as accuracy points. The marker and its appearance on an MRI scan are shown in Figure 4.9 on the next page.

Figure 4.9 MR image showing an accuracy marker, and an image of a vitamin E capsule used for accuracy measurement (inset).

4.2.4.1 Accuracy Benchmark

The aim of performing the accuracy tests was to determine whether the navigation system in ACL reconstruction achieves an accuracy which indicates the feasibility of the system for further development. Thus, the extent of this feasible accuracy range must be discussed.

The image guided neurosurgery system attained a quoted accuracy of 1.6 mm during a theatre trial using a head phantom [Watson, 2004]. Since the orthopaedic system is being developed from the neurosurgery system, it would seem that this figure represents the best accuracy that can be attained.

The accuracies of other image guided ACL reconstruction systems are difficult to find from generally available information.

The required accuracy of the system was discussed with the orthopaedic surgeon, Dr van der Merwe. He suggested that accuracies below 5 mm would be acceptable in terms of providing the surgeon with an idea of where he is placing the tunnel. This high figure is appropriate because the problem with most tunnel placement is not minor errors, but huge discrepancies in where tunnels are placed, due to a lack of orientation information in the arthroscopic procedure.

With these two figures in mind (1.6 mm best accuracy and 5 mm worst accuracy), it was decided that accuracies below 5 mm would indicate the feasibility of developing the system further, whilst accuracies of about 2 mm would indicate that a fairly high precision had been attained.

4.2.5 Registration Procedure

The procedure of registration followed is similar to that used for the neurosurgery system. Firstly the cameras are connected to a laptop via an Ethernet link. This laptop contains the navigational software packages.

The first step is to place digital markers on the MRI scans using the MRIPoint software. This involves locating the slice and position of the landmark to be used for registration. A digital marker is then placed in this position by clicking the mouse as shown in Figure 4.10 below. Once all the markers have been chosen a file is compiled storing their position information. This file is then used during navigation.

Figure 4.10 Screen from the MRIPoint software showing a digital marker.

Calibration of the 'theatre space' can now take place. This involves holding the reference frame above the area of interest (i.e. the space where navigation will take place – the knee joint). When the cameras can see all twelve reflective markers on the frame, the space is calibrated and given a Calibration Error, indicating how well the navigational space has been defined.

Registration can now begin. The navigational software prompts the user to point to each landmark in turn using the tracked pointer. An image from the navigation software is shown in Figure 4.11 on the next page.

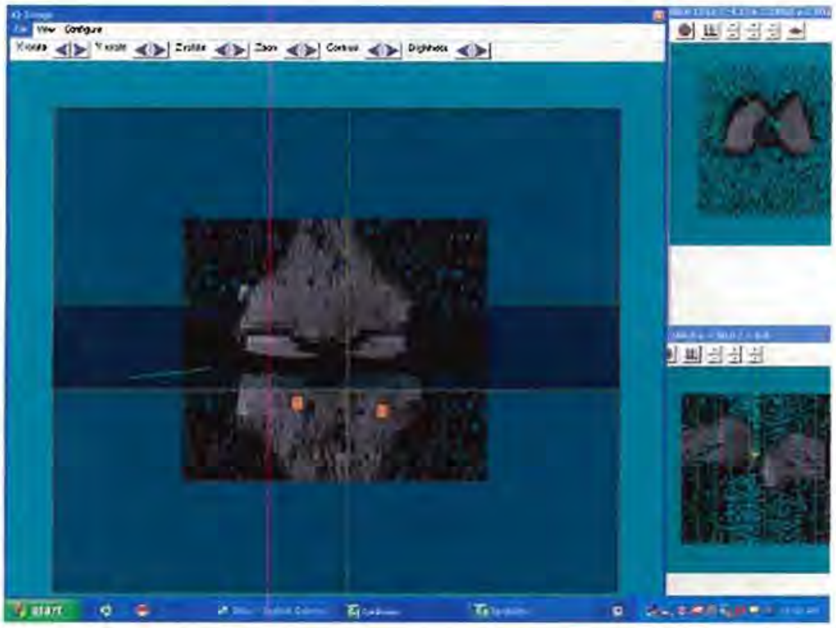

Figure 4.11 Screen shot of the navigation display.

This figure shows the display of the navigation software. The left hand image is a reconstruction of the MRI scans. The orange squares are the landmarks which must be pointed to for registration. The area on the right shows 2D views of the bones. The pointer is shown as a green circle with a green line showing its trajectory.

During registration and navigation, the three reflective markers of the pointer must point upright and towards the camera, so that the pointer's orientation in space can be ascertained. The required orientation of the pointer is shown in Figure 4.12 below. Once each marker has been pointed to, a relationship between the MRI scans and the theatre space can be made, and is given a Registration Error, based on how well the system identified the probe at each registration point.

Figure 4.12 The orientation in which the pointer must be in order for the cameras to identify it.

Navigation can now begin in either a discrete or continuous manner. As long as the cameras can see the probe in an upright position, its orientation is indicated on the MRI scans.

4.3 Aims of the Feasibility Tests

Experiments were performed to ascertain the feasibility of adapting the neurosurgery system for the orthopaedic environment. The questions to be answered by these experiments are:

- Can bony anatomical landmarks be used for registration?
- Which landmarks – number and combination – provide the best registration?
- How can the movement of the bones in surgery be dealt with whilst still providing the necessary navigational information to the surgeon, and avoiding the invasive drilling of frames into the bones?
- Is the system practical for use in surgery?

The dry bone, plastinated specimen and cadaver tests are discussed in detail in the following chapters.

5 DRY BONE REGISTRATION TESTS

Two tests were performed with the dry bones to ascertain the accuracy of using landmarks to register the tibia and femur to the MRI scans. The first test registered the two bones together, and the second registered them separately.

5.1 Initial Dry Bone Registration Test

The initial test of the use of landmarks for registration was performed using the dry bones. The main aim of this first experiment was to test the accuracy of using bony landmarks for registration. Tests were also performed to determine what effect (if any) the orientation of the bones to the cameras had.

5.1.1 Specimen Set-up

The first approach to dealing with movement of the bones was to treat the bones as one single object i.e. tibia and femur are grouped as a single entity, and registered together as one object. During registration they are held still with respect to each other and maintained in this position whilst all necessary navigation information is obtained. This simplifies the problem of bone movement, making the assumption that the bones will neither move with respect to one another, nor at all, during the navigational part of the surgery. To achieve this the bones were firmly strapped together on a board using Velcro, in an extension position. Eleven accuracy markers (fat capsules) were then attached to the bones using super glue, as shown in Figure 5.1 below.

Figure 5.1 The dry bones with eleven accuracy markers (A – K) attached.

Transverse scans of the bones were then taken using the MRI protocol described in Chapter 4.

Figure 5.2 The dry bones being scanned in the MRI machine.

Following Dr van der Merwe's advice, five bony landmarks were chosen for use in registration. These were:

1. The highest point of the articular surface of the femur, on the lateral side.
2. The highest point of the articular surface of the femur, on the medial side.
3. The highest point in the femoral notch.
4. The lateral tibial spine.
5. The medial tibial spine.

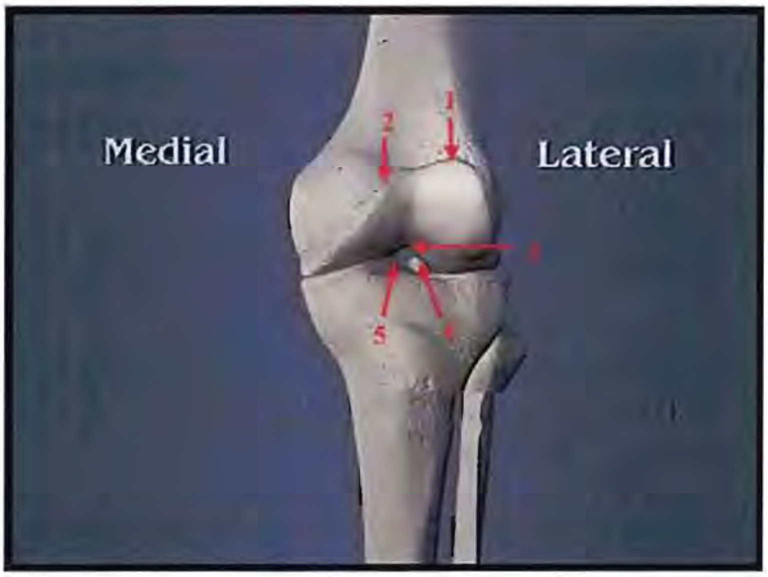

Figure 5.3 The bony landmarks to be used in registration [Smith & Nephew, 1998].

The MRI scans were imported into the MRIPoint software. Here, digital markers were placed on each of the five landmarks by the author, following the surgeon's advice on how to locate them on the scans.

5.1.2 Registration and Accuracy Testing

The bones were then placed longitudinal to the cameras as shown in Figure 5.4 below.

Figure 5.4 The navigation set up showing the bones longitudinal to the cameras.

The five landmarks were registered using the process described in Section 4.2.5. Once registration was complete each accuracy marker was pointed to in turn using the probe to determine the accuracy of the registration. The registration and accuracy measurement procedure was repeated to give a total of three tests.

The same procedure was followed with the bones aligned transversely to the cameras, as shown in Figure 5.5 below.

Figure 5.5 Navigation set up showing the bones transverse to the cameras.

5.1.3 Results

For each orientation, the results were averaged over each of the the three tests and over all the accuracy markers. The final averages were taken over the x and y measurements. The results are given in Tables 5.1 and 5.2 on the next page.

Table 5.1 Results of the registration tests with the bones aligned longitudinally to the cameras.

	Average Error [mm]	Maximum Error [mm]	Minimum Error [mm]
dx	6.1	84.8	0.2
dy	3.4	28.5	0.4
Overall	**4.8**	**84.8**	**0.2**

Table 5.2 Results of the registration tests with the bones aligned transversely to the cameras.

	Average Error [mm]	Maximum Error [mm]	Minimum Error [mm]
dx	4.2	16.9	0.3
dy	3.6	13.0	0.2
Overall	**3.9**	**16.9**	**0.2**

The average error over x and y, and over both orientations, is 4.3 mm. Placing the bones transversely to the cameras, rather than longitudinally, results in a lower average error, and lower outliers.

5.1.4 Discussion of Results

An average error of approximately 4 mm is a reasonable result, but could be improved. There are various reasons which could explain why this error is high, regardless of how well registration was performed.

Firstly, although the bones were well secured to the board, some shifting between bones may have occurred during the transport between the MRI scanner and the navigation software. This immediately introduced simple displacement errors, which would decrease the overall accuracy of the registration procedure, without indicating the precision with which registration itself was performed.

Secondly, some of the markers came loose during transport between the scanner and the navigation setup. Although their positions had been marked directly onto the bones, it was still difficult to account for their 3D volume when attempting accuracy tests. Add to this the relatively large size of the marker, any part of which could be pointed to, and further error was added to the process.

The landmarks were digitally marked on the MRI scans by the author. Although the orthopaedic surgeon had advised on the process, a lack of experience with MRIs and specific anatomic identification on them, could have led to some slightly erroneous positions being marked as landmarks. Additionally the slices taken were 3 mm thick, this means that if the landmarks were identified one slice too late or early, an error of 3 mm is instantly introduced.

A further contributor to registration error was the registration of the highest point in the femoral notch (Landmark 3 on p 48) and the two tibial spines (Landmarks 4 and 5). Although these were easy to locate, the extension orientation of the bones made it difficult to point to these landmarks whilst keeping the pointer upright and facing the cameras. Some mis-registration of these points would have contributed to an overall decrease in accuracy.

Thus it can be seen that although the overall error seems quite high, there are some simple experimental errors which have contributed to this. Considering that, the results of this experiment are encouraging for the use of bony landmarks as registration points.

5.2 Dry Bone Separate Registration Test

At this point in the tests it was decided that the assumption of treating the bones as a single entity in order to overcome relative movement problems would not be practical in surgery. Thus, a new approach was taken where the tibia and femur would be registered separately from one another, in the most appropriate position to mark tunnel positions for each bone. In surgery, the bone would then be held still whilst the surgeon uses the navigation system to locate the best tunnel orientation. Once the tunnel is marked/drilled (with the bone held still), the bone can be manipulated. However, navigation will be lost from this point onwards. If further orientation information is required, the bone must be re-registered.

This solution was discussed with Dr van der Merwe and decided as a viable approach to solving the problem of moving bones. It allows the surgeon to obtain all the navigational information he needs to improve the ACL reconstruction procedure (i.e. to place tunnel positions accurately), but does not disturb his routine surgical practice, or put the patient at extra risk by drilling trackable frames into the bones.

In order to check the initial practicality of this assumption, the dry bones were used for testing. The aim of the experiment was to determine whether the tibia and femur could be registered separately, using three landmarks on each bone.

5.2.1 Specimen Set-up

The original transverse scans of the dry bones were used for this experiment. Thus, the same eleven accuracy markers were used to determine the quality of registration (see Section 5.1).

Dr van der Merwe was consulted as to which three landmarks could be used on each bone, and his suggestions were followed.

The landmarks used on the femur are:

1. The highest point on the articular cartilage, laterally.
2. The highest point on the articular cartilage, medially.
3. The highest point in the femoral notch.

The landmarks used on the tibia are:

1. The lateral tibial spine.
2. The medial tibial spine.
3. 'Skin' marker I on the anterior surface of the tibia, slightly distal to the tibial tubercle.

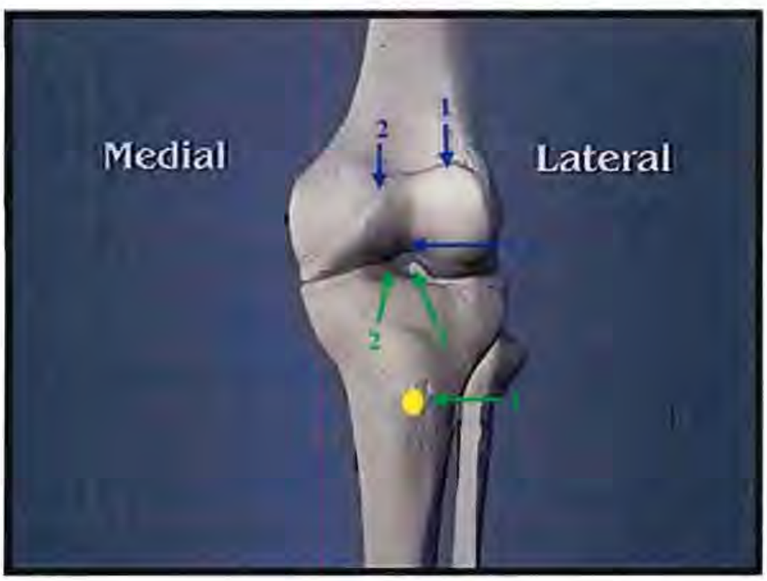

Figure 5.6 The femoral (blue) and tibial (green) landmarks to be used for registration. Tibial 'landmark' I is an accuracy marker [Smith & Nephew, 1998].

Marker I was used to represent a potential third landmark on the tibia. This test was to verify the initial assumption that three landmarks on each bone could be used for registration.

5.2.2 Registration and Accuracy Testing

After scanning, registration was performed on the femur using the three femoral landmarks. The accuracy markers on the femur (A, B, C, D, E, F) were pointed to in turn in order to determine the quality of registration. This was repeated three times.

Registration was then performed on the tibia using the three tibial landmarks. The accuracy markers on the tibia (G, H, J, K) were then pointed to in turn in order to determine the quality of registration. This was repeated three times.

5.2.3 Results

For each bone, the results were averaged over all the applicable accuracy markers, and over all three tests. They are given in tables 5.3 and 5.4 below.

Table 5.3 Registration errors for landmark registration of the femur using three landmarks.

	Average Error [mm]	Maximum Error [mm]	Minimum Error [mm]
dx	1.8	6.7	0.0
dy	1.9	4.5	0.1
Overall	**1.9**	**6.7**	**0.0**

Table 5.4 Registration errors for landmark registration of the tibia using two landmarks and a skin marker.

	Average Error [mm]	Maximum Error [mm]	Minimum Error [mm]
dx	3.7	16.7	0.3
dy	6.4	29.2	1.3
Overall	**5.1**	**29.2**	**0.3**

As can be seen, the femur achieves a lower average error than the tibia.

5.2.4 Discussion of Results

These results show excellent accuracies for the femoral registration. However, the value for the tibia is very inaccurate. This is probably due to the difficulty registering the tibial spines, especially with the tibia lying flat as it was in this experiment. However, if this accuracy can be improved, then it would seem feasible to register each bone separately, if a third tibial landmark can be found.

6 PLASTINATED SPECIMEN REGISTRATION TESTS

Following the fairly good results of the dry bone tests, it was decided to repeat the experiments using a plastinated specimen. Since this knee was articulated, it would reduce some of the errors related to relative movement between the two dry bones. It was also hoped that the better quality MR images would improve the accuracy of the registration. An additional benefit of using the plastinated specimen is that it has ligaments and muscles which create a more realistic environment in which the accessibility of the bony landmarks can be tested.

Three tests were performed. The first was to test which combination of landmarks was best to register the tibia and femur together. Two further tests were performed to determine which landmarks would be best for separate registration of the the tibia and femur.

6.1 Initial Plastinated Specimen Registration Test

The main aim of this experiment was to determine how accurate landmark registration could be with this improved specimen in comparison to the dry bones. Added to this, various different combinations of landmarks were tested to determine how many were needed to give good registration accuracy.

6.1.1 Specimen Set-up

As in the first dry bone experiment, it was assumed that the two bones would be treated as a single entity. Thus the specimen was strapped securely to a board in extension, to prevent any movement between the bones. Seven accuracy markers were attached to the specimen using tape, and their positions were marked on the tape for use in accuracy testing, as shown in Figure 6.1 below.

Figure 6.1 The seven accuracy markers (A – G) taped to the plastinated specimen.

The specimen was then MRI scanned as discussed in Chapter 4. The landmarks used in the registration tests were:

1. The highest point of the articular surface of the femur, laterally.
2. The highest point of the articular surface of the femur, medially.
3. The highest point in the femoral notch.
4. The lateral tibial spine.
5. The medial tibial spine.

G. 'Skin' marker G on the lateral surface of the tibia.

F. 'Skin' marker F on the medial surface of the tibia.

Figure 6.2 The landmarks (1- 5) and accuracy markers (G, F) used for registration [Smith & Nephew, 1998].

The landmarks G and F were accuracy markers used to represent skin markers, to determine whether these extra points might improve registration of the tibial portion of the specimen.

The registration landmarks were marked on the MRI scans using MRIPoint, in various combinations.

6.1.2 Registration and Accuracy Testing

Different combinations of landmarks were used for the registration tests, to determine which would give the best results. The combinations were:

1. Five bony landmarks: 1, 2, 3, 4, 5
2. Three bony landmarks: 1, 2, 3
3. Three bony and two skin landmarks: 1, 2, 3, G, F

Each combination was chosen to test a specific premise:

1. To repeat the experiment performed on the dry bones in order to ascertain what quantity of error was due to the movement of the bones and other errors discussed in Section 5.1.
2. To test registration of the knee using only femoral landmarks (i.e. do these provide enough spatial information for registration?)
3. To test registration using both femoral and tibial landmarks, but eliminating the tibial spines, which prove difficult to register.

The registration procedure was performed for each combination of landmarks. Each accuracy marker was pointed to in turn using the trackable probe, and compared to the position on the MRI scans. In the third case, markers G and F were not used as accuracy markers, since they were used as registration landmarks.

This process was completed four times for the first two landmark combinations (1 and 2), and twice for the final combination (3).

6.1.3 Results

For each combination, the results were averaged over all of the accuracy markers, and over all the tests, giving the following averaged results.

Table 6.1 Registration errors using five bony landmarks (1 – 5).

	Average Error [mm]	Maximum Error [mm]	Minumum Error [mm]
dx	2.2	5.9	0.1
dy	3.5	11.4	0.2
Overall	**2.9**	**11.4**	**0.1**

Table 6.2 Registration errors using three femoral bony landmarks (1 – 3).

	Average Error [mm]	Maximum Error [mm]	Minumum Error [mm]
dx	2.6	12.1	0.1
dy	2.2	11.1	0.1
Overall	**2.4**	**12.1**	**0.1**

Table 6.3 Registration errors using three bony (1 – 3) and two skin (G, F) markers.

	Average Error [mm]	Maximum Error [mm]	Minumum Error [mm]
dx	2.6	6.5	0.1
dy	2.1	3.9	0.3
Overall	**2.3**	**6.5**	**0.1**

The average error over all the tests is 2.5 mm, with the best results being shown by the last test – registration with bony landmarks and skin markers.

6.1.4 Discussion of Results

This set of tests shows a clear improvement upon the dry bone experiment, with the average error almost halving. This indicates that registration using bony landmarks is indeed feasible, and that many of the errors in the initial tests were due to movement of the bones relative to each other and poor MR imaging quality. An error of 2.5 mm (averaged over all the tests) is acceptable for a navigation system. Errors due to the large marker size, and marking of the landmarks on the MRI scans by the author instead of a radiologist or orthopaedic surgeon, could still be contributing to the registration error.

In terms of assessing which method is best, the difference between the three combinations is not significant enough to indicate a 'best combination'. However, it can be seen that the use of the tibial spines (Landmarks 4 and 5) is problematic, since in the last two tests when they are not used for registration, the average error improves slightly. However, once again, the improvement is slight (a maximum improvement of 0.5 mm), so it is difficult to draw a meaningful conclusion from this.

6.2 Plastinated Specimen Separate Registration Test 1

Having ascertained using the dry bones that separate registration was feasible, it was necessary to decide on a third tibial landmark that could be used for registration. This implies a landmark that can be identified both arthroscopically, and on the MRI scans. After discussion with the surgeon, it was decided that despite the difficulty with registering the tibial spines, they should be used as landmarks, as there are few other suitable points available arthroscopically on the tibia.

The third landmark chosen for this experiment was the centre of the medial tibial plateau and thus the aim of this experiment was to ascertain how accurate tibial registration using this third landmark would be. The experiment was performed on the plastinated specimen to improve accuracy.

6.2.1 Specimen Set-up

The plastinated bones were strapped to the board and scanned as before, with accuracy markers attached. The tibial landmarks used for registration were:

1. Lateral tibial spine
2. Medial tibial spine
3. Centre of the medial tibial plateau

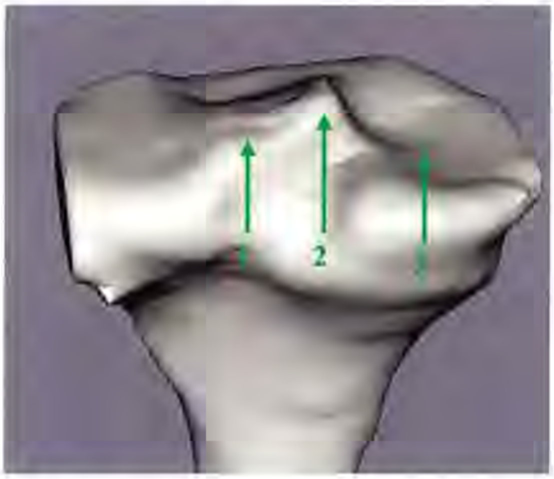

Figure 6.3 The three tibial landmarks used for registration.

6.2.2 Registration and Accuracy Testing

After scanning, the landmarks were marked on the MRI scans using MRIPoint. Registration and accuracy testing then took place as previously described.

6.2.3 Results

No results were obtainable for this experiment. The difference between the shown and actual positions of the markers could not be measured, as the positions were not visible on the same MRI slice at the same time.

6.2.4 Discussion of Results

Although this test had no results as such, it was valuable in that it indicated that this third tibial landmark – the centre of the medial plateau – is not suitable for registration. Although used in surgery as an orienting landmark, identification on the MRI scans and bones proved difficult since this is a fairly large area, not a single point. This means it is difficult to repeatably point to the same point, and to locate the same point on both the scans and on the specimen.

A further problem which could have contributed to this large inaccuracy is the fact that the centre of the medial tibial plateau is located in a similar position to the two tibial spines. It is on a similar plane to the spines, and is situated close to them. Thus it is likely that these three points together do not provide enough geometrical information to attain good registration accuracy. A point located further away is needed to provide enough spatial information for registration.

6.3 Plastinated Specimen Separate Registration Test 2

Another tibial landmark was now chosen for registration. With consultation with Dr van der Merwe, this was chosen as the tibial tuberosity. Although this cannot be pointed to arthroscopically, it can be identified over the skin. Skin movement errors should be slight since the underlying bone itself will be palpated during registration.

The aim of this experiment was twofold. Firstly, separate registration of the femur using the plastinated specimen was tested. Secondly, separate registration of the tibia using the new landmark was tested. Since this experiment was to provide an indication of the accuracy of performing this registration in a clinical setting, an MRI protocol routinely used in practice was chosen, as discussed in Chapter 4.

6.3.1 Specimen Set-Up

Ten accuracy markers were attached to the plastinated specimen as shown in Figure 6.4 below.


Figure 6.4 The ten accuracy markers (A – J) taped to the plastinated specimen.

The femoral landmarks used for registration were:

1. The highest point of the articular cartilage, laterally.
2. The highest point of the articular cartilage, medially.
3. The highest point in the femoral notch.

The tibial landmarks used for registration were:

1. The lateral tibial spine.
2. The medial tibial spine.
3. The tibial tuberosity.

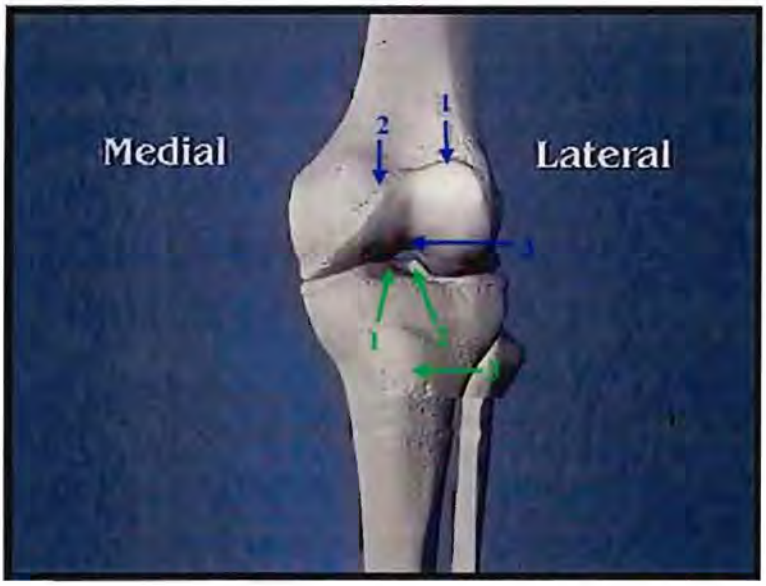

Figure 6.5 The three femoral (blue) and three tibial (green) landmarks to be used for separate registration [Smith & Nephew, 1998].

6.3.2 Registration and Accuracy Testing

After scanning, registration was performed on the femur using the three femoral landmarks. Registration was performed in flexion so that the landmarks could be pointed to more easily, whilst keeping the pointer upright. This is also the position that registration would take place in surgery.

Figure 6.6 The plastinated bones in flexion, to aid registration of the femoral notch and tibial spines.

The accuracy markers on the femur (A, B, C, D, E) were pointed to in turn in order to determine the quality of registration. This was repeated three times.

Similarly, registration was performed on the tibia using the three tibial landmarks. The accuracy markers on the tibia (F, G, H, I, J) were pointed to in turn in order to determine the quality of registration. This was repeated three times.

6.3.3 Results

The accuracy results, averaged over the three tests and all the accuracy markers, are given in Tables 6.4 and 6.5 below.

Table 6.4 Registration errors for the femur using three landmarks.

	Average Error [mm]	Maximum Error [mm]	Minimum Error [mm]
dx	1.8	7.1	0.0
dy	1.0	3.4	0.0
Overall	**1.4**	**7.1**	**0.0**

Table 6.5 Registration errors for the tibia using three landmarks.

	Average Error [mm]	Maximum Error [mm]	Minimum Error [mm]
dx	1.6	6.4	0.1
dy	2.8	5.6	0.3
Overall	**2.2**	**6.4**	**0.1**

The results show good accuracies for both tibia and femur.

6.3.4 Discussion of Results

These results are very encouraging for the use of separate registration. The accuracy result for the femur has improved due to the use of the plastinated bones, which image better. The use of the tibial tuberosity on the tibia has also greatly improved tibial registration accuracy - 2.2 mm is an acceptable figure for a preliminary system. Positioning the bones in flexion aided the registration of the femoral notch and tibial spines.

Use of the plastinated specimen and the clinical MRI protocol further reinforce the feasibility of this procedure. These landmarks can be identified with the ligaments and muscles of the knee joint present. The navigation system also functions well with clinical scans. Decrease in scan slice width might improve accuracy, but is not necessary at this stage.

7 ARTHROSCOPIC CADAVER TEST

Following the final plastinated specimen test, the basic feasibility of the system in terms of the use of bony landmarks had been established. Final testing in a more realistic surgical environment was necessary. A cadaver was chosen for the testing, which was carried out by the orthopaedic surgeon – Dr van der Merwe – in a set up similar to that used in surgery.

The aims of this experiment were to show that the bony landmarks could be reached arthroscopically, that holding the bones still to maintain registration was feasible, and that the entire system was feasible in terms of the information it supplies, and how well it fits in with the existing surgical procedure.

7.1 Specimen Set-Up

A fresh-frozen cadaver leg was defrosted at room temperature overnight. Accuracy markers were attached around the knee using tape. The leg was then MRI scanned, using the hip coil attachment. However, due to the large size of the knee, it was tightly fitted into the coil. This meant that some of the accuracy markers were shifted, and others didn't image well. The same femoral and tibial landmarks as used in the plastinated phantom test were used for registration (see Section 6.3).

Femoral Landmarks:

1. Highest point on the articular cartilage, laterally
2. Highest point on the articular cartilage, medially
3. Highest point in the femoral notch

Tibial Landmarks:

1. Lateral tibial spine
2. Medial tibial spine
3. Tibial tuberosity

After scanning, the knee was moved to an orthopaedic teaching laboratory, where it was clamped into a flexion position resembling that used in surgery. The surgeon cut the usual medial and lateral arthroscopic portals into the knee as shown in Figure 7.1 on the next page, and prepared it accordingly. The tracked pointer was inserted through one of the portals, and the arthroscopic camera through the other.

Figure 7.1 The surgeon cutting the arthroscopic portals into the cadaver knee.

In MRIPoint, the surgeon marked the three femoral and three tibial landmarks for use in registration. All of the landmarks were marked where they would be reached arthroscopically, as opposed to directly on the bone. For example, the tibial tuberosity was to be registered over the skin, so its position on the MRI scan was marked on the outside of the skin, as opposed to on the bone itself. A similar procedure was followed for the other landmarks, taking cartilage covering the bone into account.

7.2 Registration and Accuracy Testing

The registration procedure was now begun. First, the theatre space was calibrated using the reference frame, as shown in Figure 7.2 below.

Figure 7.2 Calibration of the theatre space above the knee using the reference frame.

Registration now took place using the three femoral landmarks. However, due to the position of the knee, and the fact that the pointer has to be held upright for the cameras to track it, it proved difficult to reach the three points through the normal arthroscopic portals. The surgeon therefore cut another portal proximally, so the pointer could be held upright. Registration then took place with little difficulty. The femur was clamped in place throughout the procedure, so holding it still whilst obtaining navigational information did not prove difficult.

Figure 7.3 Registration of the femur showing the cameras, pointer and arthroscopic screen.

The femur was registered with the knee in flexion, whereas it had been scanned in extension. This was a further hindrance to using the accuracy markers, as skin movement would have caused them to shift, rendering them useless as a 'ground truth' for accuracy testing. Therefore readily identifiable anatomical landmarks were used to test the accuracy. Due to the limited number of these in the knee, some repetition of the landmarks used for registration was necessary. The accuracy landmarks used were:

1. Middle of the top of the articular surface
2. Highest medial point of the articular surface
3. Highest lateral point of the articular surface
4. Lowest point of the articular surface

These landmarks are shown in Figure 7.4 on the next page.

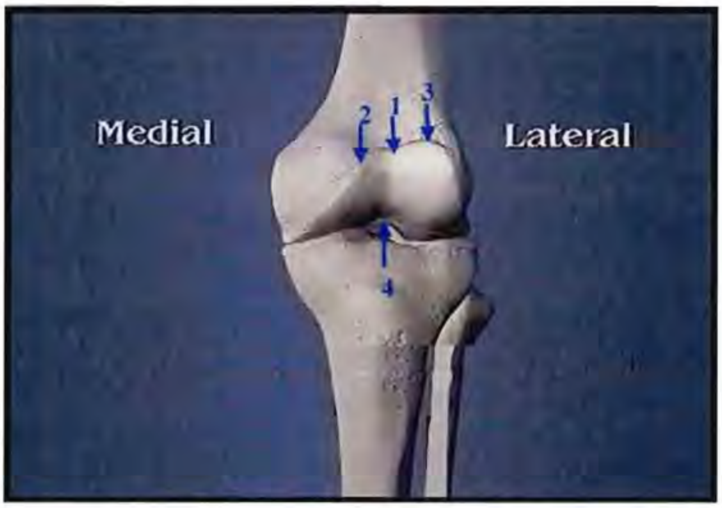

Figure 7.4 The landmarks used for accuracy testing on the femur.

Due to time constraints, the registration and accuracy testing took place only once.

The tibia was then registered using the three tibial landmarks – the two tibial spines were pointed to using the normal arthroscopic portals. The tibial tuberosity was palpated and pointed to over the skin. Holding the tibia still was slightly more difficult than holding the femur still, since it was 'dangling' from the clamp. However it was managed with some success.

Figure 7.5 Registration of the tibia showing the cameras, pointer, arthroscopic screen and laptop.

Again, anatomical landmarks were used for accuracy testing. These were:

1. Middle of the lateral tibial plateau
2. Tibial ACL insertion
3. Tibial tuberosity

The tibial accuracy landmarks are shown in Figure 7.6 below.

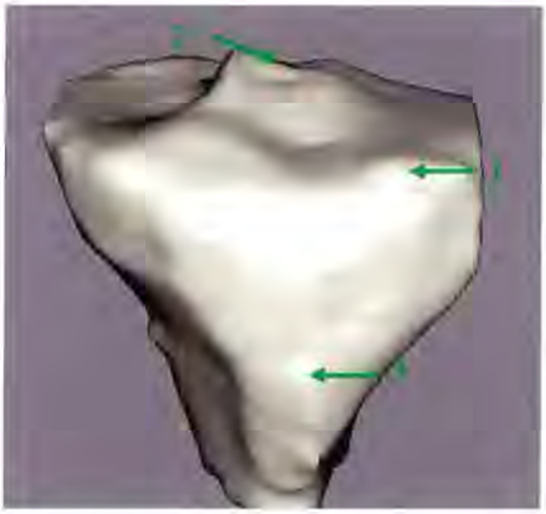

Figure 7.6 Landmarks used for accuracy testing of the tibia.

Again, only one test was performed due to time constraints.

7.3 Results

The results for the cadaver test, averaged over the three accuracy landmarks, are shown below.

Table 7.1 Registration errors for the arthroscopic registration of the cadaveric femur.

	Average Error [mm]	Maximum Error [mm]	Minimum Error [mm]
dx	3.0	5.5	0.5
dy	1.4	3.2	0.4
Overall	**2.2**	**5.5**	**0.4**

Table 7.2 Registration errors for the arthroscopic registration of the cadaveric tibia.

	Average Error [mm]	Maximum Error [mm]	Minimum Error [mm]
dx	7.4	16.0	5.1
dy	2.1	5.2	1.6
Overall	**4.8**	**16.0**	**1.6**

As can be seen in the tables, the accuracy results are slightly worse than those obtained for the plastinated specimen, but are still within acceptable limits.

7.4 Discussion of Results

The results for the cadaver test are very encouraging. The average error for the femur is 2.2 mm, which is certainly an acceptable standard for navigation. Once again, the tibial error is higher than this, at 4.8 mm. This higher error is due to several factors. The main contributor is the fact that the tibia was dangling during registration. In surgery, with a bent knee with foot resting on the table, as shown in Figure 7.7 below, it would be much easier to hold the tibia still. Movement of the tibia in this test certainly contributed to some of the loss of accuracy in the system.

Figure 7.7 Position of the knee during ACL reconstruction surgery.

Another source of error is the fact that the probe was slightly bent during the final accuracy testing of the tibia – this would have added error to the process.

However, overall, it is encouraging that registration could be performed arthroscopically – this is an important test of the feasibility of the system for surgery. In future, the navigational instruments will have to be modified to allow registration to take place with the probe upside down or at an angle. With these modifications, no extra arthroscopic portal would be necessary, and registration in general could take place more accurately.

The surgeon also has a positive opinion of the system, and how it fits into the normal surgical environment and procedure. Discussion with the surgeon revealed that holding the bones still during navigation should not be a problem in surgery, that the navigational information supplied was sufficient to improve surgery, and that the lack of invasive tracking frames in the bones was a significant improvement on currently available systems.

8.1.1 Individual Variation in ACL Insertion Position

Finding the answer to how much the position of the ACL differs between people was inspired by examination of the literature concerning ideal tunnel placement for ACL reconstruction (See Section 2.1). As discussed, the method for tunnel placement which tends to be slightly more favoured is anatomical tunnel placement i.e. placing the tunnel in a position close to the insertion of the original ACL [Harner *et al.*, 1999; Amis and Jakob, 1998; Arnold *et al.*, 2001]. In many patients, the remnants of the original ACL are no longer present and thus the surgeon must decide on a general protocol for where an anatomically placed tunnel must be.

However, in these same studies, a wide variation in natural ACL insertion position was revealed [Arnold *et al.*, 2001; Giron *et al.*, 2005; Lintner *et al.*, 2005; Musahl *et al.*, 2003]. This means that if one standard 'anatomical' approach is chosen by a surgeon, it will not result in anatomical placement of the tunnel for all his patients.

In order to confirm this thought, it was decided that a study of the placement of healthy ACLs should be performed, using 3D computer models of the knee to accurately perform this study.

8.1.2 The Bi-lateral symmetry of ACLs

If true anatomic placement is to be achieved in ACL reconstruction surgery, then it seems that the only way to achieve it is to individualise the placement for each patient, and some authors agree with this [Amis and Jakob, 1998; Howell, 1998]. CAOS provides a means of doing this, yet it seems that few systems take this opportunity, and instead continue to select a standardised placement for all patients.

The idea in this study was to ascertain whether the undamaged ACL of a patient (i.e. the ACL of the opposite knee) could be used to obtain the ideal position for the tunnels of the reconstructed ACL. In order to decide if this is feasible, the bi-lateral symmetry of the ACL in people must be shown. In other words, it must be shown that the ACL in left and right knees is placed in a similar position.

Therefore, the left and right knees of patients with no ACL damage were reconstructed, and the 3D models were measured to determine whether left and right symmetry exists. If this is the case, then an MRI of the undamaged knee will provide the positioning information required for reconstruction of the damaged ACL, and this position information will be individualised and optimised for each patient.

8.1.3 Position of the Healthy ACL in Patients who have had ACL Reconstruction

The next question to be answered is whether people who tear their ACLs have a different anatomy to those who don't. If this is the case, it would indicate that certain people have an ACL orientation which makes them prone to ACL damage.

In order to ensure that this is not true, the position of an undamaged ACL in the knee of someone whose other ACL has been damaged, must be found. This is then compared to the positions of healthy ACLs in those who have experienced no damage in either leg. If ACL damage is related only to impact, and not anatomy, as expected, then the ACLs from patients will be in a similar position to the ACLs of people who have never had an ACL injury. Again, 3D computer models are the ideal format for performing these measurements.

8.1.4 Placement of ACL Reconstruction Tunnels

If the answers to the first three questions are true, then this indicates several things. Firstly, it indicates that ACL anatomy varies widely and that an individualised placement for each person's reconstruction is desirable. Secondly, it indicates that this individualised placement information can be obtained from the healthy knee of each person and that this holds for ACL reconstruction patients, as they have the same anatomical properties as the uninjured patients who were studied. This information, together with an image guided surgery system, would allow the surgeon to place anatomic tunnels accurately for each patient.

Having answered these questions, the 3D models can now be used to examine whether ACL tunnels *are* being placed anatomically, in comparison to the undamaged ACL on the opposite knee, for each patient. This information provides insight into how surgeons are placing tunnels, and whether this can, and should, be changed. It will also provide an indication for the necessity of a CAOS system providing individualised anatomical information.

8.2 Subjects

In this study, two different sets of subjects were MRI scanned. The first was a group of 16 patients who had undergone ACL reconstruction surgery in one knee, performed by Dr van der Merwe. These patients had been studied in a previous clinical trial, so several sets of MRI scans were already available of their reconstructed knees. As will be discussed, further scans were later required of these subjects. 13 subjects were recalled, and scans of both their knees, reconstructed and healthy, were taken using a new MRI protocol. This resulted in a total of 26 sets of scans. These subjects will be referred to as the 'ACL patients' for clarity.

The second group of subjects was a group of 13 people who had experienced no previous ACL damage. Scans of their left and right knees (both undamaged) were taken. This resulted in a further 26 scans. These subjects will be referred to as the 'healthy subjects' for clarity.

8.3 Magnetic Resonance Imaging Procedure

Deciding on an appropriate protocol for the MRI scans was difficult. The ACL was the primary focus of the study, and it has been shown that T2 weighted MR images are the best choices to optimise ligament imaging. Specifically, spin-echo multi-echo or gradient-echo T2 sequences with long repetition times (TR) result in the best imaging of ligaments. Sagittal scans give the best images of the ACL, which appears as a single, dark, continuous band extending from the medial aspect of the lateral femoral condyle to the anterior tibial plateau. However, the ACL runs in an oblique course, and can sometimes be difficult to visualise on an MR scan [Berquist, 1990, Bloem and Sartoris, 1992].

Reconstructed ACLs are visualised using the same scan protocols mentioned above, as the graft is also a ligament with similar signal intensity, and the course of the reconstructed ligament is the same [Bloem and Sartoris, 1992]. Figure 8.1 below shows MRI scans of the healthy and reconstructed ACL.

Figure 8.1 Examples of MRI scans showing the natural ACL (left) and the reconstructed ACL autograft with part of the femoral tunnel (right).

However, for 3D reconstruction of the images, the tibia and femur also need to be clearly visualised. Furthermore, the subjects in the study cannot be subjected to overly long scan times. Thus, various MRI protocols were examined to decide which would give the best compromise between these three factors. These were:

- High resolution, T1 weighted spin echo with 4 mm slices
- T1 weighted spin echo with 4 mm slices
- T2 weighted spin echo with 2 mm slices

These protocols will be discussed further in the following chapters.

8.4 Mimics

As described in Chapter 1, Mimics is software developed by the Materialise company. It is used to manipulate Dicom format images from scanners to form 3D models of selected regions of anatomy. Dr Fitzpatrick and postgraduate students in the Biomedical Engineering discipline at UCD have gained much experience in the use of Mimics for this purpose, with both CT and MRI scans. They were consulted and provided advice on the best method to create 3D models. The procedure used to create these models was essentially the same for all the tasks in this thesis, and is outlined below.

First, the scans to be manipulated are selected and imported into Mimics. Their orientation details (i.e. anterior, posterior, medial, lateral etc.) must be entered. The scans are then compiled to show the original view in which they were taken (in this case sagittal), as well as the other two views – coronal and transverse. Any of these views can be selected and used for segmentation of the image.

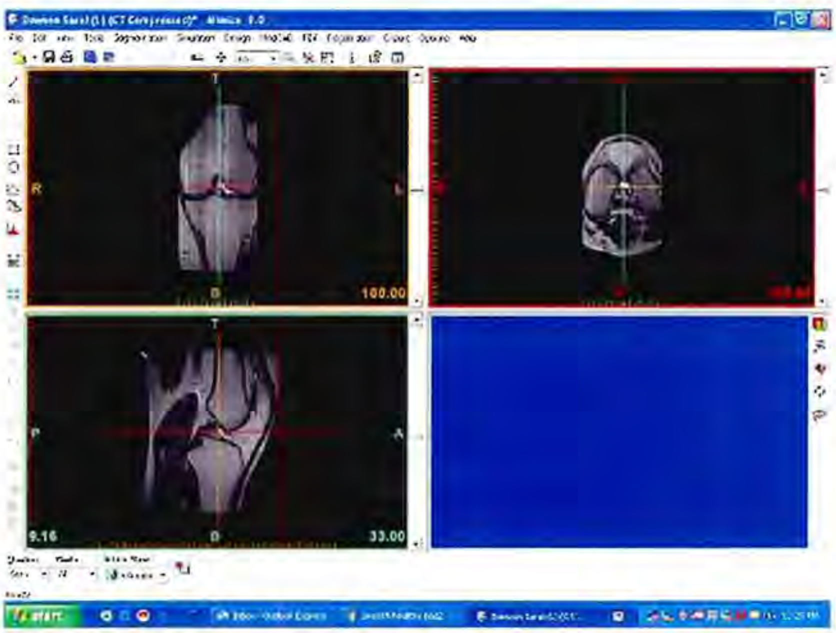

Figure 8.2 Screen shot from Mimics showing the three views of the MRI data.

A range of threshold values is then selected for the images. Essentially, a window of grey values is chosen, and all pixels with these values are selected on the MRI scans. This is shown by colouring them in. Unfortunately, in these MRI images with their wide variety of structures, threshholding did not produce a very well segmented image, as shown in Figure 8.3 on the next page.

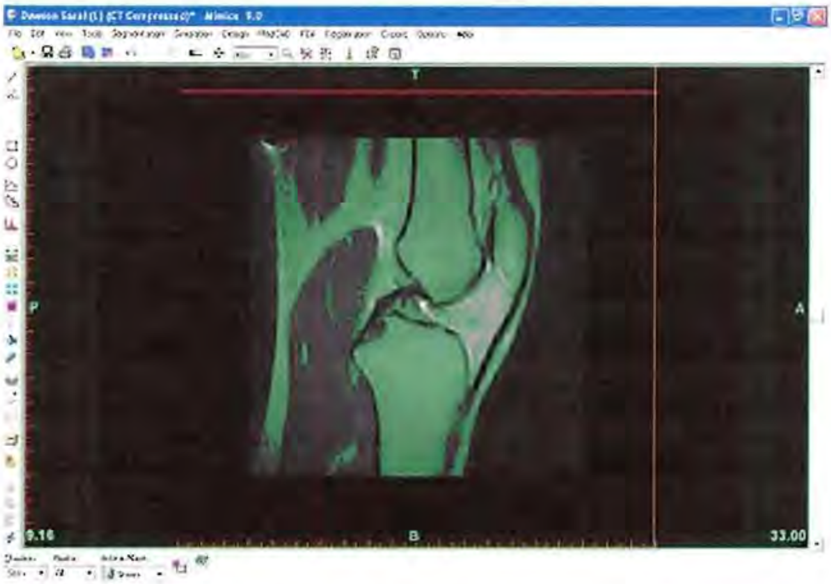

Figure 8.3 Screen shot from Mimics showing the results of applying the thresholding selection. Areas in green are those which have been selected.

At this stage, the user must manually select, on each scan slice, the area of interest. The first area considered was the bones – the tibia and femur. These were segmented together since they have similar grey value properties on the images. So, for each slice, any areas that had been erroneously selected by the threshholding operation were erased manually. Similarly, areas of the bones which had not been selected were filled in manually. The final segmentation of the bones is shown in Figure 8.4 below.

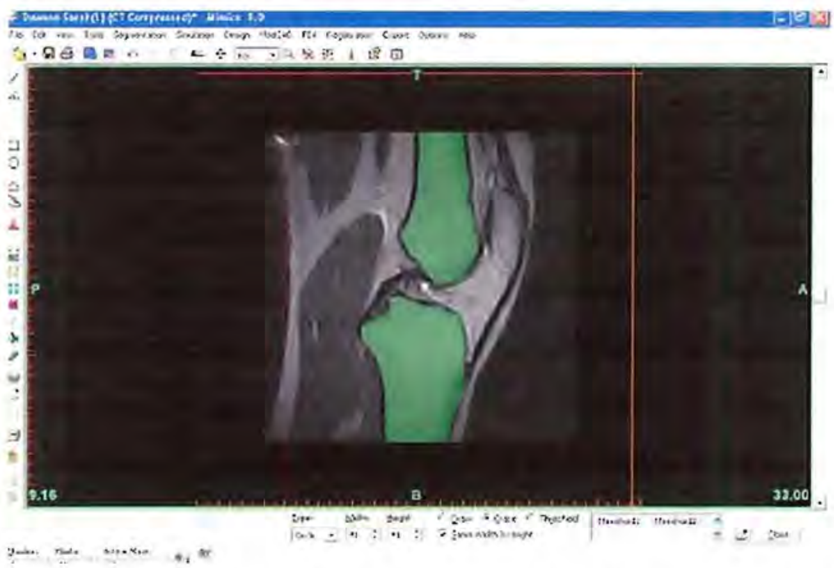

Figure 8.4 Screen shot from Mimics showing the selected tibia and femur (green) after manually erasing and filling in the appropriate areas on the scan.

Once this is complete, every scan slice shows the areas of interest (tibia and femur) coloured in the same colour. A region growing algorithm is now applied to these areas to ensure all pixels within the areas have been selected. The result of this is shown in Figure 8.5 on the next page.

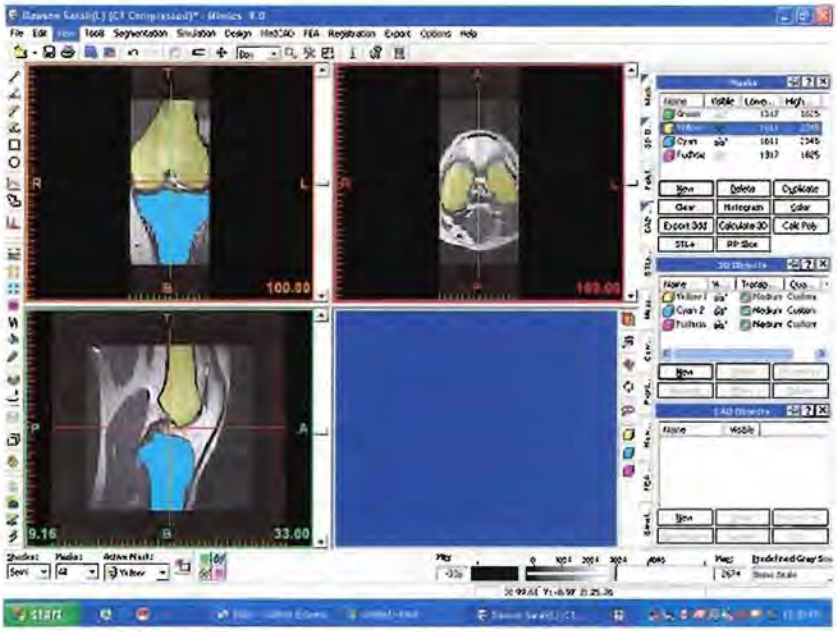

Figure 8.5 Screenshot from Mimics showing the final selection of the femur (yellow) and tibia (blue) before a 3D model is created.

Following this process for the tibia and femur, it was repeated for the ACL (or tunnels and ligament graft in the case of the damaged knee of ACL patients). In the case of the undamaged ACL, all views of the MRI scans were used, since it is a fairly difficult object to visualise. The final segmentation of the ACL is shown in Figure 8.6 below.

Figure 8.6 Screenshot from Mimics showing the final selected ACL (purple) before the 3D model is compiled.

The areas are now formed into 3D objects using the built-in Mimics function, as shown in Figure 8.7 on the next page. Various parameters regarding the formation of these models can be selected. The 3D models are then examined for any defects, missing areas etc. These can be corrected on the 2D scans, and the 3D model is then re-compiled. This 3D model is fairly rough, and further smoothing is required, as discussed in Section 8.5.

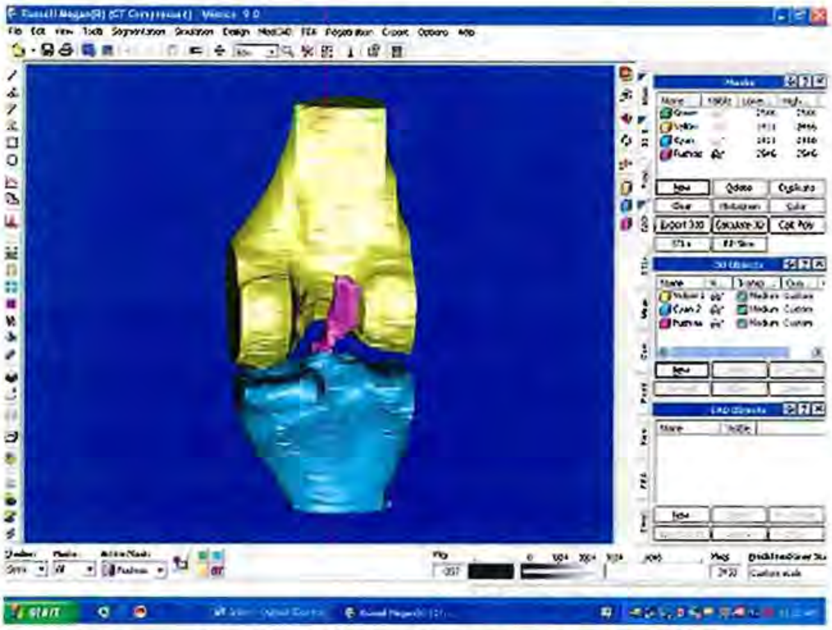

Figure 8.7 Screenshot from Mimics showing the 3D reconstructed model.

8.4.1 Discussion of Model Formation with Mimics

Mimics seems to be the benchmark program for the creation of 3D models from scan data. Although the final model produced is of good quality, and was useable in this thesis, there are various causes of error in the process, and disadvantages of the procedure.

The major downfall of creating models in this way is time. Every slice of every scan must be examined and manually manipulated so that the correct areas are selected. This is a very laborious and time consuming process, which slows down the processing of scans, and limits the number of models which can be made in a given amount of time.

This manual manipulation of scans adds other errors into the process. The most obvious of these is the subjectivity involved in selecting the regions of interest. Someone with limited anatomical knowledge finds it very difficult to know where one structure ends and another begins, especially in the case of soft tissues like the ACL, and towards the beginning and end of a set of scans, as shown in Figure 8.8 on the next page. In this study, consultation with the orthopaedic surgeon ensured that models were made accurately. However, the manual selection process must add a certain degree of error and much subjectivity into the process. This is particularly true for the ACL, which is difficult to visualise in MRI scans. Assumptions and estimates had to be made in some cases, and with so few slices going through the ACL, any mistake would contribute significantly to the final shape of the ACL in the 3D reconstruction.

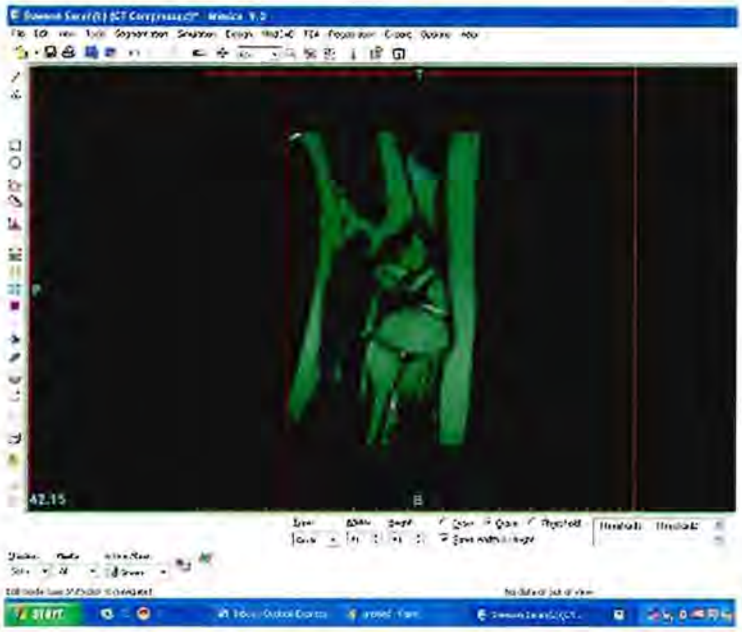

Figure 8.8 Mimics screen shot showing a difficult area of the MRI scan to segment accurately.

However, although this manual and subjective selection of models has added some error to the process, each model was completed carefully in order to minimise this error and ensure that the best accuracy possible for the final images was obtained.

8.5 Magics

The 3D model generated by Mimics is accurate, but has rough edges and discontinuities. Thus, further modification of the model is necessary and this was performed in Magics. This is another software program from the Materialise company, and is designed for processing of the 3D models obtained from Mimics. In order to import models into Magics, they must be in STL format, and Mimics provides a method for converting its models into this format.

Once in Magics, each element of the 3D model must be imported. Since each knee was to be compared to all the other knees in the study, they needed to all be of the same orientation. Therefore every right knee was flipped around the XZ axis so that it became a left knee. On this basis, all measurements taken are directly comparable to each other.

The next step in Magics is the smoothing process. Several tools are provided for this, and some experimentation with this procedure was undertaken to form the best final model. The details of the smoothing procedure used are discussed in the following chapters.

8.6 Arthron

The smoothed 3D models are now ready for measurement. The program used to perform these measurements was Arthron. This is shape analysis software for biomechanics created at University College Dublin by Goodwin Lawlor. The software provides various tools for making measurements and setting up reference axes on models.

Arthron was used to orient each set of bones and ACL to a consistent set of reference axes, so that all measurements would relate to one another. Measurements were then made on these models using Arthron. Various methods of creating the axes were used, and these are discussed in detail in the following chapters.

8.7 Statistical Analysis

Having obtained measurements from the 3D models, statistical analysis was performed in order to answer four basic questions:

- What is the variation in insertion position of the ACL in healthy people?
- Is the position of the ACL bilaterally symmetrical i.e. is the ACL in the left and right knees of healthy people in the same place?
- Is the healthy knee of ACL patients also in the same place as the ACLs of uninjured, healthy people?
- Is the reconstructed ACL in the same place as the uninjured ACL for each of the ACL patients?

These questions were answered using the Statistica data analysis software (StatSoft, Inc. (2004) Statistica version 7. www.statsoft.com.). This software was used to perform a 2-way ANOVA comparison on the data, as well as several Tukey HSD post-hoc tests. The details of the statistical analysis and results are given in Chapter 11.

9 INITIAL PROCEDURE FOR THE ANALYSIS OF 3D MODELS

Two different protocols for reconstructing 3D models of the knee using Mimics and Magics were experimented with. The first of these used routinely available MRI scans of the knee, and the second used a specialised MRI Protocol. Different ways of analysing these models by fitting reference axes to them were also tried.

9.1 3D Models using a Clinical MRI Protocol

The first set of 3D reconstructions was performed using routinely used clinical scans. Scans of 16 ACL patients were available, as they had been taken for a previous study. During these reconstructions, familiarisation with Mimics and Magics was obtained. A method for creating reference axes and performing measurements was also developed.

9.1.1 MRI Protocol

The scans used in this section of the investigation were of the ACL reconstructed knees of 16 patients who had undergone surgery by Dr Willem van der Merwe. This group of patients had been studied in a previous investigation, so the MRI scans that had been taken for that investigation were available. Since the ACL is easiest to visualise in sagittal images, only the sets of sagittal scans were reconstructed for each patient.

Two T1 weighted, sagittal scan protocols had been performed on each patient, as shown below and on the next page.

High Resolution Spin Echo T1
15 slices, 4 mm thick
TE = 26 ms, TR = 800 ms

Figure 9.1 Example of a high resolution spin echo T1 weighted scan of a reconstructed ACL.

Spin Echo T1
19 slices, 4 mm thick
TE = 26 ms, TR = 950 ms

Figure 9.2 Example of a spin echo T1 weighted scan of a reconstructed ACL.

9.1.2 3D Reconstruction

Both sets of scans were imported into Mimics and segmented and manipulated as described in Chapter 8. Since these were images of reconstructed knees, it was decided that the tunnel, screws and autograft would all be treated as one object, and segmented together, as they were difficult to differentiate from each other.

3D volumes were then created using the default settings:

- XY resolution = 1.6 mm
- Z resolution = 4.4 mm

The 3D models were converted into STL files using the default settings. These models were imported into Magics, where a smoothing algorithm was applied to them, as follows:

- *Smoothing Procedure:*
  - Smoothing Factor: 0.5
  - Shrinkage Compensation Factor: -0.5
  - Repetitions: 10
- *Triangle Reduction* with default settings.
- *Smoothing Procedure,* as above.

The goal of the smoothing procedure is to eliminate roughness and sharp edges, without losing too much anatomical detail of the models. Thus, the smoothing and shrinkage compensation factors must be negatives of each other to ensure little data loss. The repetitions are low because the slice width of the MRI scans is so large (4 mm). The choice of factors was based on trial and error and the advice of postgraduate students at UCD with experience in using Mimics and Magics with both MRI and CT data.

9.1.2.1 Discussion of Resulting 3D Models

The final models resulting from this procedure were fairly accurate, but difficult to work with for various reasons. The biggest contributing factor was the scan protocols chosen. Neither produced a significantly different model to the other. However, both shared qualities which impacted the final quality of the reconstruction.

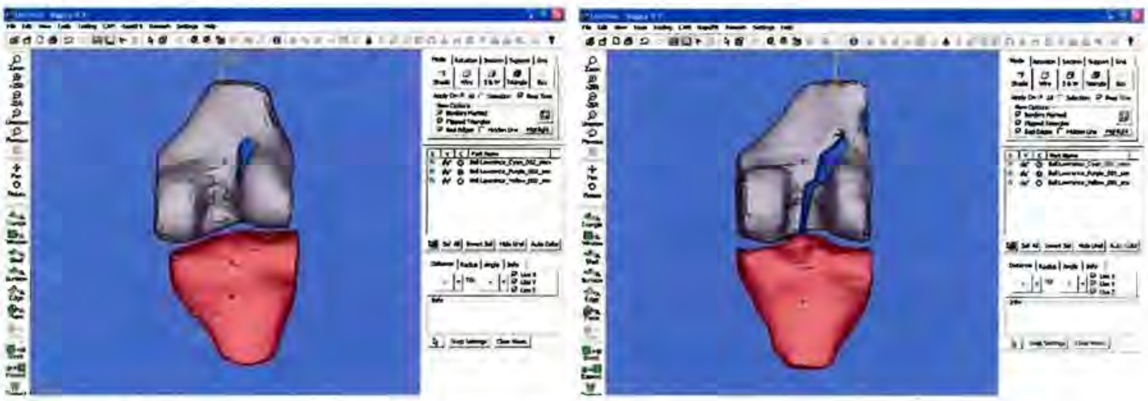

Figure 9.3 Final Magics 3D models with the high resolution spin echo (left) and spin echo (right) protocols respectively.

The first problem was that these scans had been taken at a slight angle. This meant that the tunnel and autograft were not always easily visualised. This was further impacted by the large slice width of the scans. The tunnel and graft are relatively small, and with 4 mm slices, were only visible in one or two scans for each knee. This resulted in difficulty segmenting the tunnel accurately, and a loss of detail in the final model. This large slice width also resulted in a loss of anatomical information on the bones so that normal anatomical landmarks are difficult to identify.

Since these scans were only taken for clinical use, they were focused on imaging the ACL reconstruction, and little else of the knee. This meant that large parts of the bone had been 'cut off', medially, laterally, proximally and distally, as shown in Figure 9.4 on the next page.

Figure 9.4 Images from Arthron showing the loss of information due to the angle and size of the scan.

Figure 9.4 shows a scan with the lateral edge of the knee cut off (left). The image on the right illustrates how the scans were taken at an angle. The lack of proximal and distal data is also evident, especially on the distal tibia. The 'smoothness' of the models also shows that little anatomical detail is present due to the large slice size.

All this loss of data negatively impacts the ability of the model to yield useful measurements.

However, the process did show that, although cumbersome, the Mimics procedure produced good models with the available data. The Magics procedure also produced well smoothed models.

9.1.3 Reference Axes

In order for these models to provide measurements that can be compared to each other, a set of axes must be set up on each knee. The process rotates and translates the MRI co-ordinate frame to the new reference axes. Measurements taken are therefore relative to these new axes, and are thus consistent across all the knees.

However, in order to set up axes, a repeatable method had to be chosen that could be applied to all the models. Due to the loss of data, as discussed above, the number of landmarks available for this were limited. Added to this, parts of the tibia and femur were missing due to lack of complete scan data. This further limited the landmarks that could be used.

Ideally, a set of axes should be set up on both the tibia and femur, so that tibial and femoral measurements can be made separately. However, due to the minimal data available, it was decided to set up axes relative to either the tibia *or* the femur, depending which was the most complete in each model. Only one model was used for each patient – the best of the reconstructions was chosen for each.

9.1.3.1 Method

The method chosen was to use the posterior condyles of either tibia or femur, and the anatomical axis of the bone shaft (of the same bone) to create orthogonal axes. The procedure is outlined below.

- Two points, roughly positioned on the posterior condyles, were manually selected, a and b.
- Two points, roughly positioned in the centre of the bone's shaft were manually selected, c and d.
- $V_1 = a - b$, this is a vector in the plane of the posterior condyles.
- $V_2 = c - d$, this is a vector in the direction of the anatomic axis.
- Normalise vectors V_1 and V_2: N_1 and N_2
- $N_1 \times N_2 = V_3$. This is a vector perpendicular to both the posterior condyles and the anatomic axis.
- V_3 is used in Arthron as the normal of a plane, resulting in a plane passing through the posterior condyles. This is set as the 'Epiphyseal Axis' in Arthron.
- Sets of concentric circles were then fitted to the shaft of the bone. The centroid of each circle defines the anatomical axis, which was set as the 'Diaphyseal Axis' in Arthron.
- A third axis, orthogonal to these two, is then selected by Arthron to form a set of reference axes with the mid-point between the posterior condyles being the centre of the co-ordinate system.

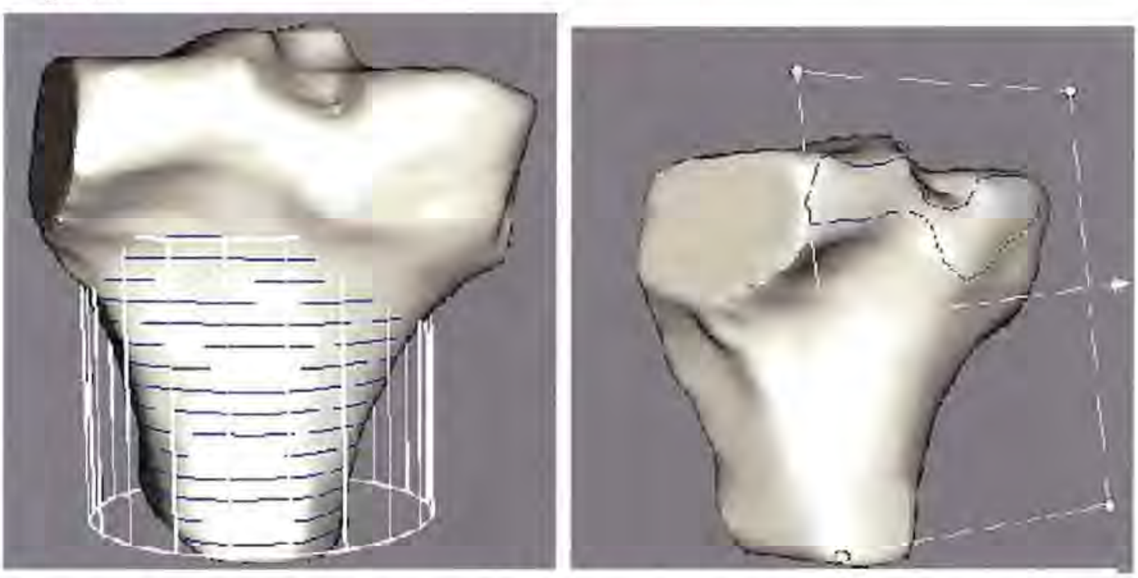

Figure 9.5 Images from Arthron showing the concentric circles used to set the 'anatomic axis' of the bone shaft (left) and to select the posterior condyles (right) for the tibia.

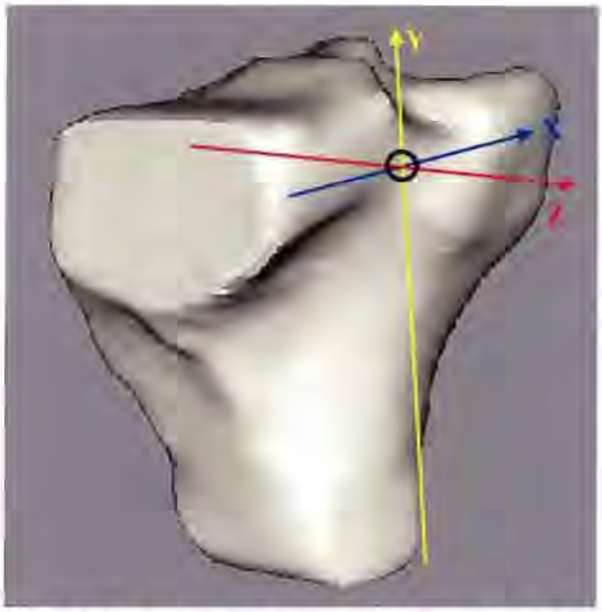

Figure 9.6 An example of the reference axes on the tibia. The X axis (blue) goes through the posterior condylar line, the Y axis (yellow) is in the direction of the anatomic axis of the bone shaft, the Z axis (red) is orthogonal to the X and Y axes. The origin is the middle of the posterior condylar line (black).

9.1.3.2 Discussion of the Reference Axes

This process of setting up the reference axes had several problems, once again mainly due to the poor initial scan data and resulting quality of the 3D models.

Firstly, some scans had neither tibia nor femur which could be used for setting up axes, so these models could not be used. Secondly, setting the reference axes to only one bone, for instance the tibia, means that measurements made on the femur are not related to any anatomical data. Thirdly, some models were referenced to the tibia, and others to the femur, depending on the information available in the model. This means that measurements between models were not comparable.

Lack of scan data resulted in models which did not have many anatomic landmarks. This meant that definition of the axes was a fairly 'rough' procedure, and was hard to accurately verify. Finally, the lack of consistency between the models meant that making a measurement that would allow normalisation for size was almost impossible. Without normalised measurements, comparison between patients could not be made.

For these reasons, this set of models and axes were abandoned, and no measurements were made on them.

9.2 3D Models using a Specialised MRI Protocol

Following the first trials using the clinical MRI scans with 4 mm slice thickness, it was decided that a better scan protocol needed to be found. This protocol would allow good imaging of the ACL or reconstruction, and have as thin a slice size as possible, to allow for model reconstruction with much detail.

9.2.1 MRI Protocol

Scans of both the left and right knees of three healthy people (i.e. with no ACL injuries or repairs) were taken. Several different protocols were experimented with, and finally, a specialised T2 weighted study was chosen:

Sagittal T2 Spin Echo
31 images, 2 mm slice thickness
TR = 4960ms, TE = 80ms

Figure 9.7 T2 spin echo MRI scan.

2 mm was the smallest slice width that the Esaote E-scan scanner could attain. The scans were also maximised in size i.e. as much of the bone as possible was scanned medially, laterally, proximally and distally. However, due to limitations of the scanner, the entire knee joint could not always be imaged in every subject.

9.2.2 3D Reconstruction

The scans were imported into Mimics and reconstructed using the procedure outlined in Chapter 8. The 3D models and STL files were created using the default Mimics parameters.

The STL files were then opened in Magics for smoothing. A new smoothing algorithm was applied to each model:

- *Filter sharp triangles* with default parameters
- *Triangle reduction* with default parameters
- *Smoothing procedure:*
    - Smoothing Factor: 0.5
    - Shrinkage Compensation Factor: -0.5
    - Repetitions: 20

This procedure was decided on with the goals of reducing rough edges, but maintaining anatomical information. Since the previous smoothing procedure had worked well, this was kept almost the same. The number of repetitions was increased, since the scan slice size had decreased.

9.2.2.1 Discussion of the Resulting 3D Models

The resulting models were much more complete than those discussed in Section 9.1.

Firstly, the decrease in slice width and increase in number of slices meant that more anatomical data was visible. Specifically, several more slices went through the ACL, allowing a more detailed reconstruction. The increase in size of the scan, i.e. covering as much of the knee joint as possible, also resulted in much more useable models where more of the tibia and femur were visible proximally, distally, medially and laterally. The T2 weighted, spin echo sequence also resulted in clearer images with the ACL being well defined in the images.

However, despite these improvements, there were still several problems with the resulting models. These can be seen in Figure 9.8 below.

Figure 9.8 The final smoothed 3D model. As can be seen the model lacks anatomical detail. The red arrow shows where the ACL ends before it reaches the femur.

Firstly, the final smoothed models seemed 'too smooth'. This means that some important anatomical data has been lost in the smoothing procedure, indicating that a new procedure is required. Also, the ACL ends before it meets the femur. At first it was assumed that this was due to cartilage or cortical bone that was not being included in the model. However, on consultation with the orthopaedic surgeon, it seemed that the insertion of the ACL was not being included in the model due to its difficulty in being visualised. A way of overcoming this to create more anatomic models was necessary.

9.2.3 Reference Axes

The reference axes were set up in Arthron as described in Section 9.1.3. The posterior condylar axis and anatomic axis through the bone shaft were again used as the primary axes, with a third, orthogonal axis being added by Arthron.

9.2.3.1 Discussion of the Reference Axes

Although the 3D models used for the set up of these axes were better, there were still problems in creating the axes. Some models still had parts of the femur or tibia missing, meaning that either tibial *or* femoral axes could be set for each model, not both. Once again, this has limits in terms of comparing measurements across all the models.

On consultation with the orthopaedic surgeon it seemed that these reference axes didn't hold much clinical significance. In other words, a surgeon receiving measurements made according to these axes would not intuitively know what they meant. This is an obvious downfall of the axes, since the data obtained from the measurements will be of most interest to orthopaedic surgeons.

The MRI scans were limited as to how much of the proximal femur and distal tibia can be imaged. Thus, when finding the anatomic axis of the bone shaft, little bone was available to make an accurate estimate of this. This meant that using the resulting estimate of the anatomic axis as an axis in the co-ordinate system was unreliable and inaccurate. The posterior condylar axis was also difficult to measure repeatably.

Furthermore, in the models, the ACL did not reach the femur. This meant that measuring the femoral insertion was difficult, if not impossible.

For these reasons, this method of reference axes was abandoned, and no measurements were taken on these models.

10 FINAL PROCEDURE FOR THE ANALYSIS OF 3D KNEE MODELS

Having completed the trial and error experiments discussed in the previous two chapters, a final procedure for creating and analysing 3D models was decided on. This included an accurate scan protocol, smoothing procedure, method for setting axes that is clinically significant, and a method for making measurements.

10.1 MRI Scan Protocol

The MRI protocol discussed in the Section 9.2 was decided as the best to use for creating 3D models. It utilised the smallest slice size available with the Esaote E-scan scanner, and the maximum visualisation of the knee joint. The T2, spin echo sequence also allowed optimal visualisation of the ACL or ACL reconstruction.

For the creation of the final models, 52 scans were taken. The ACL patients used in Section 9.1 were recalled for further scanning. 13 of these responded, and MRIs of both their healthy and ACL reconstructed knees were taken using the new scan protocol. Scans of the left and right knees of 13 healthy subjects (with no ACL damage in either knee) were also taken.

10.2 3D Reconstruction

These scans were imported into Mimics, and reconstructed into 3D volumes as outlined in Chapter 8. On consultation with a Mimics expert, the 3D models were created in Mimics using new resolution values:

- XY resolution = 0.8 mm
- Z resolution = 4.4 mm

Thus the XY resolution is twice as precise as in the previous 3D models, as shown in Figure 10.1 on the next page. STL files were then created using the default parameters.

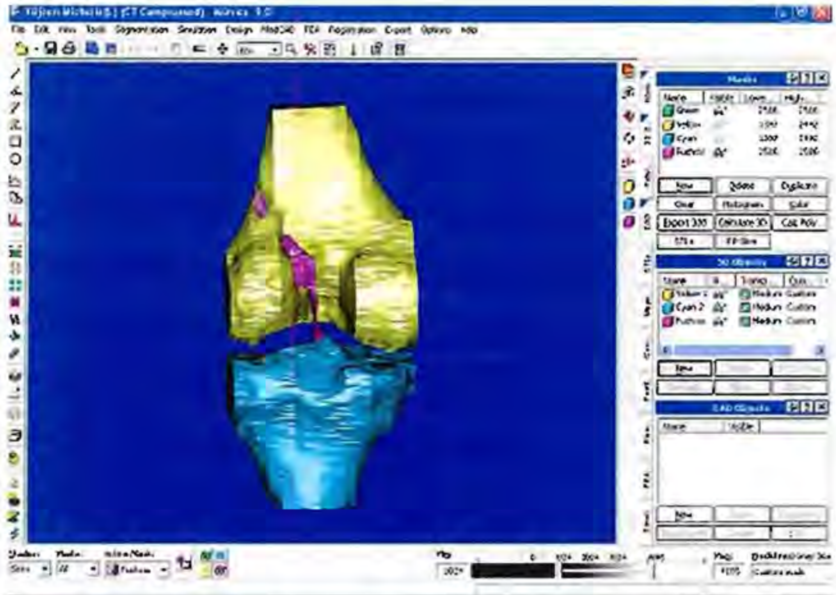

Figure 10.1 Screen shot from Mimics showing the final 3D model of a knee with a reconstructed ACL.

10.2.1 Magics Smoothing Trials

The 3D models were then imported into Magics. The models of right knees were mirrored around the XZ axis to create 'left' knees, so that all the knees are comparable to each other. A trial and error process of various smoothing algorithms was followed as described below.

10.2.1.1 Trial 1

The first algorithm was to filter sharp triangles, and perform triangle reduction with the default parameters. Smoothing was then carried out using 0.5 and -0.5 as the smoothing and shrinkage compensation factors respectively. The ideal algorithm should result in a smooth model that has not lost too much data. Loss of data is indicated by a decrease in volume and area of the image when compared to the original volume and area. For each smoothing procedure, the number of iterations was increased, and the change in volume and area of the resulting model examined for loss of detail. The original image details are given below.

Table 10.1 Volume and area representing the amount of data in the original STL image imported into Magics.

Original Image Details:	Volume:	2203mm^3
	Area	1396mm^2

The final image details, after the smoothing procedure, are given on the next page for each number of iterations.

Table 10.2 The area and volume (data) changes using the first smoothing algorithm, for various iterations.

Iterations	Volume (mm^3)	Area (mm^2)
5	2184	1312
10	2158	1281
15	2133	1259
20	2109	1241
25	2087	1225
30	2066	1212

10.2.1.2 Trial 2

The second algorithm was to first perform the Smoothing procedure (as described above), then to filter sharp triangles and perform triangle reduction. The final image details after this smoothing algorithm are given below for each number of iterations.

Table 10.3 The area and volume (data) changes using the second smoothing algorithm, for various iterations.

Iterations	Volume (mm^3)	Area (mm^2)
5	2194	1325
10	2182	1299
15	2170	1281
20	2157	1266
25	2147	1255
30	2135	1244

10.2.1.3 Discussion of Smoothing Procedures

As can be seen from the results of the two trials, there is a relationship between the number of smoothing iterations performed, and the loss of image information. However, the more iterations that are performed, the smoother the resulting model. Thus, a compromise must be made between obtaining a smooth model, and not losing too much image detail.

The results show that the second algorithm results in less image loss per iteration compared to the first algorithm. So on examination of the resulting models, this procedure using 15 iterations was chosen as the best compromise between a smooth and detailed model, and an example of a smoothed model created like this is shown in Figure 10.2 on the next page.

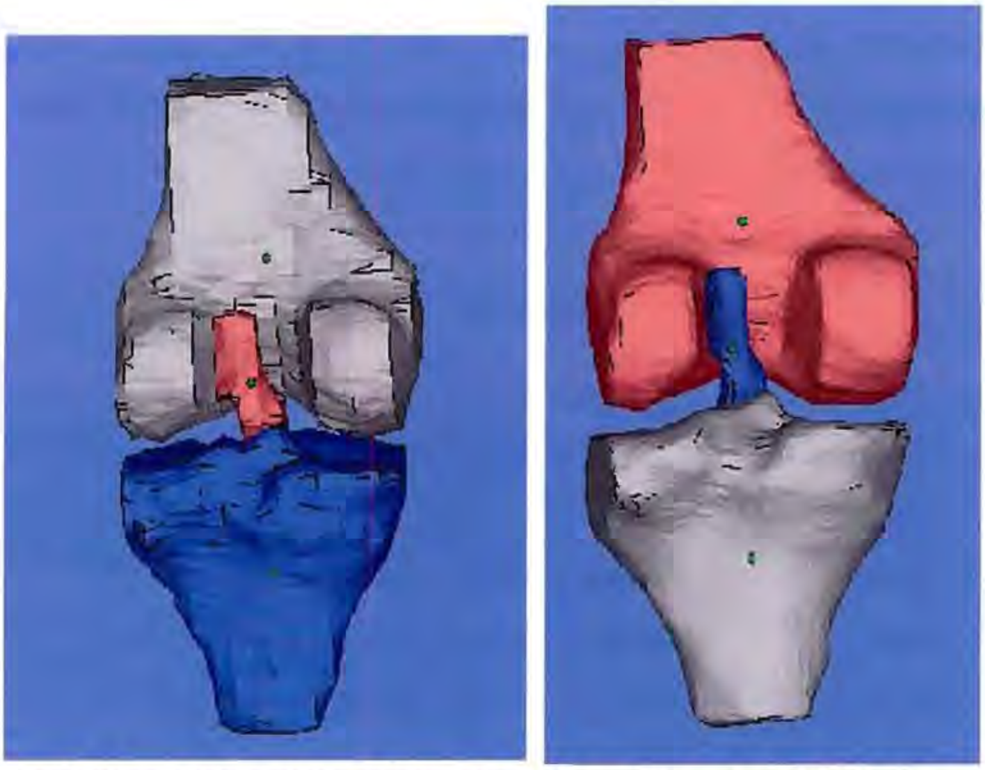

Figure 10.2 A model imported into Magics from Mimics (left) and a model after the smoothing algorithm (right).

Thus the final smoothing algorithm used is:

- *Smoothing Procedure:*
    - Smoothing Factor: 0.5
    - Shrinkage Compensation Factor: -0.5
    - Iterations: 15

- *Filter sharp triangles* with default values.
- *Triangle Reduction* with default values.

10.2.2 Discussion of the Resulting 3D Models

The models resulting from this reconstruction procedure were good. The smoothing algorithm left a sufficient amount of anatomical detail. Anatomical knowledge and familiarisation with the MRIs also resulted in more accurate models.

On consultation with Dr van der Merwe, a method for identifying the femoral insertion of the ACL on the scans was decided on, so these 3D models show the ACL in its entirety – running from the femur to the tibia. This is an important detail for the measurement and analysis of the scans.

Reconstruction of the scans of patients with repaired ACLs was also good, with good visualisation of the tunnels and autograft. The smoothed 3D models are shown in Figure 10.3 on the next page.

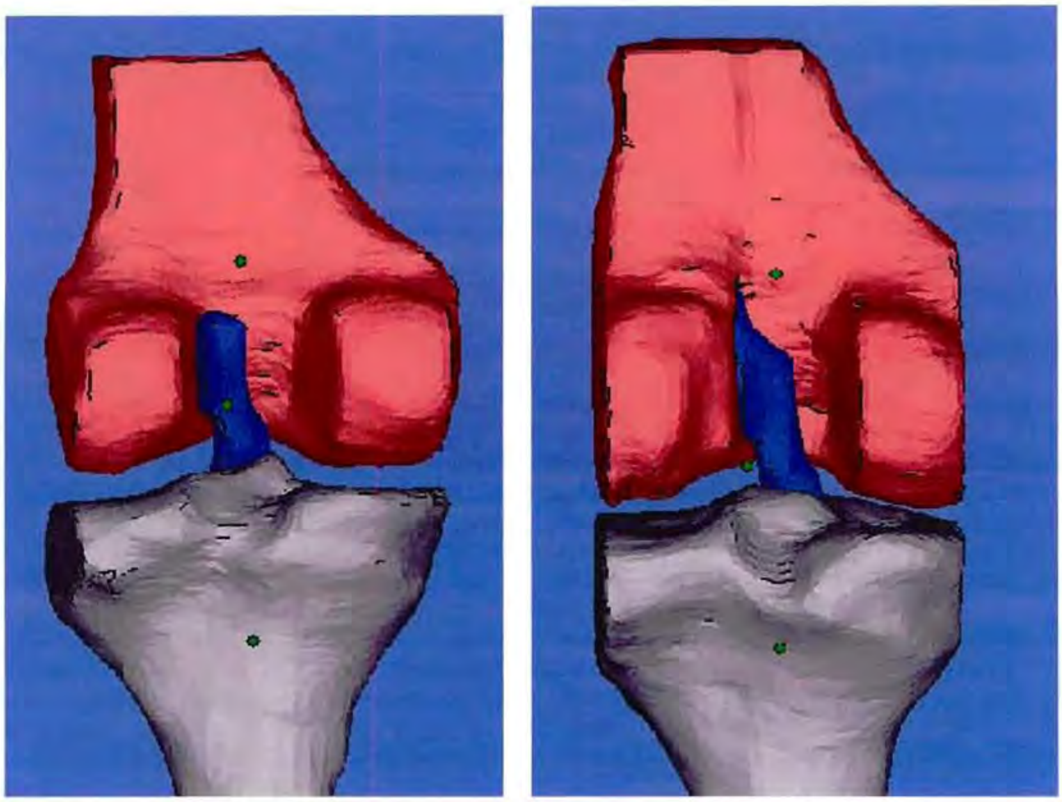

Figure 10.3 Examples of a smoothed 3D model of a healthy knee (left) and an ACL reconstructed knee (right).

However, parts of the knee proximally, distally, medially and laterally were still missing. This is due to inbuilt limitations of the scanner, and could not be overcome. This missing detail limited the procedures that could be used for setting up reference axes. Contrasting images of a complete 3D model, and one missing information proximally, distally, medially and laterally, are shown below in Figure 10.4.

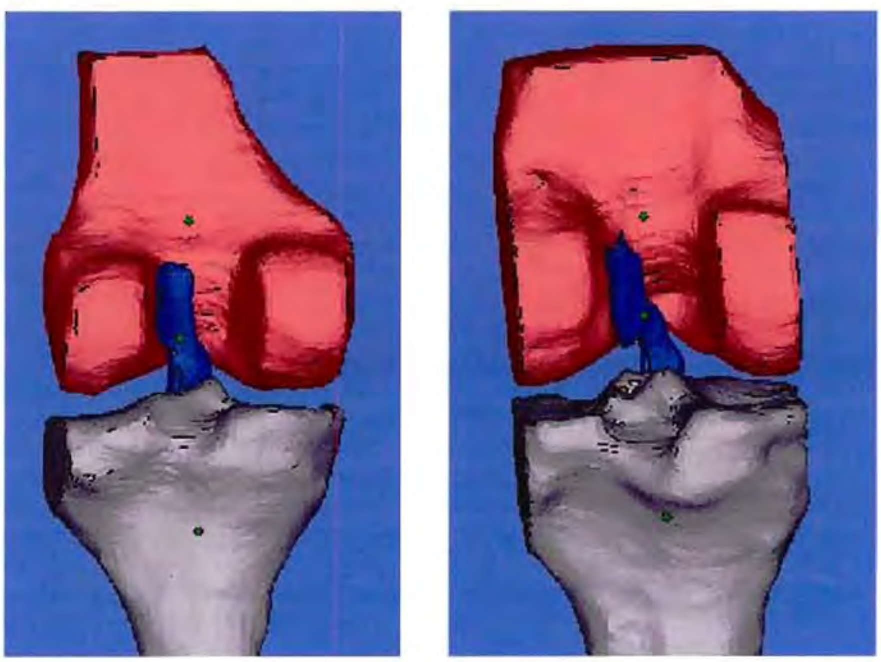

Figure10.4 3D Images of a good 3D model of a healthy knee (left) and one with data missing proximally, distally, medially and laterally (right).

10.3 Reference Axes

The aim in creating these reference axes was to provide a consistent co-ordinate system for measurement that could be applied to all the 3D models. This would allow comparison of the measurements across all the subjects. Since the resulting information is of primary interest to surgeons, it was also important that the measurements were in relation to some clinically significant landmarks, so they are easy to understand. For this purpose, Dr van der Merwe gave advice on anatomical landmarks and the set up of axes that would be relevant to orthopaedic surgeons, and this advice was incorporated into the setting up of the axes.

10.3.1 Method

Axes were set up on both the tibia and femur for each model, so that tibial measurements are relative to tibial anatomy, and femoral measurements are relative to femoral anatomy. The method used to set up the axes for each bone is discussed in detail below.

10.3.1.1 Femoral Reference Axes

- Select points on the medial and lateral posterior condyles: *a* and *b*.
- Select a point on the anterior portion of the femur, at the same height as the lateral condylar point: *c*.
- Create a medial-lateral vector: $V_{ML} = b - a$
- Create an anterior vector: $V_{ant} = b - c$
- Create a vector perpendicular to V_{ML} and V_{ant} i.e. a vector in the posterior-distal direction: $V_{PD} = V_{ML} \times V_{ant}$
- Make V_{PD} and V_{ML} into unit vectors: N_{PD}, N_{ML}
- Use N_{ML} to define the Epiphyseal axis in Arthron, and N_{PD} to define the Diaphyseal axis.
- Arthron creates a third axis orthogonal to these two (i.e. in approximately the anterior-posterior direction)

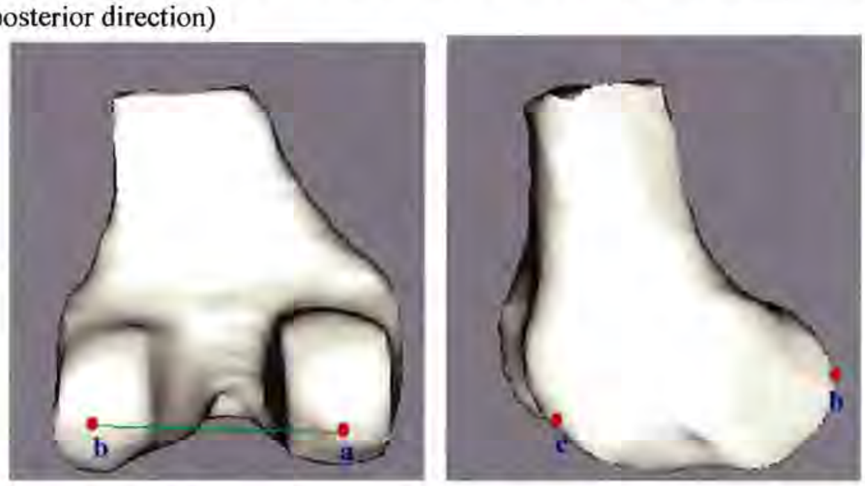

Figure 10..5 The three points a, b and c used for setting up the measurement axes of the femur.

The centre of the co-ordinate system was now be set. The first choice for doing this was to set the joining point of the mediolateral ridge over the lateral condyle, and the highest ridge in the femoral notch, as the centre. This point was consistently identifiable on healthy knee scans. However, on ACL reconstruction scans, this point often coincided with the femoral tunnel, as shown in Figure 10.6 below. Thus it was unsuitable as a centre.

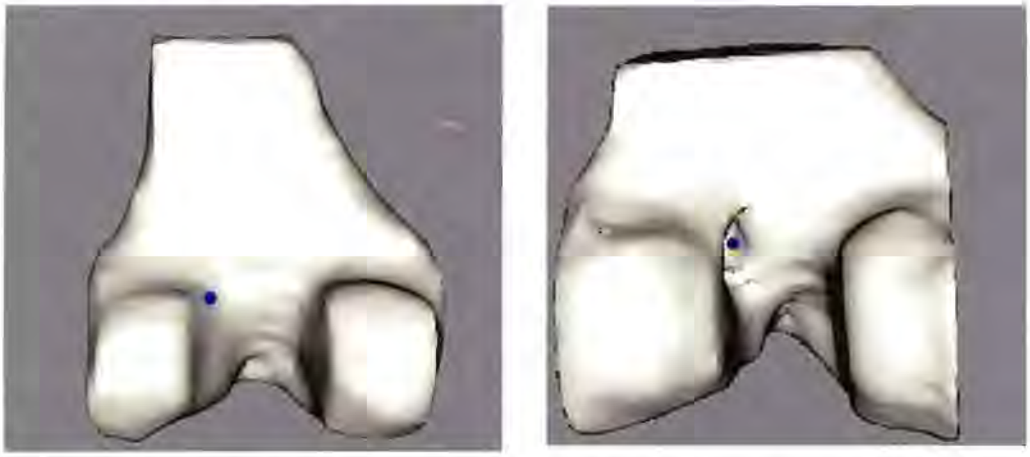

Figure 10.6 The first choice for the femoral axes origin (blue). The image on the left shows the ideal position of the origin, and on the right, how this coincides with the tunnel in an ACL reconstructed knee.

A new centre was chosen as the 12 o'clock reference point used arthroscopically (See Chapter 2). This is the highest, most central and most distal point in the femoral notch, when the femur is in 90° flexion. In this case it was set on the anterior part of the notch, whereas arthroscopically it is often defined in the posterior part of the notch, since this is more relevant for ACL tunnel drilling.

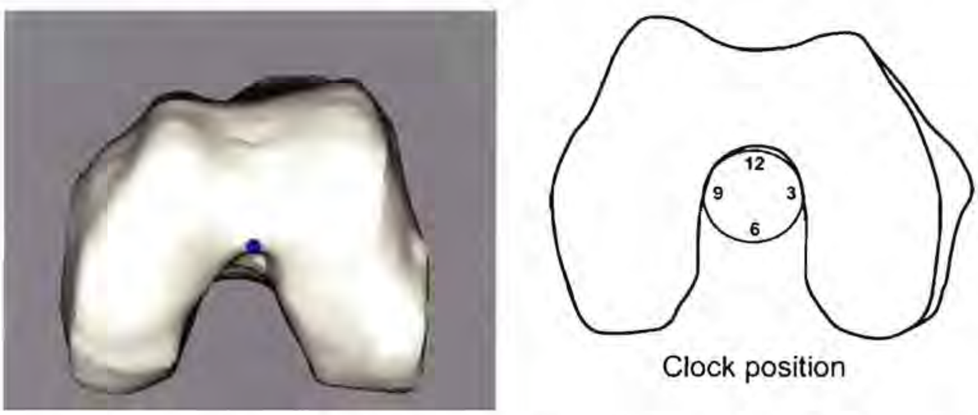

Figure10.7 The new position of the femoral origin, at the highest point of the anterior part of the femoral notch (left) and the posterior 12 o'clock reference point (right).

This procedure created a set of axes where Z points proximally (positive), X points medially (positive) and Y points posteriorly (positive), as shown in Figure 10.8 on the next page.

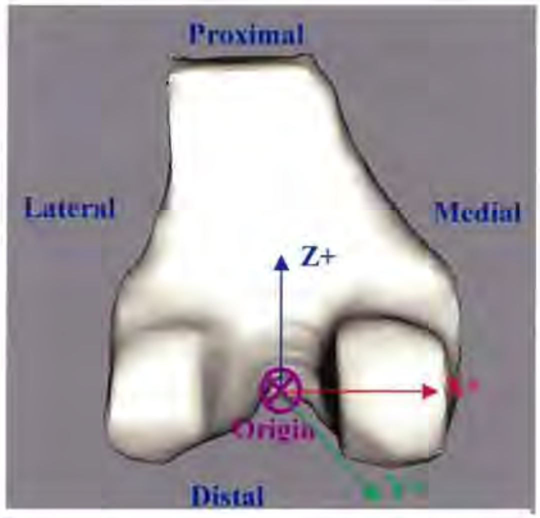

Figure 10.8 The femoral reference axes.

10.3.1.2 Tibial Reference Axes

In order to define the tibial reference axes, the following procedure was used.

- Select the mid-point between the tibial spines, and the mid-point of the tibial tuberosity, and force their proximal-distal co-ordinate to be the same (i.e. at the same height): *d*, *e*
- Select a point medial to the lateral tibial spine and force the proximal-distal co-ordinate to be the same as above: *f*
- Create an anterior-posterior vector: $V_{AP} = d - e$
- Create a medial-lateral vector: $V_{ML} = f - e$
- Create a vector orthogonal to these two i.e. pointing in the proximal-distal direction: $V_{PD} = V_{AP} \times V_{ML}$
- Make the anterior-posterior and proximal-distal vectors unit vectors: N_{AP} and N_{PD}
- Use N_{AP} to define the Epiphyseal axis in Arthron, and N_{PD} to define the Diaphyseal axis.
- Arthron creates a third, orthogonal axis pointing in approximately the medial-lateral direction.

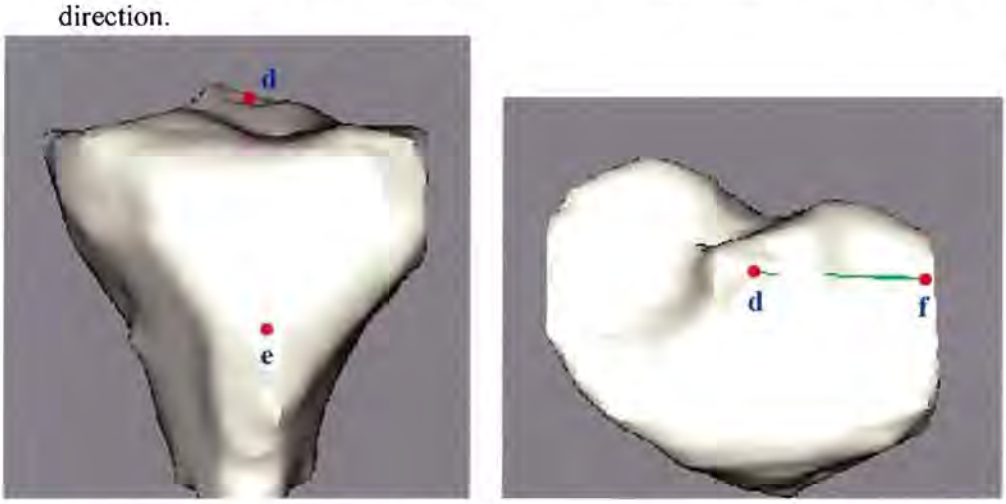

Figure10.9 The three points, d, e and f, used for setting up the measurement axes on the tibia.

The origin of the axes was chosen to be the highest point on the medial spine, as shown in Figure 10.10 below.

Figure 10.10 The origin of the tibial axes on the highest point of the medial tibial spine (blue).

This creates a set of axes where Z points proximally (positive), X points medially (positive) and Y points posteriorally (positive), as shown in Figure 10.11 below.

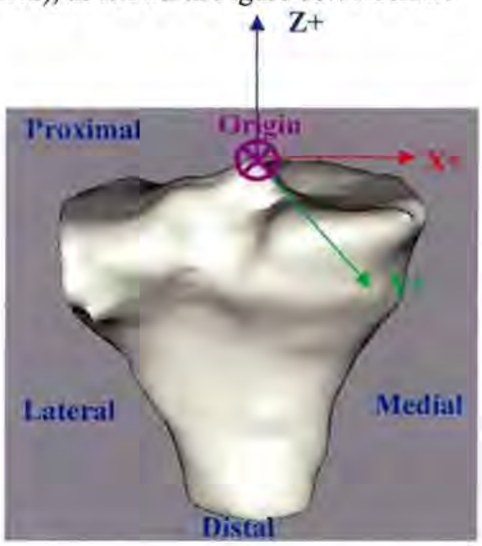

Figure 10.11 The reference axes on the tibia.

10.3.1.3 Axial Directions

Because of the peculiarities of the Arthron program, the two sets of axes, tibial and femoral, result in axes with X, Y and Z definitions as a left handed co-ordinate system, when viewing the bone from the posterior aspect. However, although a right handed system would be preferable, the two sets of axes are consistent with each other. To summarise, the following directions now apply:

- Positive X = medial; Negative X = lateral
- Positive Y = posterior; Negative Y = anterior
- Positive Z = proximal; Negative Z = distal

10.3.2 Discussion of the Reference Axes

These axes were simple to define, and measurements taken using them are intuitive to understand. However, it is important that the axes could be consistently set up, to ensure that comparable co-ordinate systems were being created for each model. Thus, a series of repeatability tests were performed to confirm that these axes could be consistently defined.

Three models were tested – two of healthy knees, and one of an ACL reconstruction knee. For each knee, five attempts were made to identify each of the points important to setting up the reference axes. These points are:

- Femoral condylar line – 2 points, *a* and *b*
- Tibial line from the mid-point of the tibial spines to the mid-point of the tubercle – 2 points, *d* and *e*
- The femoral origin – highest point in the anterior femoral notch
- Tibial origin – highest point of the medial tibial spine

The results of these repeatability tests are given below.

Table 10.4 Results of the repeatability tests for the reference axes measurements.

Point	Average Error over 5 Attempts [mm]									Average Overall Error [mm]
	Knee 1			Knee 2			Knee 3			
	x	*y*	*z*	*x*	*y*	*z*	*x*	*y*	*z*	
a	0.5	0.9	0.4	0.4	0.7	0.6	0.4	1.7	0.3	**0.7**
b	0.4	0.6	0.1	0.4	0.8	0.6	0.6	1.2	0.4	**0.6**
d	0.1	0.2	0.2	0.2	0.2	0.2	0.5	1.5	0.4	**0.4**
e	0.1	0.2	0.2	0.2	0.9	0.4	0.1	0.3	0.2	**0.3**
Femoral Centre	0.1	0.1	0.1	0.3	0.1	0.3	0.3	0.1	0.3	**0.2**
Tibial Centre	0.2	0.0	0.1	0.3	0.1	0.1	0.1	0.0	0.3	**0.6**

The error referred to is the difference between the average position of that point, and the position identified in each of the five attempts. This error is averaged over the five attempts, over all three knees, and over the x, y and z directions. Full details of the repeatability tests are given in Appendix C.

As can be seen from the results, each of the points is consistently and accurately identifiable, with average errors in identifying the same point five times not exceeding 0.7mm. This indicates that this method of setting up the axes is accurate and repeatable.

However there are still several shortcomings of this reference axis method. Due to a lack of anatomical knowledge, selection of points could be slightly different between different people, but this is difficult to measure. To address this issue, considerable care was taken to accurately set up the axes on each model.

The 3D models, although of good quality, sometimes lack detailed anatomical information that would make identification of points such as the tibial tuberosity easier. Also, lack of scan data, as mentioned previously, has limited the choices available for reference axes since only points in the centre of the knee joint can be used due to the absence of some medial, lateral, proximal and distal data. An increase in scan data both in terms of anatomical detail, and size of scan, would result in models which allow more reference axes options to be explored.

10.4 Measurements

Measurements were now taken on the models, in relation to the reference axes. Measurements of the tibial and femoral insertions of the ACL were taken on healthy knees. In the case of ACL reconstruction patients, measurements of the distal exit of the femoral tunnel, and the proximal exit of the tibial tunnel were taken. As mentioned previously, all right knees were mirrored around the XZ axis to form 'left' knees, so all knees are comparable to each other.

The ACL insertions were measured by selecting the four 'corner' points of the ligament, as illustrated in Figure 10.12 and 10.13 below. The most posterior proximal (1), anterior proximal (2), posterior distal (3) and anterior distal (4) points were selected on the femoral insertion of the ACL. The most anterior medial (5), anterior lateral (6), posterior medial (7) and posterior lateral (8) points were selected on the tibial insertion of the ACL.

Figure 10.12 The position of the ACL with respect to the femur, and the four 'corners' of the femoral insertion site (1 – 4).)

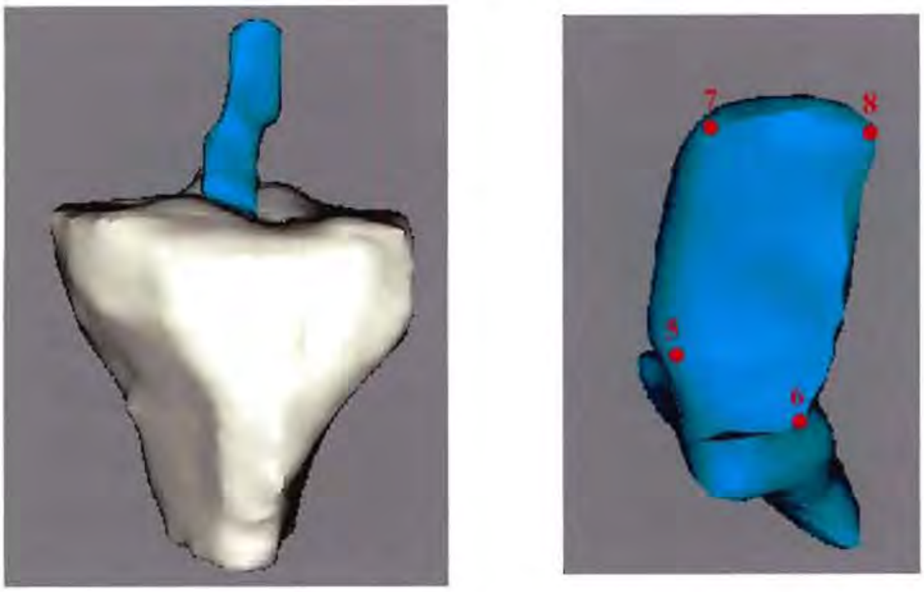

Figure 10.13 The position of the ACL with respect to the tibia, and the four 'corners' of the tibial insertion site (5 – 8).

These same four corners were selected on the tunnel exits on the femur and tibia, and are shown in Figures 10.14 below and 10.15 on the next page.

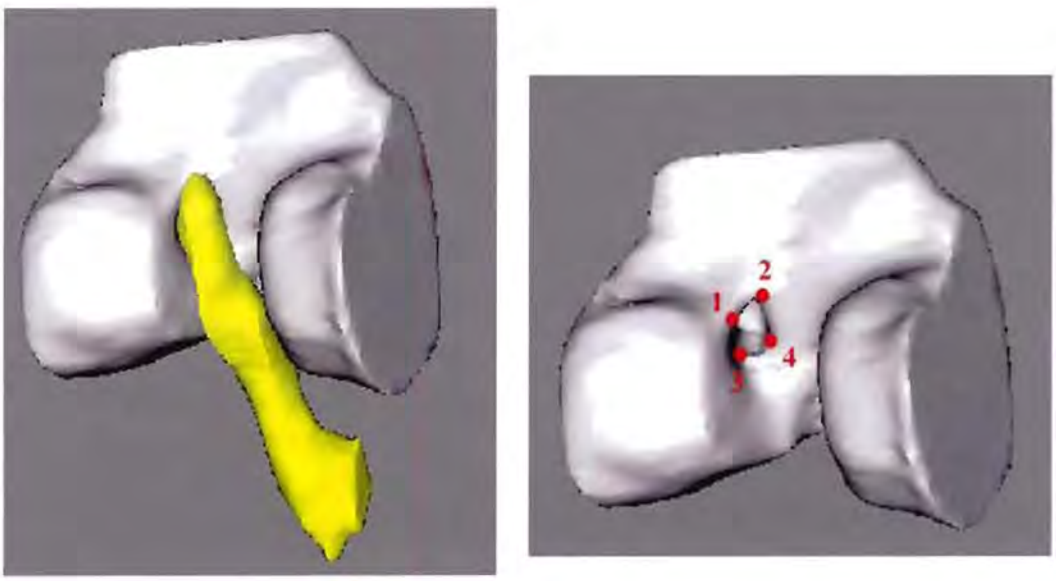

Figure 10.14 The position of the reconstructed ACL graft in the femur, and the four 'corners' of the femoral tunnel (1 – 4).

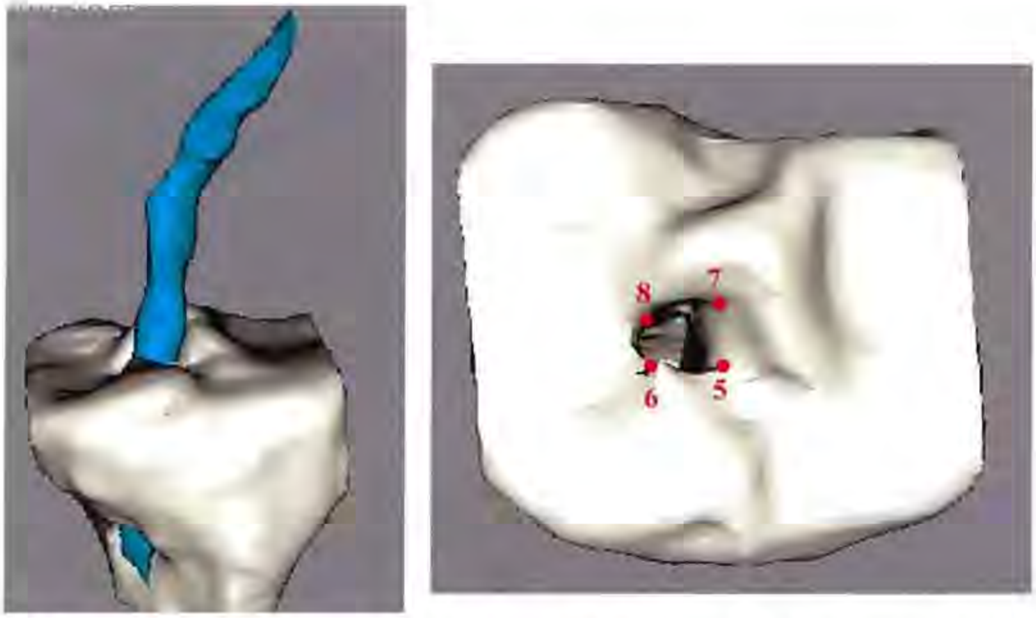

Figure 10.15 The position of the reconstructed ACL graft in the tibia, and the four 'corners' of the tibial tunnel (5 – 8).

The four points were then averaged to give an approximation of the centre of the ligament insertion or tunnel exit. For each patient, a set of tibial and femoral measurements was made for each knee.

10.4.1 Repeatability Tests

Once again, it was necessary to ensure that the measurements made of the ACL insertions and tunnels were repeatable and consistent. Thus a test of this repeatability was performed. One healthy and one reconstructed knee were chosen. On each of these knees, measurements of all the femoral and tibial points were made five times. The average position of each measurement was then compared to each of the five measurements to establish an average error in point identification. Full details of the repeatability tests can be found in Appendix C. The results are given below.

Table 10.5 Results of the repeatability tests for the measurement points on the tibia and femur.

	Average Error Measurements [mm]	
	Healthy Knee	**Reconstructed Knee**
Femoral Points:		
Posterior Proximal	0.1	0.3
Anterior Proximal	0.5	0.7
Posterior Distal	0.1	1.1
Anterior Distal	1.11	0.7
Average Femoral Error	**0.4**	**0.7**
Tibial Points		
Anterior Medial	0.2	0.4
Anterior Lateral	0.1	0.3
Posterior Medial	0.6	0.1
Posterior Lateral	0.2	0.1
Average Tibial Error	**0.3**	**0.2**
Average Overall Error	**0.3**	**0.4**

Once again, the error results are very low – below 0.5 mm – indicating that the measurement of these points is consistent and repeatable.

10.4.2 Normalisation

Every person's knee is a different size. Thus, the measurements taken above were not comparable until this difference in size had been accounted for. It was decided that one normalising measurement should be made on both the femur and tibia.

The measurement for the femur was a line drawn from the highest point of the femoral notch posteriorly, to the highest point of the intra-condylar groove anteriorly. In other words, an AP measurement of the thickness of the femur at the femoral notch, as shown in Figure 10.16 below.

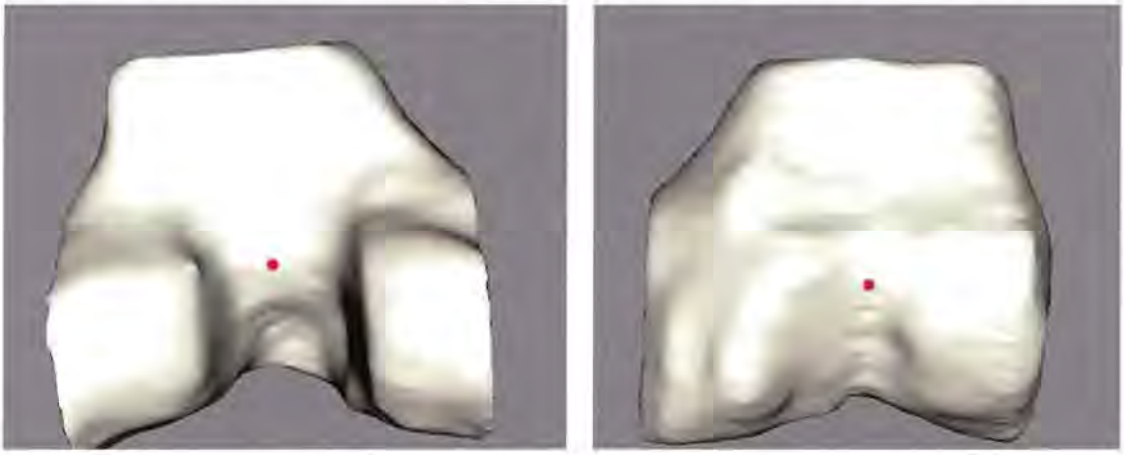

Figure 10.16 The starting (left) and ending (right) points of the AP normalising measurement in the femur.

The measurement for the tibia was a line drawn on the medial side of the tibia through the middle of the tibial plateau, from the most anterior to the most posterior point. In other words, an AP measurement of the size of the tibial plateau, as shown in Figure 10.17 below.

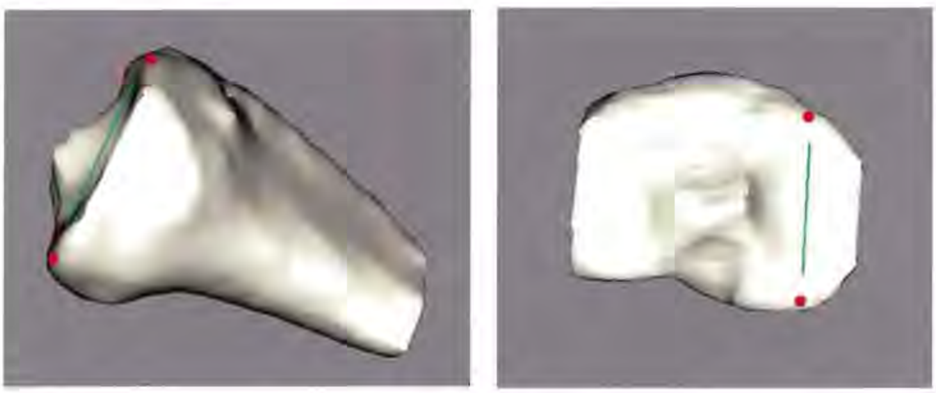

Figure 10.17 The AP normalising measurement in the tibia.

For the femur, the position of the centre of the ACL insertion, or tunnel exit, (as calculated above) was divided by the femoral normalising measurement to create a percentage value. The same procedure was followed with the tibia to create final ACL insertion, or tunnel exit measurements, that are independent of size.

10.4.2.1 Repeatability Tests

Repeatability tests were performed to ensure that these normalising measurements were consistently and repeatably performed. Two knees were chosen, and five measurements of both the femoral and tibial normalisation measurements were made. These were averaged, and each measurement was compared to the average to give an error value in the measurement. Full details of the repeatability tests can be found in Appendix C. The results are given below.

Table 10.6 Results of the repeatability tests for the normalising measurements.

	Average Error Measurement [mm]	
	Knee 1	**Knee 2**
Femur	0.2	0.1
Tibia	0.4	0.3
Average Error	0.3	0.2
Average Overall Error	**0.2**	

With an average error well below 0.5mm, the repeatability tests show that the normalisation measurements are consistently and accurately identified.

10.4.3 Discussion of the Measurement Procedure

As the repeatability tests have shown, each step of the measurement procedure, from setting the reference axes to making and normalising the measurements has been rigorously tested to check that points are consistently and accurately identifiable. Also, the process of averaging the four 'corners' of the ACL or tunnel is a good method of eliminating variation in individual point measurement, as the final figure used is an average value which will be more independent of this variation.

However, some models did prove more difficult to measure than others. Especially for the ACL reconstruction knees, the start of the femoral tunnel was sometimes difficult to see, due to the fact that the roof of the tunnel started further anteriorally on the bone than the tunnel itself, as shown in Figure 10.18 on the next page. This was either due to inaccuracy in reconstruction of the 3D models, or the fact that the tunnel had been drilled like this in surgery. The tibial tunnel exit was clearly identifiable and measurement of this tunnel was consistent.

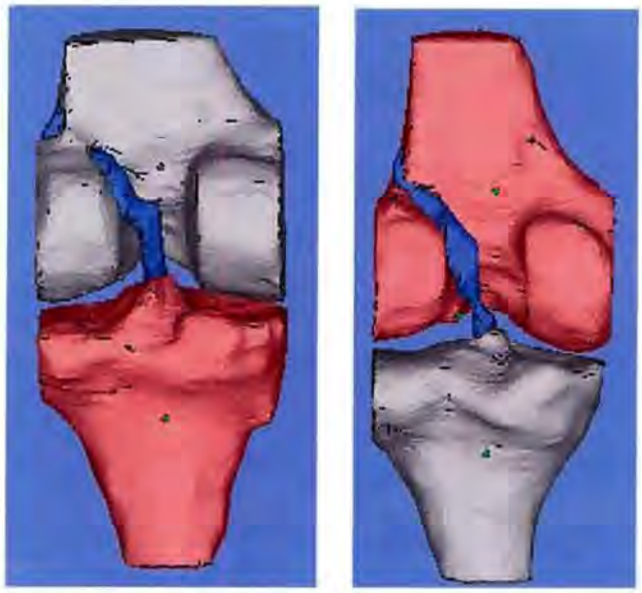

Figure 10.18 Examples of two reconstructed knees where the start of the femoral tunnel is difficult to distinguish.

Another problem was the variation in ACL insertion site anatomy. This has been shown to be a characteristic of the ACL, but still meant that the four 'corners' of the insertion sites were slightly different in some cases. Again, the averaging of the four points to create a central measurement should eliminate a lot of this measurement uncertainty.

Despite these few problems contributing to some variation and uncertainty in measurement, the procedure in general was undertaken carefully to produce useful results.

11 RESULTS AND STATISTICAL ANALYSIS OF 3D KNEE MODELS

Following the successful set up of the reference axes on each model, and the verification of the measurement and normalisation protocols, measurements were made on each of the 52 models. This chapter presents the results of those measurements, and discusses the statistical analysis performed on them to answer the four main questions of this section of the thesis.

11.1 Measurement Results

For the 13 healthy subjects, each model's co-ordinate system was set to that of the reference axes. Measurements of the ACL's femoral and tibial insertions were made using the protocol described in Section 10.4. Normalising measurements of the tibia and femur were then made, as discussed in Section 10.4.2. The final values for the normalised centres of the ACL's femoral and tibial attachments are given below.

Table 11.1 The normalised measurements of the centre of the ACL insertions in healthy knees.

Subject	Normalised ACL Insertion Measurements [%]											
	Left Femur			Left Tibia			Right Femur			Right Tibia		
	x	*y*	*z*	*x*	*y*	*z*	*x*	*y*	*z*	*x*	*y*	*z*
MR	-20.8	33.8	39.5	-3.9	-33.8	39.5	-22.8	64.7	30.3	0.7	-64.7	30.3
SD	-23.5	63.8	37.5	-3.0	-63.8	37.5	-21.5	64.2	40.8	-0.5	-64.2	40.8
JT	-14.2	59.3	35.9	1.5	-59.3	35.9	-19.6	58.7	30.0	1.1	-58.7	30.0
AR	-23.2	65.4	31.1	2.4	-65.4	31.1	-18.4	56.9	38.1	-2.1	-56.9	38.1
MB	-21.8	57.6	38.8	4.4	-57.6	38.8	-23.4	46.9	41.1	-4.5	-46.9	41.1
AH	-15.7	58.9	41.6	2.4	-58.9	41.6	-25.1	64.0	41.1	0.9	-64.0	41.1
AC	-17.3	13.5	28.8	-1.3	-13.5	28.8	-36.2	65.4	43.2	-5.7	-65.4	43.2
AW	-24.5	58.6	43.1	-9.1	-58.6	43.1	-25.7	56.8	40.1	-6.9	-56.8	40.1
DS	-21.1	57.6	33.9	2.2	-57.6	33.9	-19.3	51.3	45.8	-0.9	-51.3	45.8
EE	-22.9	35.5	40.9	12.5	-35.5	40.9	-23.2	55.9	43.1	8.3	-55.9	43.1
A1	-10.3	66.3	39.5	2.1	-66.3	39.5	-14.8	67.1	40.7	-1.4	-67.1	40.7
A2	-21.4	61.1	38.0	-0.4	-61.1	38.0	-18.3	58.4	33.0	-0.8	-58.4	33.0
A3	-22.4	61.7	54.0	0.1	-61.7	54.0	-18.6	56.3	43.9	-1.7	-56.3	43.9
Mean	-19.9	53.3	38.7	0.8	-53.3	38.7	-22.1	59.0	39.3	-1.0	-59.0	39.3
Std. Deviation	4.3	15.7	6.2	5.0	15.7	6.2	5.3	5.9	5.1	3.7	5.9	5.1

For the 13 ACL patients, each model's co-ordinate system was set to that of the reference axes. On each healthy knee, the ACL's femoral and tibial insertions were measured. On each reconstructed knee, the position of the femoral and tibial tunnel exits were measured. Normalising measurements of the tibia and femur were made on each model. The final values for the normalised centres of the ACL's femoral and tibial attachments, or tunnel exits, are given below.

Table 11.2 The normalised measurements of the centre of the exit of the femoral and tibial tunnels in the patients' knees.

Subject	Normalised Tunnel/ACL Insertion Measurements [%]											
	Reconstructed Femur			Reconstructed Tibia			Healthy Femur			Healthy Tibia		
	x	*y*	*z*	*x*	*y*	*z*	*x*	*y*	*z*	*x*	*y*	*z*
AB	-14.0	47.3	54.4	-7.7	-47.3	54.4	-16.2	63.1	31.3	1.6	-63.1	31.3
MB	-23.1	44.3	53.0	5.4	-44.3	53.0	-20.3	21.1	48.3	-2.0	-21.1	48.3
SL	-15.3	56.8	47.7	0.5	-56.8	47.7	-16.3	50.9	32.7	0.9	-50.9	32.7
TC	-23.6	36.4	59.8	11.0	-36.4	59.8	-21.5	47.6	37.8	4.2	-47.6	37.8
LB	-26.2	38.8	63.0	5.1	-38.8	63.0	-33.5	47.0	44.4	0.7	-47.0	44.4
CW	-17.8	48.5	42.7	-0.2	-48.5	42.7	-19.6	26.2	39.0	-0.3	-26.2	39.0
CvK	-26.5	51.1	49.1	2.0	-51.1	49.1	-23.4	60.1	41.8	5.2	-60.1	41.8
IR	-18.7	49.1	63.1	9.6	-49.1	63.1	-24.1	53.3	40.5	4.7	-53.3	40.5
JS	-14.8	47.1	47.2	13.0	-47.1	47.2	-14.2	57.2	37.5	4.2	-57.2	37.5
MV	-19.4	52.0	49.6	15.1	-52.0	49.6	-30.2	64.0	35.2	22.3	-64.0	35.2
BB	-9.3	48.3	47.4	-4.1	-48.3	47.4	-18.8	54.0	40.4	-7.3	-54.0	40.4
RvS	-19.1	52.4	52.8	0.6	-52.4	52.8	-18.4	55.9	37.7	5.7	-55.9	37.7
CP	-15.2	3.6	-1.0	1.9	-3.6	-1.0	-10.4	9.4	-18.0	6.6	-9.4	-18.0
Mean	-18.7	44.3	48.4	4.0	-44.3	48.4	-20.5	46.9	34.5	3.6	-46.9	34.5
Std. Deviation	5.1	13.4	16.1	6.7	13.4	16.1	6.3	17.1	16.4	6.8	17.1	16.4

From examination of the results, a high variability between people can already be observed. Statistical Analysis of the data was now performed.

11.2 Statistical Analysis

The statistical analysis was performed in Statistica. The test chosen was a 2-way ANOVA (Analysis of Variance) test. Tests were performed on the femoral and tibial data separately. The data was grouped in the following way:

- Subjects who had had reconstruction on one knee were labelled as group 'ACL'.
- Healthy subjects were labelled as group 'Control'.
- The knees were grouped as either 'Ipsilateral' or 'Contralateral'.
- 'Ipsilateral' is the reconstructed knee of ACL patients, and the left knee of healthy subjects.
- 'Contralateral' is the healthy knee of ACL patients, and the right knee of healthy subjects.

The results were analysed further with Tukey HSD post-hoc tests, to answer the four major questions, as discussed in detail below. Results were considered significant if $p<0.005$.

11.2.1 Individual Variation in ACL Insertion Position

The first question to be answered was simply "How much does the insertion position of the ACL differ between healthy people?" To answer this, a basic statistical analysis of the tibial and femoral data in the healthy subjects was performed. This resulted in figures for the variability between different people. The data for the tibia and femur are given below in Tables 11.3 and 11.4 and Figure 11.1 and 11.2.

Table 11.3 The variation of the femoral insertion site (%) in healthy knees.

	Mean	Minimum	Maximum	Std. Deviation
Femur x	-21.0	-36.2	-10.3	4.8
Femur y	56.1	13.5	67.1	12.0
Femur z	39.0	28.8	54.0	5.6

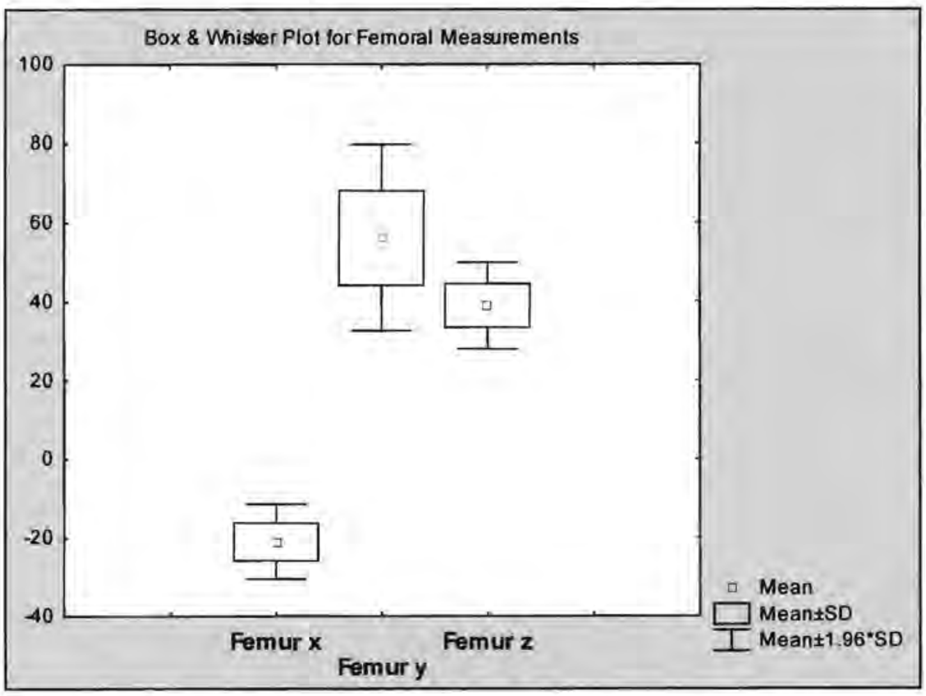

Figure11.1 A Box and Whisker plot showing the mean, standard deviation and 95% confidence levels of the femoral insertion site in healthy subjects.

Table 11.4 The variation of the tibial insertion site (%) in healthy knees.

	Mean	Minimum	Maximum	Std. Deviation
Tibia x	-0.1	-9.1	12.6	4.4
Tibia y	-56.1	-67.1	-13.5	12.0
Tibia z	39.0	28.8	54.0	5.6

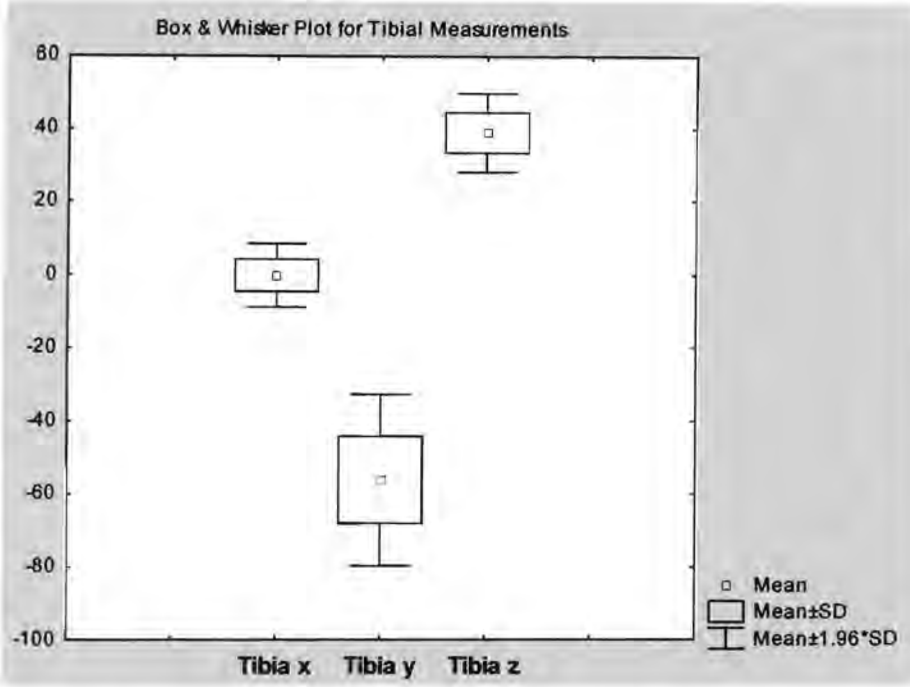

Figure11.2 Box and whisker plot showing the mean, standard deviation and 95% confidence levels for the tibial insertion site in healthy subjects.

These box and whisker plots illustrate the data for the femoral and tibial x, y and z co-ordinates respectively. The bigger boxes represent the standard deviation of the measurements, and the 'whiskers' represent 1.96 times the standard deviation, which is the 95% normal confidence interval for individual observations around the mean.

11.2.1.1 Discussion of Results

As the plots and data illustrate, there is quite a large variation between different knees for both femoral and tibial data. Comparing the minimum and maximum values for each measurement gives a good idea of the range of placements of the ligament. For instance, subject A could have a femoral insertion which lies at 13.5% in the AP direction (y co-ordinate). Subject B could have a femoral ACL insertion which lies at 67% in the AP direction. This is an extremely large variation, which could be due to some measurement errors etc. This could also be an 'outlier' or exceptional case. However, even if only half of this variation is present, it still illustrates the point that one, standard anatomical placement should not be prescribed for each and every patient. No two people are alike, and similarly, neither are their ACLs. An individualised anatomic placement for each patient must arguably provide the best reconstruction for each person. Clearly, if anatomic ACL reconstruction is to be pursued, it must be anatomic for each person individually.

11.2.2 The Bi-lateral Symmetry of ACLs

If the healthy ACL position is to be used to provide a surgeon with a good anatomic idea of where his reconstruction should be placed in the damaged knee, it must first be established that the ACL is symmetrical in left and right knees i.e. that the ACL in each knee is in a similar position. In order to verify this, a post-hoc analysis was performed examining the position of the ACL in the x, y and z directions, for the tibia and femur, in each of the healthy subjects. The results of this analysis are given below.

Femur:

- **x-values:** no significant difference ($p = 0.9999$)
- **y-vales:** no significant difference ($p = 0.8206$)
- **z-values:** no significant difference ($p = 1.0000$)

Tibia:

- **x-values:** no significant difference ($p = 0.9958$)
- **y-values:** no significant difference ($p = 0.9999$)
- **z-values:** no significant difference ($p = 0.9794$)

11.2.2.1 Discussion of Results

These results indicate that there is no significant difference in the position of the ACL in the left and right knees of the same subject for either tibia or femur. This means that, as expected, the ACL is symmetrical between both knees. These results can be seen in the Box and Whisker plots in Figures 11.3 and 11.6.

Since the symmetry of the ACL has now been proven, it shows that for a patient who has torn one ACL, the position of the ACL in the other, undamaged knee can be used in pre-operative planning. This will give the patient a precise anatomical reconstruction which is individualised for his particular anatomy.

11.2.3 Position of the ACL in Patients who have had ACL Reconstruction

The next question to be answered is whether the healthy knee of people who have undergone an ACL reconstruction (in the other knee) is similar to other healthy people's knees. In other words, is there any difference in the placement of the ACL between the healthy knee, and other normal subjects who have had no ACL damage in either knee.

Answering this question serves two purposes. Firstly, it verifies that there is no difference between the models made for the healthy and ACL groups. If the ACLs all lie in the same positions, then it can be assumed that all the models are comparable to each other. This is important in answering the next question.

However, answering the question also verifies the fact that anatomically, there is no difference between those 'prone' to tearing an ACL, and those who have had no damage to their ACLs.

For this purpose, the contralateral (healthy) knees of the ACL reconstruction group were compared to both knees of the healthy subjects group, and the results are given below. The results can be seen visually in the Box and Whisker plots in Figures 11.3 and 11.6.

Femur:

- **x-values:** no significant difference ($p=1.0000$ (L); $p = 1.0000$ (R))
- **y-values:** no significant difference ($p= 0.9558$ (L); $p = 0.7711$ (R))
- **z-values:** no significant difference ($p = 0.9986$ (L); $p = 0.9997$ (R))

Tibia:

- **x-values:** no significant difference ($p = 0.9890$ (L), $p = 0.9617$ (R))
- **y-values:** no significant difference ($p = 0.9999$ (L), $p = 0.9993$ (R))
- **z-values:** no significant difference ($p = 0.9318$ (L), $p = 0.9881$ (R))

11.2.3.1 Discussion of Results

The results show that there is no significant difference between the healthy knees in the two groups. This indicates that there is no significant difference between the position of the ACL in either healthy knee of the control group, and the healthy knee of patients in the ACL group i.e. all healthy ACLs are in approximately the same position, regardless of whether the other knee underwent ACL reconstruction, as expected.

Thus these results verify that the two groups (ACL reconstruction and healthy) are comparable to each other, and that there is no underlying anatomical difference that makes any particular person prone to tearing their ACL.

11.2.4 Placement of ACL Reconstruction Tunnels

Accuracy of comparison between the groups has been verified. The question can now be asked "How well are ACL tunnels placed currently?" In order to answer this question, the reconstructed knees were compared with the healthy knees for each subject in the ACL reconstruction group. The benchmark used for a 'good' reconstruction is one which is placed in the same position as the healthy ACL of the opposite knee.

All the reconstructions have been performed by Dr van der Merwe, who is an experienced orthopaedic surgeon. All of the patients in this group are clinically successful, and in terms of conventional analysis of the reconstructions, have had well performed surgeries. The results of the comparisons between legs for the femoral positions are given below, and can be seen in the Box and Whisker plot in Figure 11.3.

11.2.4.1 Femoral Results

- **x-values:** no significant difference ($p = 0.9999$)
- **y-values:** no significant difference ($p = 0.9995$)
- **z-values:** **significant difference** ($\boldsymbol{p = 0.0035}$)

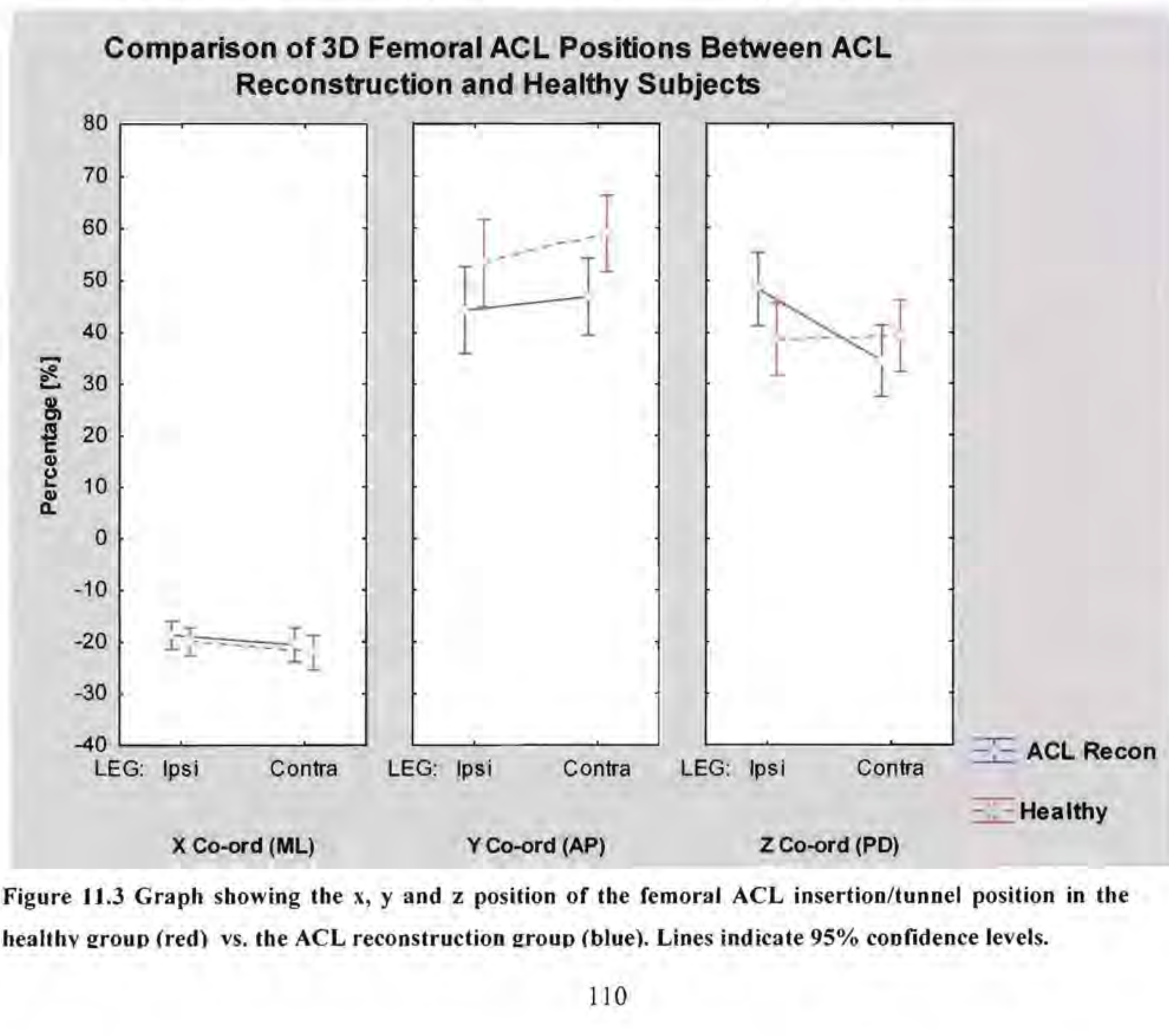

Figure 11.3 Graph showing the x, y and z position of the femoral ACL insertion/tunnel position in the healthy group (red) vs. the ACL reconstruction group (blue). Lines indicate 95% confidence levels.

11.2.4.2 Discussion of Femoral Results

For the femur, the results indicate that, on the whole, the tunnels in the study were placed well i.e. that they matched anatomically with the position of the original ACL. This is true for the x (mediolateral) and y (anterioposterior) co-ordinates. However, the z-values show a difference between the healthy and reconstructed positions. Examination of the graph shows that the z values are more positive for the reconstructed (ipsilateral) knees than the healthy (contralateral) knees. This means that the tunnel is drilled more proximally on the femur than the ACL inserts. This relationship can also be observed in the models, as shown in Figure 11.4 below.

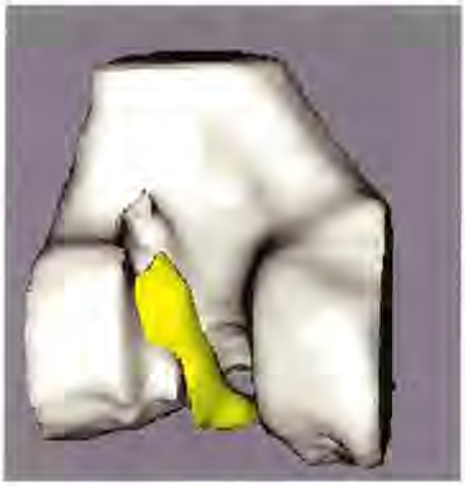

Figure 11.4 Model showing the natural ACL (yellow), super-imposed on the ACL reconstructed femur. The tunnel is higher than the ACL insertion.

From examination of the literature, it does seem that even surgeons who aim for an 'anatomical' reconstruction specify a tunnel position which is higher than the position of the native ACL. For example, Markolf *et al.* (2002) say the best position for the femoral tunnel based on anatomical reconstruction is 11 o'clock. However, Arnold *et al.* (2002) say the position of the natural ACL spreads from 7.30 to 11 o'clock. Thus, the problem would seem to be that drilling a single hole cannot replicate the extent of coverage of the natural ACL footprint. Double bundle ACL reconstruction has been proposed as a solution to this, but is beyond the scope of this thesis.

Discussion with the surgeon revealed that he deliberately aims to drill his tunnels higher in the femoral notch than the attachment of the ACL. This could be warranted, since when the position of the *graft* (not tunnel) is examined on the models, it does line up well with the position of the healthy ACL (transposed onto that knee), as seen in Figure 11.5 on the next page.

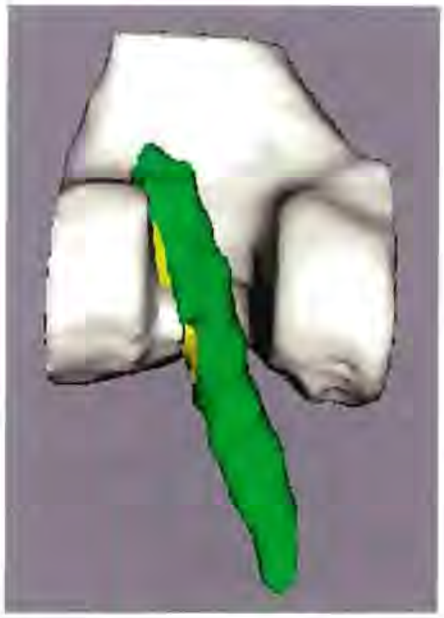

Figure 11.5 The ACL graft (green) super-imposed on the natural ACL (yellow) shows that the graft and ACL line up well despite the tunnel being drilled higher than the ACL insertion.

These results are interesting, and leave the debate open as to whether the tunnel positions chosen by surgeons should be changed or not.

The results for comparison of the tibial measurements on the healthy and reconstructed knees are given below and shown in the Box and Whisker plot in Figure 11.6 on the next page.

11.2.4.3 Tibial Results

- **x-values** no significant difference ($p = 1.0000$)
- **y-values** **significant difference** (**$p = 0.0040$**)
- **z-values** no significant difference ($p = 0.2342$)

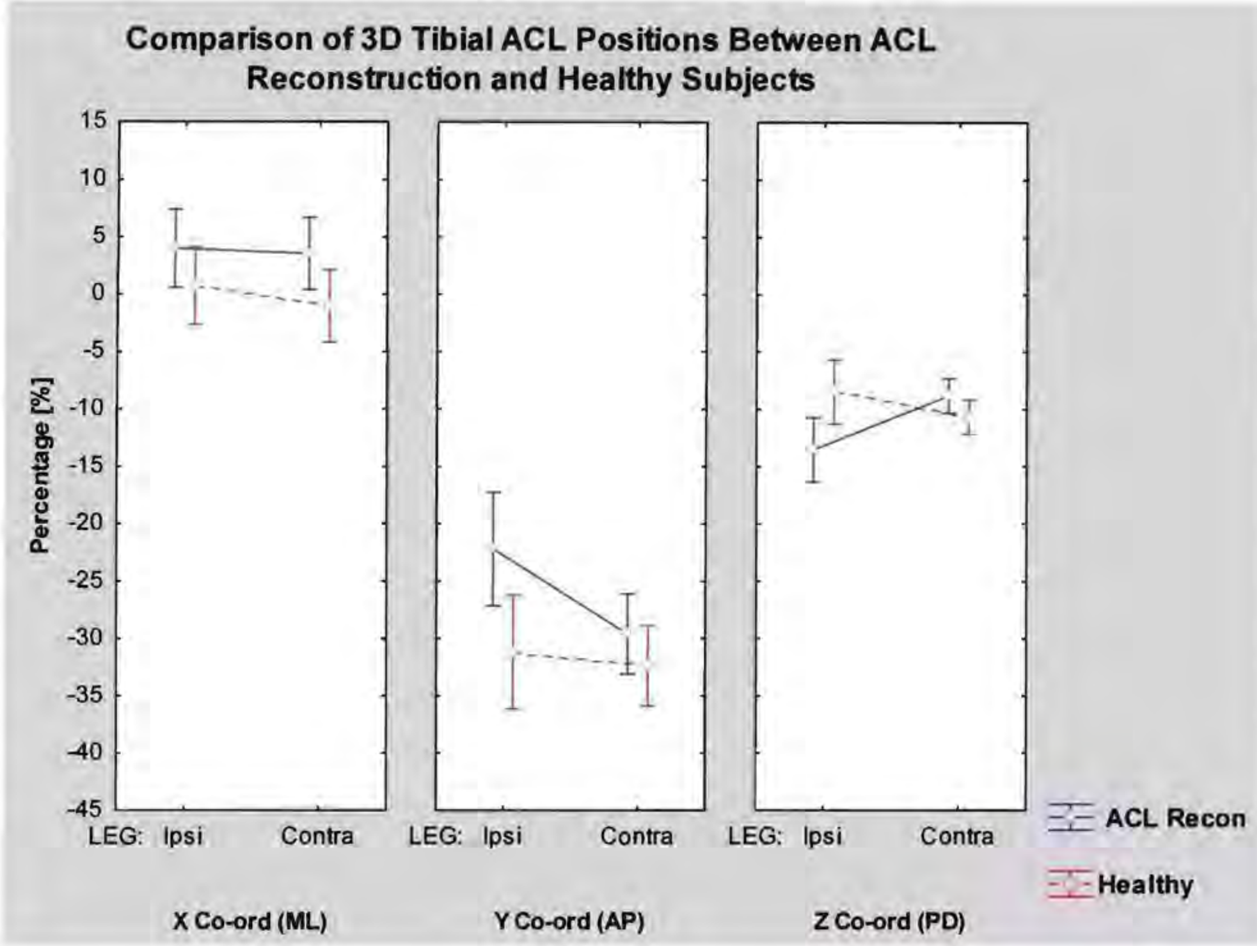

Figure 11.6 Graph showing the x, y and z position of the tibial ACL insertion/tunnel position in the healthy group (red) vs. the ACL reconstruction group (blue). Lines indicate 95% confidence levels.

11.2.4.4 Discussion of Tibial Results

For the tibia, the results again indicate that on the whole the tunnel is placed well i.e. matches with the position of the healthy ACL. This is true for the x (mediolateral) and z (proximodistal) co-ordinates. However, there is a difference in placement for the y (anteroposterior) co-ordinate. Examination of the graph shows that the y values are more positive for the reconstructed (ipsilateral) knee than the healthy (contralateral) knee. This means the tunnel is placed more posteriorly than the attachment of the native ACL.

Examination of the models shows that in general, the size of the tunnel is smaller than the size of the ACL attachment, as shown in Figure 11.7 on the next page. The tunnel is usually drilled in the most posterior part of the attachment. However, since the natural ACL's footprint extends anteriorally from this position, its centre (the value used in this comparison) will be more anterior than the tunnel's centre. As with the femoral results, it can be seen that the tunnels are placed accurately. However this difference in tunnel vs. footprint size results in the measurement discrepancy.

Figure 11.7 The natural ACL (blue) super-imposed on the ACL reconstructed tibia showing how the tibial footprint extends posterior to the tibial tunnel.

Discussion with the surgeon revealed that he does aim to place his tunnel in the posterior part of the footprint. He also said that many surgeons place their tunnel even further posterior than this, aiming for the centre of the tibial spines.

Again, on examination of the *graft* as opposed to the tunnel position, it seems that the reconstructed and natural ACLs line up well (when super-imposed on each other), as shown in Figure 11.8 below. Perhaps this indicates that current tunnel positions are effective. Again, perhaps double bundle ACL reconstruction would address the problem of small tunnel size compared to natural ACL footprint.

Figure 11.8 The ACL graft (green) super-imposed on the natural ACL (blue) shows how the two line up well despite the tunnel being more anterior than the ACL insertion.

12 CONCLUSIONS

In this chapter, the results are used to draw conclusions for the two sections of the thesis.

12.1 Feasibility of Adapting the Image Guided Neurosurgery System for Orthopaedic Surgery

The overall goal of this section was to decide whether the image guided neurosurgery system could be adapted for use in an orthopaedic setting, specifically for ACL reconstruction surgery, and what this adaptation would entail. This question was answered in four sections.

12.1.1 The Use of Bony Anatomical Landmarks and MRI Scans

The problem to be addressed here is the fact that the neurosurgery system uses surface fiducials and CT scans for registration. This is not feasible in knee surgery. The proposed solution to this problem was to use bony anatomical landmarks and MRI scans for registration.

During the various feasibility tests, with dry bones, plastinated specimens and a cadaver leg using MRI images, good accuracy results were obtained:

For the bones registered together, the best accuracy attained was 2.5 mm, averaged over all the combinations of landmarks used for the plastinated specimen test (Chapter 6).For the bones registered separately, the best accuracy for the femur was 1.4 mm, and for the tibia was 2.2 mm, for the plastinated specimen test (Chapter 6).For the cadaver test, the accuracies were 2.2 mm for the femur and 4.8 mm for the tibia (Chapter 7).

Of these 'best results', the highest error is 4.8 mm. As discussed in Chapter 7, there were contributing factors to this error apart from the registration process, such as difficulty keeping the tibia still and a slightly bent navigation probe. The slice width (3 mm) of the MRI scans could also contribute to higher inaccuracies.

As discussed in Chapter 4, accuracies better than 5 mm indicate a feasible system, and accuracies around 2 mm indicate that a good precision has been attained. Considering this, it seems clear from these accuracy results that registration using bony landmarks and MRI scans is indeed feasible, and for the femur, excellent. The cadaver test proves that these landmarks can be reached arthroscopically, and identified on MRI, and the accuracy they provide in these preliminary feasibility studies indicates that they are suitable for use in orthopaedic navigation.

Thus, the conclusion drawn from the results is that bony anatomical landmarks and MRI scans can be used for registration.

12.1.2 The Best Landmarks for Registration

Various combinations of landmarks were tested to determine which would give the best accuracy of registration.

The first of these tests was registering the tibia and femur together using five landmarks, 3 femoral landmarks and 3 femoral landmarks with 2 tibial skin markers (Chapter 6) The accuracy results for these tests indicate that registration without the two tibial spines results in a better overall registration. However, since few bony landmarks are available arthroscopically, it also seems impossible to reject these points as tibial landmarks.

Further tests with the dry bone specimen indicated that three landmarks on the femur, and three on the tibia provide enough spatial information to register each bone separately (Chapter 5).

Further tests were performed to determine a suitable third tibial landmark. Use of the centre of the medial tibial plateau resulted in registration with errors too large to be measured (Chapter 6). However, use of the tibial tuberosity, palpated cutaneously, resulted in accuracies of 2.2 mm for the plastinated specimen, which is within an acceptable range for initial tests (Chapter 6).

Thus, the final conclusion as to which landmarks are most suitable for registration is:

Femoral Landmarks:

1. *Highest point of the articular surface, laterally*
2. *Highest point of the articular surface, medially*
3. *Highest point of the femoral notc.*

Tibial Landmarks:

1. *Lateral tibial spine*
2. *Medial tibial spine*
3. *Tibial tuberosity*

12.1.3 Movement of the Knee During Surgery

A major problem in adapting the neurosurgery system for use in ACL reconstruction surgery is that the knee is constantly being manipulated. Registration can only be maintained if the bones are held still, or if trackable frames are drilled into them to account for their movement (as in current navigated ACL reconstruction systems).

However, an aim of this project was to come up with a solution to the problem of movement whilst at the same time avoiding the invasive process of using trackable frames. The first solution to this was to register both bones together and keep them still during surgery. However, on consultation with the orthopaedic surgeon, this was deemed impractical in terms of the surgical environment.

A final solution was decided on as registering the tibia and femur separately. Each bone is registered, held still, and the required tunnel position information is gained from the navigation system, and marked on the bone. The bone can then be manipulated, but must be re-registered if further navigational information is required.

This has several advantages in that it reduces the invasiveness currently found in ACL navigation systems. It also provides the surgeon with the necessary navigational information to improve the reconstruction. However, it does not over-complicate the surgery, or the operating theatre environment, and the system can be removed as soon as the necessary information is obtained. Thus it is a simple solution, which is not invasive to the surgeon's normal operating practice.

Thus, the final conclusion is that this solution to the movement of bones is both feasible, and possibly an improvement on current systems.

12.1.4 Practicality of the System in Surgery

The overall test of the feasibility of the system was to subject it to the typical surgical environment. This was done using a cadaver knee, with an orthopaedic surgeon performing the registration and navigation procedure (see Chapter 7).

The accuracy results of this test (2.2 mm for the femur and 4.8 mm for the tibia) were acceptable for a preliminary trial of the system. Feedback from the orthopaedic surgeon also indicated that the system was practical to use in surgery – it was easy to operate, the necessary steps could be completed without interfering in the surgery, and the necessary navigational information was provided.

Thus the final conclusion for use of this modified neurosurgery system in orthopaedic surgery is that it is practical and feasible to use.

12.2 Creation and Analysis of 3D Models of MRI Scans

The overall goal of this section of the thesis was to use accurate 3D models of the knee to perform anatomical studies on healthy ACLs and knees which had undergone ACL reconstruction. Conclusions are made about the process used to create the 3D models. Conclusions are also made about the four main questions posed at the beginning of the study.

12.2.1 Measurement Procedure

Various different aspects of the procedure of creating and analysing the 3D models were examined. A scan protocol for creating 3D models was developed, as well as a procedure for creating smooth models. A procedure for creating a consistent co-ordinate system was developed, as well as methods for measuring the ACL insertion/tunnel position and for making normalising measurements.

The conclusions are:

- *The best scan protocol for creating 3D models using the Esaote E-scan is a Sagittal T2 Spin Echo scan with 2mm slice thickness, and TR = 4960ms, TE = 80ms.*

- *The best smoothing algorithm to apply in Magics is:*

    - *Smoothing Procedure:*
        - *Smoothing Factor:* *0.5*
        - *Shrinkage Compensation Factor:* *-0.5*
        - *Iterations:* *15*

    - *Filter sharp triangles with default values.*
    - *Triangle Reduction with default values.*

- *The method for creating a co-ordinate system discussed in Section 10.3 is the best method that can be applied to these 3D models.*

- *The measurement protocol outlined in Section 10.4 can be accurately and repeatable applied and gives good results.*

12.2.2 Individual Variation in ACL Insertion Position

The first aspect of ACL anatomy examined was how much the position of the ACL differs between various people. With the standard deviation of measurements varying between 4.4% and 12%, a wide variation between different people can be seen for both the tibia and femur. This certainly indicates that using a standard placement of ACL reconstruction tunnel for all people will not result in a good, anatomical reconstruction for everyone treated.

Thus, the conclusion is that there is a wide variation of ACL tunnel position between people indicating that individualised anatomical placement of the reconstructed ACL is advisable.

12.2.3 The Bi-lateral Symmetry of ACLs

The question to be answered here is whether the ACL insertions in the left knee are symmetrical to those in the right knee, for healthy knees. The statistical analysis shows no significant difference between the insertion positions of the ACL (x, y and z co-ordinates) between the left and right knees of the same subject. This information indicates that the insertion position in an undamaged knee can be used to give the surgeon an accurate idea of where to place the graft in a repair of the damaged knee.

Thus it can be concluded that the ACL is bi-laterally symmetrical, and that the healthy ACL can thus be used to guide the surgeon in the repair of a damaged ACL in the opposite knee.

12.2.4 The Position of the Healthy ACL in Patients who have had ACL Reconstruction

The issue addressed here is whether the healthy ACL position in a person whose other knee has had an ACL reconstruction, is the same as the ACL position in people who have not torn an ACL in either knee. The statistical analysis showed no significant difference between the two groups of ACL positions. This information shows that the two groups of models can be compared to one another, and that people who have torn one ACL are no different anatomically to those who have never torn an ACL.

The conclusion is that all healthy ACLs have insertions in similar positions. Thus the two groups of models can be compared to each other, and there is no anatomic predisposition to tearing an ACL.

12.2.5 Placement of ACL Reconstruction Tunnels

The fourth analysis undertaken was a comparison between the healthy and reconstructed knees of the ACL reconstruction group of subjects. The point of this comparison was to ascertain whether the tibial and femoral tunnels in the ACL reconstructed knees had been drilled in the same position as the ACL inserts in the healthy knees.

The statistical analysis showed that on the whole, the tunnels were accurately anatomically placed. However, the femoral tunnels were placed more proximally than the ACL insertions, and the tibial tunnels were placed more posteriorly than the ACL insertions. This was confirmed by the orthopaedic surgeon as being his surgical practice.

Thus a conclusion can be made that ACL reconstruction tunnels are placed more proximally than the femoral insertion and more posteriorally than the tibial insertion. However, no conclusion can be made as to how effective the resulting reconstruction is.

13 RECOMMENDATIONS

On the basis of the conclusions, the following recommendations for each section of the thesis are made.

13.1 Feasibility of Adapting the Image Guided Neurosurgery System for Orthopaedic Surgery

In order to produce a commercially viable system, the following steps should be taken:

13.1.1 Use Thinner MRI Slices

In order to improve the accuracy of the system, trials using MRI slices of 2 mm or below should be performed. Although this may alter the routine clinical MRIs used, and lengthen the time for each scan, a compromise should be made since it is possible that thinner slices will improve the navigation accuracies.

13.1.2 Eliminate Tibial Spines as Landmarks

Although the use of the tibial spines provides sufficient accuracy for a prototype system, in general, they prove difficult to identify using the probe. Although it seems unlikely that other suitable tibial landmarks can be found, alternative tibial landmarks should be tested to see if an improvement in tibial accuracy can be attained.

13.1.3 Modify the Probe

Although it has been accepted that the navigation system is still a prototype, some modifications of the navigation tool are necessary. Currently the landmarks cannot be identified without the cutting of a third arthroscopic portal – this will never be accepted in practice. Instead, the design of the probe should be altered so that it can be held in a variety of positions when registering fiducials.

13.1.4 Perform Surgical Tests

Once these changes have been tested and implemented, a series of trials in surgery are necessary to test the real feasibility of this system, specifically the limited navigation provided and the necessity of holding the knee still whilst navigation is performed.

13.2 Creation and Analysis of 3D Models of MRI Scans

The following recommendations about creating and analysing 3D models, and anatomical studies involving these models, are made.

13.2.1 Use Thin MRI Scan Slices

In order to obtain the most accurate and anatomically detailed models, the thinnest scan slice size possible must be utilised – preferably less than 2 mm.

13.2.2 Create full 3D Models

In order for the most accurate co-ordinate systems to be applied and measurements to be made, models which have full anatomical detail proximally, distally, medially and laterally are necessary.

13.2.3 Use 3D Models for further Anatomical Studies

The use of 3D models in this thesis, despite the limitations of the scan data and the inexperience of the user, has provided interesting and invaluable anatomical data. It is recommended that further studies using such models are performed since there are a variety of anatomical issues which can be studied in a non-invasive manner using this approach. It is especially recommended that these studies are tied to clinical data to determine how tunnel placement affects the outcome of patients.

13.2.4 Incorporate Individualised Anatomic Placement into Image Guided ACL Reconstruction Systems

This project has illustrated that the undamaged ACL can be used to find the best position for reconstruction of a torn ACL in the opposite knee. It has also illustrated the wide variety of insertion site areas in healthy ACLs, which supports the need to individualise ACL reconstruction for each patient. Thus it is recommended that image guided ACL systems use this anatomic information in guiding surgeons during surgery.

APPENDIX A – DETAILS OF THE IMAGE GUIDED NEUROSURGERY SYSTEM

This Appendix provides a full description of the hardware and software used in the Image Guided Neurosurgery System. It should be noted that this system is still a prototype system. To orient the reader, a detailed description of the navigation procedure for neurosurgery using this system is also provided.

Typical Surgical Procedure

The procedure for a neurosurgical operation involving the removal of a tumour or lesion starts with the scanning of the lesion using CT scanning. Four or five adhesive fiducial markers are fixed to the patient's scalp around the area containing the lesion prior to scanning to obtain good coverage of the area of interest. These fiducials have a ball bearing at their centre. The lesion is then scanned; approximately twelve slices are taken, as well as a slice through each of the fiducial markers. The order in which the fiducial markers are scanned is important for patient registration that occurs later in the procedure. Dicom images are loaded onto the laptop, either via the network or from CD.

Once on the laptop, the lesion is outlined and fiducial points on the images are marked using locally developed MRIPoint software. This process is performed manually and in consultation with the neurosurgeon. The images are then compiled to produce a 3D representation of the scanned portion of the patient's head. The CT coordinates of the lesion and fiducials are stored in text files on the laptop.

The patient is now moved to theatre and anaesthetised; the cameras are positioned above the surgical table and connected to the laptop via an Ethernet connection. The control frame is positioned above the head of the patient and a pair of images is taken to calibrate the operating space.

Figure A.1 Setup of the image guided neurosurgery system with a head phantom [Watson, 2004].

Patient registration entails measuring and recording the coordinates of each of the fiducial markers in theatre space using the two cameras. During registration the tip of the probe is positioned on the centre of each fiducial with the three reflective markers angled towards the cameras. At each position, the cameras are triggered to capture a pair of images and compute the coordinates of the markers. These are transformed to find the tip coordinates that represent the coordinates of the fiducial. Once all the fiducials have been measured the transformation parameters between physical and CT space are computed. Prior to registration the patient's head is clamped in a Mayfield clamp.

After registration the fiducials are removed. The head is now covered in sterile drapes. The neurosurgeon performs the craniotomy. It is critical that nothing is disturbed during this stage of the procedure.

After the craniotomy three burr holes are drilled in the patient's skull and measured using the procedure previously described. The theatre and CT space coordinates of these three points are saved to files thus allowing for re-registration of the system if the patient subsequently moves or the cameras are bumped. Measurements of the position of the tip of the probe can now be performed as and when required by the surgeon. The position of the tip is displayed on the nearest CT slice or can be viewed using the 3D image that was reconstructed from the CT scans.

Smart Cameras

The cameras were designed by Electronic Development House (EDH, Stellenbosch, South Africa). Each camera contains StrongArm SA110 206MHz processor running a version of Debian Linux adapted for the cameras.

Each camera has a Sony CCD area imager with 512 x 492 pixel resolution, providing a 256 level grey-scale image. The lenses on the cameras are Yamano 16 mm manual iris lenses. The cameras are placed 0.4 m apart.

Each camera has its own IP address for communication over the network.

Figure A.2 One of the smart cameras [Watson, 2004].

Camera Enclosure and Stand

The camera enclosure contains the two cameras, their power supply unit and the hub. The hub is an 8 port, 10Mbsps Ethernet hub which links the two cameras and the laptop. A board of infrared LEDs lies between the cameras. The cameras are triggered almost simultaneously, and every second line of LEDs flashes for each camera.

The cameras are normally mounted on a specifically designed stand, which clamps to the foot of the surgical table in neurosurgery.

Figure A.3 The cameras in the camera enclosure [Watson, 2004].

Control Frame

The control frame is a grid of 6 mm steel bars enclosing a volume. 12 flattened, reflective circular plates are attached at the intersecting points of the grid. This frame is used for calibration of the operating space.

Probe

The probe contains three circular, reflective markers arranged in a cross formation. The probe can be sterilised in an autoclave prior to performing an operation. During the operation, the tip of the probe is placed at a point of interest in the surgical space, leaving the three markers visible to the cameras. The co-ordinates of the three markers are used to calculate the co-ordinates of the tip of the probe

Software

There are two parts to the software – the graphical user interface (GUI) running on the laptop, and the imaging component running off the smart cameras.

Graphical User Interface

The GUI is called Siigns (Stereo-photgrammetric Interactive Image-Guided Neurosurgical System). There are three phases to the operation of the GUI.

Image Acquisition and Manipulation

The program used in this part of the procedure is MRIPointWin. This is a Dicom format image viewer designed specifically for use with the Siigns program. This program can be used to mark a Region of Interest (ROI) such as a tumour on CT or MRI scans. It is also used to digitally mark where the fiducials on the head are in the CT scans.

Once the ROI and fiducials have been marked, the CT scans are compiled into a 3D image of the head showing the ROI in black, and the fiducials. Various viewing formats for this image can be chosen. This image is shown during the operation, with a green cross representing the tip of the probe – this position is updated as the tip is moved.

Camera Set-up and Patient Registration

In this phase, the cameras can be calibrated and focused, and adjusted for various light conditions. Calibration takes place using the frame.

Patient registration is performed once the cameras have been set up. The user is instructed to point to each previously marked fiducial in turn (in the same order as they were marked). The cameras are triggered for each fiducial, and the cameras identify the co-ordinates of the three markers of the probe. These 2D co-ordinates are downloaded from each camera to the laptop, where they are transformed into 3D co-ordinates using the Direct Linear Transform.

The position of these 3D markers are used to determine the position of the tip of the probe, and thus the physical co-ordinates of the fiducials. These are then related to the CT co-ordinates of the fiducials to provide registration of theatre space and CT space.

Position Measurements

Once registration is complete, the probe can be used for navigation. It can either provide continuous, real-time navigation, or discrete navigation – i.e. updating its position on the click of a button. In both these navigation types, the position of the probe is shown as a green cross on the 3D model of the CT scans. On the left of the screen, it is also shown as a green cross in two 2D views of the scans.

Client-Server Communication with the Smart Cameras

The Siigns application on the laptop acts as a server to the two client cameras. The cameras run client programs which allow them to respond to instructions from the laptop. The three main functions of the client program are:

GetImage: Takes an image and downloads it to the laptop
Calibrate: Takes an image, runs the pattern recognition algorithm on the image and downloads a text file containing the 2D co-ordinates of the 12 markers of the control frame.
Measure: Takes an image, runs the pattern recognition algorithm on the image and downloads a text file containing the 2D co-ordinates of the three markers on the probe.

[Watson, 2004]

Appendix B – Full Results of the Feasibility Tests

In this appendix, the full results of all the feasibility tests are provided.

Dry Bone Registration Test

Registration with Bones Longitudinal to the Camera

See Chapter 5 for a description of the experiment.

Calibration Error:		1.2 mm
Registration Error:		
	Test 1:	9.4 mm
	Test 2:	5.6 mm
	Test 3:	7.5 mm

All errors obtained from the navigation system are an indication of how well calibration and registration has taken place.

Results for the first tests are shown in the table on the next page.

Table B.1 Results of the first dry bone tests with bones longitudinal to the cameras.

		Accuracy Marker Error Measurements [mm]												
		A	**B**	**C**	**D**	**E**	**F**	**G**	**H**	**I**	**J**	**K**	**Average**	**Overall**
Test 1	**dx**	6.4	5.9	4.0	4.5	1.7	2.6	6.2	5.7	x	x	6.7		
	dy	6.2	0.6	1.2	0.6	3.6	0.9	3.0	2.2	y	y	4.5		
Test 2	**dx**	3.0	4.2	x	x	3.5	x	84.8	x	x	x	x		
	dy	0.4	0.7	y	y	3.1	y	28.5	y	y	y	y		
Test 3	**dx**	3.0	0.8	2.4	6.4	0.5	0.2	2.4	0.3	2.9	x	3.0		
	dy	1.1	1.1	3.4	2.5	3.5	2.7	2.2	2.8	0.4	y	10.5		
Average Error [mm]	**dx**	4.1	3.6	3.2	5.4	1.8	1.4	31.2	3.0	2.9	x	4.8	**6.1**	**4.8**
	dy	2.6	0.8	2.3	1.6	3.8	1.8	11.2	2.5	0.4	y	7.5	**3.4**	
Maximum Error [mm]	**dx**	6.4	5.9	4.0	6.4	3.2	2.6	84.8	5.7	2.9	x	6.7	**84.8**	**84.8**
	dy	6.2	1.1	3.4	2.5	3.6	2.7	28.5	2.8	0.4	y	10.5	**28.5**	
Minimum Error [mm]	**dx**	3.0	0.8	2.4	4.5	0.5	0.2	2.4	0.3	2.9	x	3.0	**0.2**	**0.2**
	dy	0.4	0.6	1.2	0.6	3.1	0.9	2.2	2.2	0.4	y	4.5	**0.4**	

The average errors in the table are simple averages taken by dividing the total error by the number of tests. These are then further averaged over all the markers, and finally over dx and dy.

Where readings are replaced with 'x' or 'y', this indicates that a measurement could not be made for that marker, since the probe and marker were not visible on the same slice. In these situations, averages were made only over the number of readings available.

Registration with Bones Transverse to the Cameras

Calibration Error:		1.1 mm
Registration Error:		
	Test 1:	18.6 mm
	Test 2:	5.6 mm
	Test 3:	4.5 mm

All errors obtained from the navigation system are an indication of how well calibration and registration has taken place.

Results for the second tests are shown in the table below:

Table B.2 Results of the first dry bone tests with bones transverse to the cameras.

		Accuracy Marker Error Measurements [mm]												
		A	**B**	**C**	**D**	**E**	**F**	**G**	**H**	**I**	**J**	**K**	**Average**	**Overall**
Test 1	**dx**	6.9	16.8	x	x	x	16.9	3.9	5.2	4.5	x	x		
	dy	5.1	5.7	y	y	y	5.9	0.6	12.0	4.5	y	y		
Test 2	**dx**	1.6	2.1	1.1	0.9	2.8	0.9	1.9	3.6	x	x	4.0		
	dy	0.4	0.2	2.9	3.9	4.6	2.7	1.1	8.9	y	y	2.0		
Test 3	**dx**	0.3	2.6	0.3	0.4	7.7	1.6	7.1	x	6.8	x	x		
	dy	0.5	2.3	2.7	2.9	2.6	2.0	4.5	y	3.1	y	y		
Average Error [mm]	**dx**	3.0	7.2	0.7	0.7	5.3	6.4	4.3	4.4	5.7	x	4.0	**4.2**	**4.0**
	dy	2.0	2.7	2.8	3.4	3.6	3.5	2.1	10.9	3.8	y	2.0	**3.6**	
Maximum Error [mm]	**dx**	7.0	16.8	1.1	0.9	7.7	16.9	7.1	5.2	7.0	x	4.0	**16.9**	**16.9**
	dy	5.1	5.7	2.9	3.9	4.6	5.9	4.5	13.0	5.1	y	1.6	**13.0**	
Minimum Error [mm]	**dx**	0.3	2.1	0.3	0.4	2.8	0.9	2.0	3.6	0.3	x	4.0	**0.3**	
	dy	0.4	0.2	2.7	2.9	2.6	2.0	0.6	8.9	0.5	y	1.6	**0.2**	**0.2**

Plastinated Specimen Registration Test

See Chapter 6 for a description of the experiment.

Calibration Error: 1.4 mm

Registration using Five Bony Landmarks

Results for the first registration tests using the plastinated specimen are given below. Five bony landmarks were tested in this experiment.

1. The highest point of the articular surface of the femur, on the lateral side.
2. The highest point of the articular surface of the femur, on the medial side.
3. The highest point in the femoral notch.
4. The lateral tibial spine.
5. The medial tibial spine.

Registration Error:

Test 1:	9.9 mm
Test 2:	6.9 mm
Test 3:	4.1 mm
Test 4:	4.7 mm

Table B.3 Results of the first plastinated specimen tests using five bony landmarks.

		Accuracy Marker Error Measurements [mm]								
		A	**B**	**C**	**D**	**E**	**F**	**G**	**Average**	**Overall**
Test 1	**dx**	1.9	1.2	2.8	4.2	1.0	0.8	0.3		
	dy	1.4	0.2	0.4	3.3	7.3	11.4	4.3		
Test 2	**dx**	3.2	0.8	2.8	1.2	2.4	2.5	0.4		
	dy	0.5	3.8	4.1	1.2	2.3	5.2	0.4		
Test 3	**dx**	4.1	4.3	0.4	2.4	5.9	4.7	2.3		
	dy	1.2	3.4	4.3	5.8	2.1	2.5	4.2		
Test 4	**dx**	1.6	0.8	1.2	3.3	0.1	1.5	3.5		
	dy	1.7	2.9	5.9	2.6	1.2	5.5	9.8		
Average Error [mm]	**dx**	2.7	1.8	1.8	2.8	2.4	2.4	1.7	**2.2**	**2.9**
	dy	1.2	2.6	3.7	3.2	3.3	6.6	4.7	**3.5**	
Maximum Error [mm]	**dx**	4.1	4.3	2.8	4.2	5.9	4.7	3.5	**5.9**	
	dy	1.7	3.8	5.9	5.8	7.3	11.4	9.8	**11.4**	**11.4**
Minimum Error [mm]	**dx**	1.6	0.8	0.4	1.2	0.1	0.8	0.3	**0.1**	**0.1**
	dy	0.5	0.2	0.4	1.2	1.2	2.5	0.4	**0.2**	

Registration Using Three Bony Landmarks

Results for the first registration tests using the plastinated specimen are given below. Three bony landmarks were tested in this experiment.

1. The highest point of the articular surface of the femur, on the lateral side.
2. The highest point of the articular surface of the femur, on the medial side.
3. The highest point in the femoral notch.

Registration Error:

Test 1:	7.0 mm
Test 2:	3.6 mm
Test 3:	4.3 mm
Test 4:	4.0 mm

Table B.4 Results of the first plastinated specimen tests using three bony landmarks.

		Accuracy Marker Error Measurements [mm]								
		A	**B**	**C**	**D**	**E**	**F**	**G**	**Average**	**Overall**
Test 1	**dx**	1.0	1.9	1.7	2.4	6.3	12.1	2.9		
	dy	0.1	11.1	0.7	2.1	1.9	0.3	0.8		
Test 2	**dx**	0.9	0.6	0.2	0.5	0.3	1.8	0.5		
	dy	3.7	1.3	1.3	1.3	2.2	2.6	8.1		
Test 3	**dx**	0.5	0.4	3.8	2.7	0.8	4.9	2.9		
	dy	0.1	2.5	2.7	0.1	0.3	3.4	1.3		
Test 4	**dx**	3.2	1.7	0.1	1.1	5.6	8.0	3.4		
	dy	0.4	0.5	1.6	2.1	2.5	1.5	5.1		
Average Error [mm]	**dx**	1.4	1.2	1.5	1.7	3.2	6.7	2.4	**2.6**	**2.4**
	dy	1.1	3.9	1.6	1.4	1.7	2.0	3.8	**2.2**	
Maximum Error [mm]	**dx**	3.2	1.9	3.8	2.7	6.3	12.1	3.4	**12.1**	**12.1**
	dy	3.7	11.1	2.7	2.1	2.5	3.4	8.1	**11.1**	
Minimum Error [mm]	**dx**	1.6	0.8	0.4	1.2	0.1	0.8	0.3	**0.1**	**0.1**
	dy	0.5	0.2	0.4	1.2	1.2	2.5	0.4	**0.2**	

Registration Using Three Bony and Two Skin Landmarks

Results for the first registration tests using the plastinated specimen are given below. Three bony landmarks and two skin landmarks were tested in this experiment.

1. The highest point of the articular surface of the femur, on the lateral side.
2. The highest point of the articular surface of the femur, on the medial side.
3. The highest point in the femoral notch.

G. 'Skin' marker on the lateral surface of the tibia.
F. 'Skin' marker on the medial surface of the tibia.

Registration Error:

Test 1:	6.5 mm
Test 2:	22.7 mm

Table B.5 Results of the first plastinated specimen tests using bony and skin landmarks.

		Accuracy Marker Error Measurements [mm]						
		A	**B**	**C**	**D**	**E**	**Average**	**Overall**
Test 1	**dx**	1.7	0.1	1.8	1.5	2.7		
	dy	3.4	2.4	3.9	0.5	0.3		
Test 2	**dx**	0.2	5.6	6.5	3.0	x		
	dy	3.4	2.0	2.6	2.0	y		
Average Error [mm]	**dx**	1.0	2.9	4.1	2.3	2.7	**2.6**	**2.3**
	dy	3.4	2.2	3.2	1.2	0.3	**2.1**	
Maximum Error [mm]	**dx**	1.7	5.6	6.5	3.0	2.7	**6.5**	**6.5**
	dy	3.4	2.4	3.9	2.0	0.3	**3.9**	
Minimum Error [mm]	**dx**	0.2	0.1	1.8	1.5	2.7	**0.1**	**0.1**
	dy	3.4	2.0	2.6	0.5	0.3	**0.3**	

Dry Bone Separate Registration Test

See Chapter 5 for a description of this experiment.

Calibration Error: 1.9 mm

Registration of the Femur

The femur was registered with the following landmarks:

1. The highest point on the articular cartilage, laterally.
2. The highest point on the articular cartilage, medially.
3. The highest point in the femoral notch.

Registration Error:

Test 1:	3.8 mm
Test 2:	3.0 mm
Test 3:	5.2 mm

The results for registration of the femur are given below:

Table B.6 Results of the separate registration of the femur of the dry bones specimen.

		Accuracy Marker Error Measurements [mm]							
		A	**B**	**C**	**D**	**E**	**F**	**Average**	**Overall**
Test 1	**dx**	0.1	4.5	3.8	2.8	1.8	6.7		
	dy	4.5	3.1	0.9	2.3	3.5	2.8		
Test 2	**dx**	1.6	1.3	0.6	0.5	2.4	0.5		
	dy	1.1	2.9	1.4	1.3	2.5	1.2		
Test 3	**dx**	0.5	1.2	1.1	1.5	0.0	2.2		
	dy	0.1	1.3	0.3	1.5	1.3	1.9		
Average Error [mm]	**dx**	0.7	2.3	1.8	1.6	1.4	3.1	**1.8**	
	dy	1.9	2.4	0.9	1.7	2.5	1.9	**1.9**	**1.9**
Maximum Error [mm]	**dx**	1.6	4.5	3.8	2.8	2.4	6.7	**6.7**	**6.7**
	dy	4.5	3.1	1.4	2.3	3.5	2.8	**4.5**	
Minimum Error [mm]	**dx**	0.1	1.2	0.6	0.5	0.0	0.5	**0.0**	**0.0**
	dy	0.1	1.3	0.3	1.3	1.3	1.2	**0.1**	

Registration of the Tibia

The tibia was registered with the following landmarks:

1. The lateral tibial spine.
2. The medial tibial spine.
3. 'Skin' marker I on the anterior surface of the tibia.

Registration Error:

Test 1:	3.2 mm
Test 2:	2.8 mm
Test 3:	5.9 mm

The results for registration of the tibia are given below:

Table B.7 Results of the separate registration of the tibia of the dry bone specimen.

		Accuracy Marker Error Measurements [mm]					
		G	**H**	**J**	**K**	**Average**	**Overall**
Test 1	**dx**	9.8	16.7	0.7	2.8		
	dy	4.1	29.2	7.0	8.2		
Test 2	**dx**	0.3	4.2	x	2.0		
	dy	3.7	1.3	y	2.6		
Test 3	**dx**	2.7	0.9	x	3.3		
	dy	2.3	1.3	y	3.7		
Average Error [mm]	**dx**	4.3	7.3	0.7	2.7	**3.7**	
	dy	3.4	10.6	7.0	4.8	**6.4**	**5.1**
Maximum Error [mm]	**dx**	9.8	16.7	0.7	3.3	**16.7**	
	dy	4.1	29.2	7.0	8.2	**29.2**	**29.2**
Minimum Error [mm]	**dx**	0.3	0.9	0.7	2.0	**0.3**	**0.3**
	dy	2.3	1.3	7.0	2.6	**1.3**	

Plastinated Specimen Separate Registration Test

See Chapter 6 for a description of the experiment.

Calibration Error: 1.3 mm

Registration of the Femur

The femur was registered with the following landmarks:

1. The highest point on the articular cartilage, laterally.
2. The highest point on the articular cartilage, medially.
3. The highest point in the femoral notch.

Registration Error:

Test 1: 5.4 mm

Test 2: 4.0 mm

Test 3: 5.1 mm

The results for registration of the femur are given below:

Table B.8 Results of the separate registration of the femur of the plastinated specimen.

		Accuracy Marker Error Measurements [mm]						
		A	**B**	**C**	**D**	**E**	**Average**	**Overall**
Test 1	**dx**	0.0	0.5	0.2	6.1	1.2		
	dy	0.3	0.8	0.0	0.2	0.9		
Test 2	**dx**	0.7	0.7	1.4	3.1	2.9		
	dy	0.6	0.7	0.4	1.2	1.8		
Test 3	**dx**	1.6	0.1	0.1	7.1	0.7		
	dy	3.4	0.8	0.0	2.8	0.2		
Average Error [mm]	**dx**	0.8	0.4	0.6	5.4	1.6	**1.8**	**1.4**
	dy	1.4	0.8	0.1	1.4	1.0	**1.0**	
Minimum Error [mm]	**dx**	0.0	0.1	0.1	3.1	0.7	**0.1**	
	dy	0.3	0.7	0.0	0.2	0.2	**0.0**	**0.0**
Maximum Error [mm]	**dx**	1.6	0.7	1.4	7.1	2.9	**7.1**	**7.1**
	dy	3.4	0.8	0.4	2.8	1.8	**3.4**	

Registration of the Tibia

The tibia was registered with the following landmarks:

1. The lateral tibial spine.
2. The medial tibial spine.
3. 'Skin' marker I on the anterior surface of the tibia.

Registration Error:

Test 1:	7.3 mm
Test 2:	9.2 mm
Test 3:	6.0 mm

The results for registration of the tibia are given below:

Table B.9 Results of the separate registration of the tibia of the plastinated specimen.

		Accuracy Marker Error Measurements [mm]						
		A	**B**	**C**	**D**	**E**	**Average**	**Overall**
Test 1	**dx**	2.0	0.6	6.4	0.5	0.1		
	dy	0.3	0.5	5.4	2.3	2.6		
Test 2	**dx**	1.7	0.8	4.1	2.0	3.8		
	dy	5.1	2.1	5.6	1.3	4.7		
Test 3	**dx**	0.4	0.4	0.8	0.8	0.2		
	dy	1.2	0.7	5.2	4.9	0.6		
Average Error [mm]	**dx**	1.4	0.6	3.8	1.1	1.4	1.6	**2.2**
	dy	2.2	1.1	5.4	2.8	2.6	2.8	
Minimum Error [mm]	**dx**	0.4	0.4	0.8	0.5	0.1	**0.1**	**0.1**
	dy	0.3	0.5	5.2	1.3	0.6	**0.3**	
Maximum Error [mm]	**dx**	2.0	0.8	6.4	2.0	3.8	**6.4**	**6.4**
	dy	5.1	2.1	5.6	4.9	4.7	**5.6**	

Arthroscopic Cadaver Test

See Chapter 7 for a description of the experiment.

Calibration Error: 1.1 mm

Registration Error: 5.5 mm

Registration of the Femur

The femur was registered with the following landmarks:

1. The highest point on the articular cartilage, laterally.
2. The highest point on the articular cartilage, medially.
3. The highest point in the femoral notch.

The results for registration of the femur are given on the next page.

Table B.10 Results of the separate registration of the femur of the cadaver leg.

		Accuracy Marker Error Measurements [mm]						
		Lowest point of Trochlea	Middle of the top of the articular surface	Medial highest point of the articular surface	Lateral Highest point of the articular surface	Highest point of the notch	Average	Overall
Test 1	**dx**	5.5	0.5	5.3	0.8	0.5		
	dy	0.4	1.3	3.2	0.5	1.3		
Average Error [mm]	**dx**						**3.0**	**2.2**
	dy						**1.4**	
Maximum Error [mm]	**dx**						**5.5**	**5.5**
	dy						**3.2**	
Minimum Error [mm]	**dx**						**0.5**	
	dy						**0.4**	**0.4**

Registration of the Tibia

The tibia was registered with the following landmarks:

1. The lateral tibial spine.
2. The medial tibial spine.
3. 'Skin' marker I on the anterior surface of the tibia.

The results for registration of the tibia are given below:

Table B.11Results of the separate registration of the tibia of the cadaver leg.

		Accuracy Marker Error Measurements [mm]				
		Middle of the lateral tibial plateau	Tibial ACL Insertion	Tibial Tuberosity	Average	Overall
Test 1	**dx**	5.1	8.5	16.0		
	dy	1.7	1.6	5.2		
Average Error [mm]	**dx**				**7.4**	**4.8**
	dy				**2.1**	
Maximum Error [mm]	**dx**				**16.0**	**16.0**
	dy				**5.2**	
Minimum Error [mm]	**dx**				**5.1**	
	dy				**1.6**	**1.6**

APPENDIX C – REPEATABILITY TESTS

This appendix gives the full results of the repeatability tests described in Chapter 10.

Repeatability of the Measurements for the Reference Axes

This test was conducted to ascertain how repeatably the measurements used to set up the reference axes could be selected.

Knee 1

Measurements of the Posterior Condylar Line

Table C.1 Repeatability measurements and results for the posterior condylar line for healthy knee 1.

	Medial Point [mm]			Lateral Point [mm]		
	x	y	z	x	y	z
Attempt 1	120.1	-96.3	34.5	125.8	-98.0	-11.5
Attempt 2	120.1	-96.4	33.5	125.7	-98.03	-11.6
Attempt 3	121.6	-93.6	34.4	126.8	-96.4	-11.2
Attempt 4	121.0	-94.7	33.8	126.2	-97.6	-11.5
Attempt 5	120.9	-95.1	33.8	126.5	-96.8	-11.5
Average Value	**120.7**	**-95.2**	**34.0**	**126.2**	**-97.4**	**-11.5**
Error 1	0.6	1.1	0.5	0.4	0.6	0.1
Error 2	0.7	1.2	0.5	0.5	0.7	0.1
Error 3	0.8	1.6	0.4	0.6	1.0	0.3
Error 4	0.3	0.5	0.2	0.0	0.2	0.1
Error 5	0.1	0.6	0.2	0.3	0.5	0.0
Average Error	**0.5**	**0.9**	**0.4**	**0.4**	**0.6**	**0.1**
Average x Error				**0.4**		
Average y Error				**0.8**		
Average z Error				**0.2**		
Average Overall Error				**0.5**		

Measurements of the Middle of the Tibial Spines to the Middle of the Tibial Tuberosity

Table C.2 Repeatability measurements and results for the tibial measurements for healthy knee 1.

	Posterior Point [mm]			Anterior Point [mm]		
	x	y	z	x	y	z
Attempt 1	108.4	-105.3	14.3	76.9	-145.7	19.9
Attempt 2	108.2	-105.6	14.4	76.9	-145.8	19.8
Attempt 3	108.5	-105.2	14.0	76.9	-145.3	19.4
Attempt 4	108.6	-105.1	13.9	76.8	-145.3	19.7
Attempt 5	108.6	-105.1	14.1	76.8	-145.4	20.0
Average Value	**108.5**	**-105.3**	**14.1**	**76.9**	**-145.5**	**19.8**
Error 1	0.1	0.1	0.1	0.0	0.2	0.6
Error 2	0.2	0.3	0.2	0.1	0.3	0.1
Error 3	0.1	0.1	0.1	0.1	0.2	0.3
Error 4	0.1	0.2	0.3	0.0	0.2	0.1
Error 5	0.2	0.1	0.0	0.1	0.1	0.2
Average Error	**0.1**	**0.1**	**0.2**	**0.1**	**0.2**	**0.2**
Average x Error			**0.1**			
Average y Error			**0.2**			
Average z Error			**0.2**			
Average Overall Error			**0.1**			

Measurements of the Femoral Origin

Table C.3 Repeatability measurements for the femoral origin for healthy knee 1.

	Point [mm]		
	x	y	z
Attempt 1	27.4	-9.8	-23.4
Attempt 2	27.4	-10.3	-23.7
Attempt 3	27.3	-9.9	-23.4
Attempt 4	27.4	-9.8	-23.4
Attempt 5	27.3	-9.9	-23.4
Average Value	**27.4**	**-10.0**	**-23.5**
Error 1	0.0	0.1	0.0
Error 2	0.1	0.3	0.3
Error 3	0.1	0.1	0.1
Error 4	0.0	0.1	0.0
Error 5	0.1	0.1	0.1
Average Error	**0.1**	**0.1**	**0.1**
Average Overall Error		**0.1**	

Measurements of the Tibial Origin

Table C.4 Repeatability results for the Tibial origin for healthy knee 1.

	Point [mm]		
	x	y	z
Attempt 1	110.4	-102.9	7.6
Attempt 2	110.5	-103.0	7.4
Attempt 3	109.9	-102.9	7.4
Attempt 4	110.3	-102.9	7.4
Attempt 5	110.8	-103.0	7.7
Average Value	**110.4**	**-102.9**	**7.5**
Error 1	0.0	0.1	0.1
Error 2	0.1	0.1	0.1
Error 3	0.5	0.0	0.1
Error 4	0.0	0.0	0.1
Error 5	0.4	0.0	0.2
Average Error	**0.2**	**0.0**	**0.1**
Average Overall Error		**0.1**	

Knee 2

Measurements of the Posterior Condylar Line

Table C.5 Repeatability measurements and results for the posterior condylar line for healthy knee 2.

	Medial Point [mm]			Lateral Point [mm]		
	x	y	z	x	y	z
Attempt 1	133.2	-88.8	57.9	134.9	-90.7	11.3
Attempt 2	134.0	-87.2	58.6	134.6	-90.9	12.6
Attempt 3	133.8	-87.5	59.8	135.8	-88.1	12.1
Attempt 4	133.4	-88.3	59.2	135.4	-89.7	11.7
Attempt 5	132.7	-89.3	59.4	135.0	-90.0	13.2
Average Value	**133.4**	**-88.2**	**59.0**	**135.1**	**-89.9**	**12.2**
Error 1	0.2	0.6	1.1	0.2	0.8	0.9
Error 2	0.6	1.0	0.4	0.5	1.0	0.4
Error 3	0.4	0.8	0.8	0.7	1.8	0.1
Error 4	0.0	0.1	0.2	0.2	0.2	0.5
Error 5	0.7	1.1	0.5	0.2	0.1	1.0
Average Error	**0.4**	**0.7**	**0.6**	**0.4**	**0.8**	**0.6**
Average x Error			**0.4**			
Average y Error			**0.7**			
Average z Error			**0.6**			
Average Overall Error			**0.6**			

Measurements of the Middle of the Tibial Spines to the Middle of the Tibial Tuberosity

Table C.6 Repeatability measurements and results for the tibial measurements for healthy knee 2.

	Posterior Point [mm]			Anterior Point [mm]		
	x	y	z	x	y	z
Attempt 1	109.4	-102.3	38.6	72.4	-152.3	41.8
Attempt 2	109.2	-102.4	38.7	72.7	-154.7	40.8
Attempt 3	108.9	-102.5	38.5	72.7	-154.8	40.8
Attempt 4	108.6	-102.8	38.4	72.3	-155.2	40.5
Attempt 5	108.8	-102.6	38.2	72.6	-155.3	41.1
Average Value	**109.0**	**-102.5**	**38.5**	**72.5**	**-154.5**	**41.0**
Error 1	0.4	0.2	0.2	0.1	2.1	0.8
Error 2	0.2	0.1	0.3	0.2	0.2	0.2
Error 3	0.1	0.0	0.0	0.2	0.3	0.2
Error 4	0.4	0.3	0.1	0.3	0.7	0.5
Error 5	0.2	0.1	0.3	0.1	0.9	0.1
Average Error	**0.2**	**0.2**	**0.2**	**0.2**	**0.9**	**0.4**
Average x Error			**0.2**			
Average y Error			**0.5**			
Average z Error			**0.3**			
Average Overall Error			**0.3**			

Measurements of the Femoral Origin

Table C.7 Repeatability measurements and results for the femoral origin for healthy knee 2.

	Point [mm]		
	x	y	z
Attempt 1	21.0	-11.8	-25.1
Attempt 2	21.8	-12.1	-25.8
Attempt 3	21.5	-11.8	-25.5
Attempt 4	21.8	-12.1	-25.8
Attempt 5	21.0	-11.8	-25.1
Average Value	**21.4**	**-11.9**	**-25.5**
Error 1	0.4	0.1	0.3
Error 2	0.4	0.2	0.3
Error 3	0.1	0.1	0.0
Error 4	0.1	0.2	0.3
Error 5	0.4	0.1	0.3
Average Error	**0.3**	**0.1**	**0.3**
Average Overall Error		**0.3**	

Measurement of the Tibial Origin

Table C.8 Repeatability measurements and results for the tibial origin for healthy knee 2.

	Point [mm]		
	x	y	z
Attempt 1	113.6	-101.7	34.5
Attempt 2	112.9	-101.4	34.4
Attempt 3	113.1	-101.5	34.4
Attempt 4	113.2	-101.6	34.2
Attempt 5	113.7	-101.7	34.7
Average Value	**113.3**	**-101.6**	**34.4**
Error 1	0.3	0.2	0.1
Error 2	0.4	0.2	0.0
Error 3	0.2	0.1	0.0
Error 4	0.1	0.0	0.3
Error 5	0.4	0.1	0.2
Average Error	**0.3**	**0.1**	**0.1**
Average Overall Error		**0.2**	

Knee 3

Measurement of the Posterior Condylar Line

Table C.9 Repeatability measurements and results for the posterior condylar line for the reconstructed knee.

	Medial Point [mm]			Lateral Point [mm]		
	x	y	z	x	y	z
Attempt 1	64.9	-82.0	-59.1	53.9	-84.2	-14.8
Attempt 2	64.8	-80.4	-59.8	53.6	-81.5	-15.9
Attempt 3	65.9	-85.7	-59.9	55.2	-86.0	-15.1
Attempt 4	65.2	-83.4	-58.9	54.3	-84.1	-16.2
Attempt 5	65.7	-84.9	-59.4	55.1	-85.7	-15.5
Average Value	**65.3**	**-83.3**	**-59.4**	**54.4**	**-84.3**	**-15.5**
Error 1	0.4	1.3	0.4	0.5	0.1	0.7
Error 2	0.5	2.9	0.4	0.8	2.8	0.4
Error 3	0.6	2.4	0.5	0.8	1.7	0.4
Error 4	0.1	0.1	0.5	0.1	0.2	0.7
Error 5	0.4	1.6	0.0	0.7	1.4	0.0
Average Error	**0.4**	**1.8**	**0.3**	**0.6**	**1.2**	**0.4**
Average x Error				**0.5**		
Average y Error				**1.5**		
Average z Error				**0.4**		
Average Overall Error				**0.8**		

Measurements of the Middle of the Tibial Spines to the Middle of the Tibial Tuberosity

Table C.10 Repeatability measurements and results for the tibial measurements for the reconstructed knee.

	Posterior Point [mm]			Anterior Point[mm]		
	x	y	z	x	y	z
Attempt 1	81.4	-94.8	-36.3	119.1	-142.2	-39.6
Attempt 2	81.6	-94.9	-36.5	119.1	-141.8	-40.4
Attempt 3	812.0	-94.9	-36.4	119.0	-142.4	-39.8
Attempt 4	81.8	-95.0	-36.8	119.0	-142.3	-39.8
Attempt 5	81.9	-94.9	-36.4	118.9	-142.9	-39.7
Average Value	**81.7**	**-94.9**	**-36.5**	**119.0**	**-142.3**	**-39.9**
Error 1	0.4	0.1	0.1	0.1	0.1	0.3
Error 2	0.1	0.0	0.0	0.1	0.5	0.5
Error 3	0.2	0.1	0.1	0.0	0.1	0.1
Error 4	0.1	0.1	0.3	0.0	0.0	0.1
Error 5	0.2	0.0	0.1	0.2	0.5	0.1
Average Error	**0.2**	**0.0**	**0.1**	**0.1**	**0.3**	**0.2**
Average x Error			**0.1**			
Average y Error			**0.2**			
Average z Error			**0.2**			
Average Overall Error			**0.2**			

Measurement of the Femoral Origin

Table C.11 Repeatability measurements and results for the femoral origin for the reconstructed knee.

	Point [mm]		
	x	y	z
Attempt 1	21.2	-15.7	-30.3
Attempt 2	20.7	-15.9	-30.0
Attempt 3	20.6	-16.0	-30.0
Attempt 4	21.2	-15.7	-30.3
Attempt 5	20.6	-16.0	-30.0
Average Value	**20.8**	**-15.8**	**-30.1**
Error 1	0.3	0.2	0.2
Error 2	0.2	0.0	0.1
Error 3	0.2	0.1	0.1
Error 4	0.3	0.2	0.2
Error 5	0.2	0.1	0.1
Average Error	**0.3**	**0.1**	**0.2**
Average Overall Error		**0.2**	

Measurement of the Tibial Origin

Table C.12 Repeatability measurements and results for the tibial origin for the reconstructed knee.

	Point [mm]		
	x	y	z
Attempt 1	78.0	-93.8	-32.0
Attempt 2	78.0	-94.0	-32.2
Attempt 3	78.0	-93.9	-32.0
Attempt 4	77.6	-93.9	-32.6
Attempt 5	77.9	-93.9	-31.8
Average Value	**77.8**	**-93.9**	**-32.1**
Error 1	0.2	0.1	0.1
Error 2	0.1	0.1	0.1
Error 3	0.1	0.0	0.1
Error 4	0.2	0.1	0.5
Error 5	0.1	0.0	0.3
Average Error	**0.1**	**0.0**	**0.3**
Average Overall Error		**0.1**	

Repeatability of the Measurements of the ACL Insertion and Tunnel Positions

These tests were carried out to ensure that the four 'corners' measured for the tibial and femoral ACL insertion sites, or tunnel exits, were repeatable.

Healthy Knee

Femoral Measurements

Table C.13 Repeatability measurements for the four femoral points of the ACL insertion.

	FEMUR											
	Post Prox			**Ant Prox**			**Post Dist**			**Ant Dist**		
	x	y	z	x	y	z	x	y	z	x	y	z
Test 1	-3.1	-1.4	-1.5	5.0	-4.3	-0.1	-3.06	-2.0	-17.0	6.2	-4.5	-15.2
Test 2	-3.2	-1.4	-1.7	4.7	-2.8	-0.2	-3.01	-2.0	-16.9	5.5	-3.8	-16.2
Test 3	-3.1	-1.3	-1.5	4.6	-4.0	0.3	-3.14	-2.0	-16.8	4.9	-3.5	-16.7
Test 4	-3.0	-1.4	-1.4	4.5	-3.9	0.2	-3.38	-2.0	-16.6	2.8	-2.9	-17.4
Test 5	-3.2	-1.4	-1.5	3.1	-2.3	-0.2	-3.30	-2.1	-17.0	1.6	-1.5	-15.4
Average	**-3.1**	**-1.4**	**-1.5**	**4.4**	**-3.5**	**0.0**	**-3.18**	**-2.0**	**-16.8**	**4.2**	**-3.2**	**-16.2**
Error 1	0.0	0.0	0.0	0.6	0.8	0.1	0.12	0.0	0.2	2.0	1.3	1.0
Error 2	0.1	0.0	0.1	0.3	0.7	0.1	0.17	0.0	0.0	1.3	0.6	0.0
Error 3	0.0	0.0	0.0	0.4	0.6	0.3	0.04	0.0	0.1	0.7	0.2	0.5
Error 4	0.1	0.0	0.1	0.1	0.4	0.2	0.20	0.0	0.3	1.4	0.4	1.2
Error 5	0.1	0.0	0.0	1.3	1.1	0.2	0.12	0.1	0.2	2.6	1.8	0.8
Average Error	**0.1**	**0.0**	**0.1**	**0.5**	**0.7**	**0.2**	**0.13**	**0.1**	**0.1**	**1.6**	**0.9**	**0.7**
Average Point Error		**0.1**			**0.5**			**0.1**			**1.1**	
Average x Error							**0.6**					
Average y Error							**0.4**					
Average z Error							**0.2**					
Average Overall Error							**0.4**					

Tibial Measurements

Table C.14 Repeatability measurements for the four points of the tibial insertion.

	TIBIA											
	Ant Med			Ant Lat			Post Med			Post Lat		
	x	y	Z	x	y	z	x	y	z	x	y	z
Test 1	-3.4	19.1	-6.7	3.9	15.0	-3.4	-7.5	4.0	2.2	1.5	4.6	2.0
Test 2	-3.4	19.1	-6.7	4.1	15.4	-3.4	-7.4	3.3	2.6	1.8	4.8	2.0
Test 3	-3.4	20.2	-6.8	4.0	15.2	-3.4	-6.7	4.7	1.0	1.6	4.8	1.2
Test 4	-3.5	19.4	-6.8	4.2	15.0	-3.3	-7.0	4.3	1.5	1.6	4.6	2.1
Test 5	-3.5	19.0	-6.8	4.3	15.5	-3.2	-7.4	3.9	-2.1	1.7	4.7	1.8
Average	**-3.4**	**19.4**	**-6.8**	**4.1**	**15.2**	**-3.3**	**-7.2**	**4.0**	**1.0**	**1.6**	**4.7**	**1.8**
Error 1	0.0	0.3	0.0	0.2	0.2	0.1	0.3	0.0	1.2	0.1	0.1	0.2
Error 2	0.1	0.3	0.1	0.0	0.1	0.0	0.2	0.8	1.5	0.1	0.1	0.2
Error 3	0.0	0.8	0.1	0.1	0.0	0.1	0.5	0.7	0.0	0.1	0.1	0.6
Error 4	0.0	0.1	0.0	0.1	0.2	0.1	0.2	0.3	0.4	0.1	0.1	0.3
Error 5	0.1	0.4	0.0	0.2	0.3	0.1	0.2	0.1	3.2	0.0	0.0	0.0
Average Error	**0.0**	**0.4**	**0.1**	**0.1**	**0.2**	**0.1**	**0.3**	**0.4**	**1.3**	**0.1**	**0.1**	**0.3**
Average Point Error		**0.2**			**0.1**			**0.6**			**0.2**	
Average x Error						**0.1**						
Average y Error						**0.2**						
Average z Error						**0.4**						
Average Overall Error						**0.3**						

Reconstructed Knee

Femoral Measurements

Table C.15 Repeatability measurements for the four points of the femoral tunnel.

	FEMUR											
	Post Prox			Ant Prox			Post Dist			Ant Dist		
	x	y	z	x	Y	z	x	y	z	x	y	z
Test 1	-8.6	3.3	-3.0	0.2	1.7	-0.0	-6.6	2.8	-9.3	0.3	-2.3	-4.4
Test 2	-8.4	3.0	-3.8	0.0	-1.9	-0.7	-7.6	2.1	-9.8	-0.5	-3.6	-7.0
Test 3	-9.1	3.0	-3.8	-0.2	-2.4	0.7	-7.6	-0.6	-13.4	-1.0	-2.6	-8.4
Test 4	-8.4	2.9	-4.2	0.0	-3.3	-1.0	-4.9	1.0	-10.9	-0.5	-3.7	-7.4
Test 5	-9.1	2.8	-4.3	-0.1	-3.9	-0.7	-8.2	0.2	-12.4	-0.9	-4.0	-8.5
Average	**-8.7**	**3.0**	**-3.8**	**-0.0**	**-1.9**	**-0.3**	**-7.0**	**1.1**	**-11.1**	**-0.5**	**-3.3**	**-7.1**
Error 1	0.1	0.3	0.8	0.2	3.7	0.3	0.4	1.7	1.9	0.8	1.0	2.8
Error 2	0.3	0.0	0.1	0.0	0.1	0.3	0.6	1.0	1.3	0.1	0.4	0.1
Error 3	0.3	0.0	0.1	0.2	0.4	1.1	0.6	1.7	2.3	0.5	0.6	1.3
Error 4	0.3	0.1	0.4	0.0	1.3	0.7	2.1	0.1	0.3	0.0	0.5	0.3
Error 5	0.4	0.2	0.5	0.1	2.0	0.4	1.2	0.9	1.2	0.4	0.7	1.4
Average Error	**0.3**	**0.1**	**0.4**	**0.1**	**1.5**	**0.6**	**1.0**	**1.1**	**1.4**	**0.3**	**0.6**	**1.2**
Average Point Error		**0.3**			**0.7**			**1.1**			**0.7**	
Average x Error						**0.4**						
Average y Error						**0.8**						
Average z Error						**0.8**						
Average Overall Error						**0.7**						

Tibial Measurements

Table C.16 Repeatability measurements and results for the four points of the tibial tunnel.

	TIBIA											
	Ant Med			Ant Lat			Post Med			Post Lat		
	x	y	z	x	y	z	x	y	z	x	y	z
Test 1	-0.0	16.2	-6.3	5.2	15.7	-5.4	0.3	13.5	-6.3	4.6	13.2	-5.1
Test 2	0.1	16.3	-6.3	5.2	15.9	-5.3	0.1	13.4	-6.2	4.4	13.0	-5.1
Test 3	1.0	16.0	-6.7	4.4	15.6	-6.6	0.8	13.2	-6.2	4.3	13.0	-5.2
Test 4	-0.9	16.3	-6.0	5.4	15.9	-5.2	0.4	13.4	-6.3	4.3	13.1	-5.2
Test 5	0.9	17.1	-5.6	5.3	16.1	-5.2	0.3	13.4	-6.2	4.7	12.9	-4.9
Average	**0.2**	**16.4**	**-6.2**	**5.1**	**15.8**	**-5.5**	**0.4**	**13.4**	**-6.2**	**4.5**	**13.0**	**-5.1**
Error 1	0.2	0.1	0.1	0.1	0.2	0.1	0.1	0.1	0.1	0.1	0.1	0.0
Error 2	0.1	0.1	0.1	0.1	0.1	0.2	0.2	0.1	0.1	0.1	0.0	0.1
Error 3	0.8	0.4	0.5	0.7	0.2	1.1	0.4	0.2	0.0	0.2	0.0	0.1
Error 4	1.1	0.1	0.2	0.3	0.0	0.3	0.0	0.0	0.1	0.1	0.0	0.1
Error 5	0.7	0.7	0.6	0.2	0.3	0.4	0.1	0.0	0.1	0.3	0.2	0.2
Average Error	**0.6**	**0.3**	**0.3**	**0.3**	**0.1**	**0.4**	**0.6**	**0.1**	**0.1**	**0.2**	**0.1**	**0.1**
Average Point Error		**0.4**			**0.3**			**0.1**			**0.1**	
Average x Error							**0.3**					
Average y Error							**0.1**					
Average z Error							**0.2**					
Average Overall Error							**0.2**					

Repeatability Tests for Normalisation Measurements

These tests were conducted to ensure that the measurements used to normalise the ACL positions for size, were repeatable.

Table C.17 Repeatability measurements and results for the normalisation measurements.

	Knee 1		Knee 2	
	Femur	**Tibia**	**Femur**	**Tibia**
Test 1	37.7	41.0	33.7	41.78
Test 2	38.4	39.5	34.0	41.9
Test 3	38.1	40.5	33.7	42.6
Test 4	38.1	40.7	33.7	41.5
Test 5	38.0	40.4	33.9	41.6
Average	**38.1**	**40.4**	**33.8**	**41.9**
Error 1	0.4	0.6	0.0	0.1
Error 2	0.4	1.0	0.1	0.1
Error 3	0.1	0.1	0.1	0.8
Error 4	0.0	0.3	0.1	0.4
Error 5	0.1	0.0	0.1	0.3
Average Error	**0.8**	**0.4**	**0.1**	**0.3**
Average Overall Error		**0.2**		

REFERENCES

Aglietti P, Zaccherotti G, Simeone AJV, Buzzi R (1998) "Anatomic versus non-anatomic tibial fixation in anterior cruciate ligament reconstruction with bone-patellar tendon-bone graft", *Knee Surgery Sports Traumatology, Arthroscopy*, 6 [Suppl 1]: S43 – S48

Amiot LP, Poulin F (2004) "Computed Tomography-Based Navigation for Hip, Knee and Spine Surgery", *Clinical Orthopaedics and Related Research*, 421: 77 – 86

Amis AA, Jakob RP (1998) "Anterior cruciate ligament graft positiong, tensioning and twisting", *Knee Surgery, Sports Traumatology, Arthroscopy*, 6 [Suppl 1]: S2 – S12

Arnold MP, Kooloos J, van Kampen A (2001) "Single-incision technique misses the anatomical femoral anterior cruciate ligament insertion: a cadaver study", *Knee Surgery, Sports Traumatology, Arthroscopy*, 9: 194 – 199

Bäthis H, Perlick L, Tingart M, Lüring C, Perlick C, Grifka J (2004) "Radiological results of image-based and non-image-based computer-assisted total knee arthroplasty", *International Orthopaedics*, 28: 87 – 90

Bernard M, Hertel P, Hornung H, Cierinski T (1997) "Femoral insertion of the ACL. Radiographic quadrant method", *American Journal of Knee Surgery*, 10(1): 14 – 21

Berquist TH (Editor), (1990) "*MRI of the musculoskeletal system*", 2nd edition, Raven Press New York

Bloem JL, Sartoris DJ (Editors) (1992) "*MRI and CT of the Musculoskeletal system – a text-atlas*", Williams and Wilkins, Batimore, pp 421 – 433

Burkart A, Debski RE, McMahon PJ, Rudy T, Fu FH, Musahl V, van Scycoc A, Woo S L-Y (2001) "Precision of ACL tunnel placement using traditional and robotic techniques", *Computer Aided Surgery*, 6: 270 – 278

Cain EL Jr, Clancy EG (2002) "Anatomic endoscopic anterior cruciate ligament reconstruction with patella tendon authograft", *Orthopedic Clinics of North America*, 33: 717 – 725

Degenhart M (2004) "Computer-navigated ACL reconstruction with the OrthoPilot", *Surgical Technology International*, 12: 245-51

Delp SL, Stulberf SD, Davies B, Picard F, Leitner F (1998) "Computer Assisted Knee Replacement", *Clinical Orthopaedics and Related Research*, 354: 49 – 56

DiGioia AM III, Jaramaz B, Colgan BD (1998) "Computer Assisted Orthopaedic Surgery – Image Guided and Robotic Assistive Technologies", *Clinical Orthopaedics and Related Research*, 354: 8 – 16

Duthon VB, Abrassart S, Barea C, Ménétrey J (2000) "Anatomy of the Anterior Cruciate Ligament, a Multimedia Approach", *ESSKA 2000, Athens*

Eriksson E (1997) "How good are the results of ACL reconstruction?",*Knee Surgery, Sports Traumatology, Arthroscopy*, 5: 137

Fleute M, Lavallée S, Julliard R (1999) "Incorporating a statistically based shape model into a system for cmputer-assisted anterior cruciate ligament surgery", *Medical Image Analysis*, 3(3): 209-222

Fu FH, Musahl V (2001) "The Future of Knee Ligament Surgery", *Journal of Orthopaedic Surgery (Hong Kong)*, 9(2): 77 - 80

Gebhard F, Krettek C, Hüfner T (2004) "Editorial", *Injury*, 35: S-A1

Girgis FG, Marshall JL, al Monajem ARS (1975) "The crucuate ligaments of the knee joint – anatomical, functional and experimental analysis", Clinical *Orthopaedics and Related Research*, 106: 216 – 231

Giron F, Cuomo P, Aglietti P, Bull AMJ, Amis AA (2005) "Femoral attachment of the anterior cruciate ligament", *Knee Surgery, Sports Traumatology, Arthroscopy*, Nov 10: E-published ahead of print

Giron F, Aglietti P, Cuomo P (2000) "Femoral Insertion of the ACL", *ESSKA 2000, Athens*

Harner CD, Fu FH, Irrgang JJ, Vogrin TM (2001) "Anterior and posterior cruciate ligament reconstruction in the new millennium: a global perspective", *Knee Surgery, Sports Traumatology, Arthroscopy*, 9: 330-336

Harner CD, Hyun Baek G, Vogrin TM, Carlin GJ, Kashiwaguchi S, Woo SL-Y (1999) "Quantitative analysis of human cruciate ligament insertions", *Arthroscopy*, 15 (7): 741 – 749

Howell SM (1998) "Principles for placing the tibial tunnel and avoiding roof impingement during reconstruction of a torn anterior cruciate ligament", *Knee Surgery, Sports Traumatology, Arthroscopy*, 6 [Suppl 1]: S49 – S55

Howell SM, Clark JA, Blasier RD (1991) "Serial magnetic resonance imaging of hamstring anterior cruciate ligament autografts during the first year of implantation – a preliminary study", *The American Journal of Sports Medicine*, 19 (1): 42 – 47

Hüfner T, Gebhard F, Grützner PA, Messmer P, Stöckle U, Krettek C (2004) "Which navigation when?", *Injury*, 35: S-A30 – S-A34

Hughston JC (1993) *"Knee Ligaments – Injury and Repair"*, Mosby, St Louis, pp 22 – 27, 370 – 376

Jackson DW (Editor), Arnoczky SP, Frank CB, Woo SLY, Simon TM (1993) *"The Anterior Cruciate Ligament – Current and Future Concepts"*, Raven Press, New York, pp 7- 10, 39 – 43, 305 – 320

Järvelä T, Paakkala T, Järvelä K, Kannus P, Markku J (2001) "Graft placement after the anterior cruciate ligament reconstruction: a new method to evaluate the femoral and tibial placements of the graft", *The Knee*, 8: 219 – 227

Jenny JY, Boeri C (2004) "Low reproducibility of the intra-operative measurement of the transepicondylar axis during total knee replacement.", *Acta Orthopaedica Scandinavia*, 75(1): 74 – 77

Jonsson H, Elmqvist LG, Kärrholm, Tegner Y (1994) "Over-the-top or tunnel reconstruction of the anterior cruciate ligament? – a prospective randomised study of 54 patients", *Journal of Bone and Joint Surgery [British]*, 76-B: 82 – 87

Joskowicz L, Taylor RH (2001) "Computers in Imaging and Guided Surgery", *Computers in Science and Engineering*, 3(5): 65 – 72

Julliard R, Lavallée S, Dessenne V (1998) "Computer Assisted Reconstruction of the Anterior Cruciate Ligament", *Clinical Orthopaedics and Related Research*, 354: 57-64

Jyrkinsen L, Ojala R, Haataja L, Blanco R, Klemola R, Silven O, Tervonen O (2000) "Managing the Complexity of the User Interface of a MRI Guided Surgery System", *6th ERCIM Workshop "User Interfaces for All"*

Klos TV, Banks SA, Havets RJ, Cook FF (2000) "Sagittal plane imaging parameters for computer-assisted fluoroscopic anterior cruciate ligament reconstruction", *Computer Aided Surgery*, 5(1):28-34

Klos TVS, Habets RJE, Banks AZ, Banks SA, Devilee RJJ, Cook FF (1998) "Computer Assistance in Arthroscopic Anterior Cruciate Ligament Reconstruction", *Clinical Orthopaedics and Related Research*, 354: 65-69

Kohn D, Busche T, Carls J (1998) "Drill hole positions in endoscopic anterior cruciate reconstruction: results of an advanced arthoscopy course", *Knee Surgery, Sports Traumatology, Arthroscopy*, 6 [Suppl 1]: S13 – S15

Langlotz F (2004) "Potential pitfalls of computer aided orthopaedic surgery", *Injury*, 35: S-A17 – S-A23

Lintner DM, Dewitt SE, Moseley JB (1996) "Radiographic evaluation of native anterior cruciate ligament attachments and graft placement for reconstruction", *The American Journal of Sports Medicine*, 24 (1): 72 – 82

Markolf KL, Hame S, Hunter DM, Oakes DA, Zoric B, Gause P, Finerman GAM (2002) "Effects of femoral tunnel placement on knee laxity and forces in an anterior cruciate ligament graft", *Journal of Orthopaedic Research*, 20: 1016- 1024

Mohsen AMMA, Phillips R (2004) "Letter of the reviewers", *Injury*, 35: S-A2 – S-A5

Moody JE, Constantinos N, Picard F, Levison T, Jaramaz B, DiGioia AM, Reverte CF (2002) "Computer-Integrated Anterior Cruciate Ligament Reconstruction System", *The Journal of Bone and Joint Surgery*; 84-A(2): 99-101

Müller-Alsbach UW and Stäubli AE (2004) "Computer aided ACL reconstruction", *Injury*, 35: S-A65 – S-A67

Musahl V, Plakseychuk A, van Scycoc A, Sasaki T, Debski RE, McMahon PJ, Fu FH (2005) "Varyinbg femoral tunnels between the anatomical footprint and isometric positions", *The American Journal of Sports Medicine*, 33(5): 712 – 718

Musahl V, Burkart A, Debski RE, van Scycoc A, Fu FH, Woo SL-Y (2003) "Anterior Cruciate Ligament Tunnel Placement: Comparison of Insertion Site Anatomy with the Guidelines of a Computer-Assisted Surgical System", *Arthroscopy*, 19(2): 154-160

Musahl V, Burkart A, Debski RE, van Scycoc A, Fu FH, Woo SL-Y (2002) *i* "Accuracy of Anterior Cruciate Ligament Tunnel Placement with an Active Robotic System: A Cadaveric Study", *Arthroscopy*, 18(9): 968-973

Musahl V, Plakseychuk A, Fu FH (2002) *ii* "Current opinion on computer-aided surgical navigation and robotics – role in the treatment of sports-related injuries", *Sports Medicine*, 32(13) 809 – 818

Nizard RS, Porcher R, Ravaud P, Vangaver E, Hannouche D, Bizot P, Sedel L (2004) "Use of the Cusum Technique for Evaluation of a CT-based Navigation System for Total Knee Replacement", *Clinical Orthopaedics and Related Research*, 425: 180 – 188

Nebelung W, Wuschech H (2005) "Thirty-five years of follow-up of anterior cruciate ligament-deficient knees in high-level athletes", *Arthroscopy*, 21(6): 696 – 702

Neyret JP, Dojcinovic S, Lustig S (2000) "Best Images of Ligament Insertions of the Knee", *ESSKA 2000, Athens*

Noble PC, Sugano N, Johnston JD, Thompson MT, Conditt MA, Engh CA, Mathis KB (2003) "Computer Simulation: How Can it Help the Surgeon Optimize Implant Precision?", *Clinical Orthopaedics and Related Research*, 417: 242 – 252

Nolte LP, Beutler T (2004) "Basic Principles of CAOS", *Injury*, 35: S-A6 – S-A16

Picard F, DiGioia AM, Moody J, Martinek V, Fu FH, Rytel M, Nikou C, LaBarca RS, Jaramaz B (2001) "Accuracy in Tunnel placement for ACL Reconstruction. Comparison of Traditional Arthroscopic and Computer-Assisted Navigation Techniques", *Computer Aided Surgery*, 6:279-289

Porter ML, Gambhir AK, Pradhan N (2004) "Image-Guided Surgery for Total Knee Replacement", *The Journal of Bone and Joint Surgery [Am]*, 86-A (5): 1096

Sati M, Stäubli HU, Bourquin Y, Kunz M, Nolte LP (2002) "Real-time computerized In Situ Guidance System for ACL Graft Replacement", *Computer Aided Surgery*, 7(1): 25-40

Schep NWL, Stavenuiter MHJ, Diekerhof CH, Martens EP, van Haeff M, Broeders IAMJ, Saris DBF (2005) "Intersurgeon variance in computer-assisted planning of anterior cruciate ligament reconstruction", *Arthroscopy*, 8: 942 – 947

Shea KG, Apel PJ, Pfeiffer RP, Showaiter LD, Traughber PD (2002) "The tibial attachment of the anterior cruciate ligament in children and adolescents: analysis of magnetic resonance imaging", *Knee Surgery, Sports Traumatology, Arthroscopy*, 10: 102 – 108

Sikorski JM, Chauhan S (2003) "Aspects of current management – computer-assisted orthopaedic surgery: do we need CAOS?", *The Journal of Bone and Joint Surgery (British)*, 85-B: 319 – 323

Simon DA, O'Toole RV, Blackwell M, Morgan F, DiGioia AM, Kanade T (1995) "Accuracy Validation in Image-Guided Orthopaedic Surgery", *Proceedings of the Second International Symposium of Medical Robotics and Computer Assisted Surgery*, MRCAS, Baltimore, pp185 - 192

Smith & Nephew (1998) "Femoral Component External Rotation in Total Knee Arthroplasty" *Technical Summary CD for Genesis II*

Staubli HU, Raushning W (1994) "Tibial attachment area of the anterior cruciate ligament in the extended knee position. Anatomy and crysosections in vitro complemented by magnetic resonance arthrography in vivo", *Knee Surgery, Sports Traumatology, Arthroscopy*, 2(3): 138 – 46

Stulberg, SD (2003) "How Accurate is Current TKR Instrumentation?", *Clinical Orthopaedics and Related Research*, 416: 177 – 184

Topliss C, Webb J (2001) "An audit of tunnel position in anterior cruciate ligament reconstruction", *The Knee*, 8: 59 – 63

Watson MJ (2004) "*Development of an interactive, image guided neurosurgical system*", Masters Thesis in Biomedical Engineering, Department of Human Biology, University of Cape Town

Yasuda K, Kondo E, Ichiyama H, Kitamura B, Tanabe Y, Tohyama H, Minami A (2004) "Anatomical reconstruction of the anteromedial and posterolateral bundles of the anterior cruciate ligament using hamstring tendon grafts", *Arthroscopy*, 20 (10): 1015 – 1025

Zavras TD, Race A, Amis AA (2005) "The effect of femoral attachment location on anterior cruciate ligament reconstruction: graft tension patterns and restoration of normal anterior-posterior laxity patterns", *Knee Surgery, Sports Traumatology, Arthroscopy*, 13: 92 – 100